ROLES FOR THE DNA DAMAGE CHECKPOINT GENE *HUS1* IN RESPONDING TO ENDOGENOUS AND EXOGENOUS STRESSES IN VIVO

A Dissertation

Presented to the Faculty of the Graduate School

of Cornell University

In Partial Fulfillment of the Requirements for the Degree of

Doctor of Philosophy

by
Gabriel Balmus, D.V.M.
January 2013

ROLES FOR THE DNA DAMAGE CHECKPOINT GENE *HUS1* IN RESPONDING TO ENDOGENOUS AND EXOGENOUS STRESSES IN VIVO

Gabriel Balmus, D.V.M., Ph.D.
Cornell University 2013

The DNA damage response (DDR) represents the primary line of defense against exogenous and endogenous genotoxic agents that threaten the stability of our genomes. The ATM and ATR pathways are central to the response to DNA-damage and their understanding can bring important information in the fight against inborn disease and cancer.

While the roles for the ATM pathway in *DDR* are well understood, the lack of a model organism for the ATR pathway has impeded its understanding. Here I show how we use *Hus1*, a component of the RAD9-RAD1-HUS1 heterotrimeric clamp and a vital member of the ATR pathway, to deregulate the ATR pathway and dissect its importance in development and disease. This was done by engineering in mice a *Hus1* allelic series by combining the wild-type ($Hus1^{+}$) with a hypomorphic ($Hus1^{neo}$) or null ($Hus1^{-/-}$) alleles. As opposed to the germline constitutive deletion that leads to embryonic lethality, *Hus1* hypomorphic mice are born at expected frequencies and show no overt phenotype but have increased levels of genomic instability. Thus they have enough *Hus1* to deal with physiologic stress and could be used for our research.

To investigate the *in vivo* physiologic relationship between the ATM and ATR pathways I crossed the *Hus1* allelic series on an *Atm* null background and showed that the interaction between the two pathways is critical for normal development. When the two pathways are deregulated simultaneously a synthetic lethal interaction is created. While part of the *Hus1*/*Atm* double mutant mice die during development due an apparent incapability to deal with replication stress, the survivors suffer from developmental defects including dwarfism and skeletal defects. To further understand the interplay between these two pathways in response to genotoxins *Hus1* single mutant and *Hus1*/*Atm* double mutant mice were subjected to specific genotoxin treatments. This analysis showed that in adult tissues there is a clear separation of function between the ATM and ATR pathways, with ATM being the main responder to DNA breaks while the ATR pathway responds mainly to replication stress such as that caused by mitomycin C. In summary this thesis brings important new information about the relationship between the two main DDR response pathways leaded by ATM and ATR and substantiates their joint role in development and disease. Moreover we now have a better understanding of how these interactions can be used for creating better therapies.

BIOGRAPHICAL SKETCH

Gabriel Balmus was born on August 15, 1980 in Targu Neamt, Romania. In 1999 he graduated from „Stefan cel Mare" National College in Targu Neamt, Neamt, Romania and in 2000 entered the University of Agricultural Studies and Veterinary Medicine „Ion Ionescu de la Brad", Iasi, Romania to study veterinary medicine. Here he started to be involved in research under the guidance of Prof. Dr. Marius P. Cirlan working on a mouse model of neonatal jaundice. His research effort was acknowledged in 2003 when he received an Erasmus European Union Scholarship at University of Studies "Federico II", Naples, Italy where in the Laboratory of Prof. Dr. Dino Di Beradino participated to the description of the alpaca (*Lama pacos*) karyotype. In 2004 he was admitted to the Welcome Trust Fundamentals of Veterinary Science Summer School at Cambridge University, Cambridge, United Kingdom where in the Laboratory of Prof. Dr. Malcolm Ferguson-Smith at the Cambridge Center of Comparative Genomics started to work on describing the camel (*Camelus dromedarius*) karyotype. He followed up his work at Cambridge Center of Comparative Genomics during 2005 and 2006 to finish his work on describing the Artiodactyl ancestral karyotype. During this time he also participated to the karyotype description of the common shrew (*Sorex araneus*). In 2006 he was awarded the title of Doctor in Veterinary Medicine from University of Agricultural Studies and Veterinary Medicine „Ion Ionescu de la Brad", Iasi, Romania. Gabriel then moved to Ithaca where he joined the Laboratory of Dr. Robert S. Weiss as a postdoctoral associate. In 2007 he

started his Ph.D. studies in the field of Molecular and Integrative Physiology under the guidance of Dr. Robert S. Weiss. He is studying the cooperative roles of the *Hus1* and *Atm* genes in genome maintenance and development.

I lovingly dedicate this thesis to my wife Daniela Balmus, who supported me each step of the way.

ACKNOWLEDGEMENTS

I would like to acknowledge the many people who have facilitated my work and supported my efforts throughout graduate school. First, I would like to thank my advisor Dr. Robert S. Weiss for the trust he invested in me. Through his guidance, patience and professionalism he has been a real inspiration, a mentor. Moreover, he has helped me develop the technical and intellectual skills needed to become an independent scientist.

I would also like to acknowledge my committee members, Dr. Eric Alani, Dr. John Schimenti and Dr. Alexander Nikitin. Their expertise and encouragements were critical for my professional development.

Especially I want to thank the Weiss lab members present and past. Min Zhu for starting the *Hus1/Atm* project. Jennifer Page, Xia Xu and Stephanie Yazinsky for they have always helped me in my day to day endeavors. I would like to especially thank former undergraduates Sucheta Mukerije and Josette Pierre as well as current undergraduate Aaron Oswald for their help with my projects. I want to thank all current lab members Minxing Li, Pei Xin Lim, Dr. Erin K. Daugherity, Dr. Amy Lyndaker, Dr. Kelly Hume, Jack Stupinsky, Claire Anderson and Tim Pierpont for their suggestions, helpful discussions and friendship.

I would also like to acknowledge my former mentor Prof. Dr. Marius Cirlan who has played a major contribution to my career. He has always been close to me and encouraged me each step of the way.

Finally, I would like to acknowledge the unrelenting support and love of my family especially to my wife Daniela who has made it all possible.

TABLE OF CONTENTS

LIST OF FIGURES

LIST OF TABLES

CHAPTER 1

LITERATURE REVIEW

1.1 **DNA damage response**

Our genomes are exposed daily to tens of thousands of DNA lesions that can impair normal cellular processes and can eventually lead to disease and death. DNA-damaging agents are both exogenous and endogenous in nature and can cause a variety of DNA lesions, from single base deletions to single and double stranded DNA breaks (SSBs; DSBs) (Jackson and Bartek 2009). No matter the origin and type of lesions, in order to maintain homeostasis, replication fidelity, and impede cancer formation, eukaryotic cells have to neutralize these existential threats; the necessary response to damage is repair. However, if the injuries overwhelm the repair mechanisms viable alternatives are senescence or programmed cell death (Branzei and Foiani 2008). The DNA damage response (DDR) encompasses a signal transduction network that senses these lesions and triggers a series of posttranslational and transcriptional modifications that direct cell fate (Shiloh 2003).

Figure 1.1 Simplified view of the roles DNA-PK, ATM and ATR in DDR. The ATM and DNA-PK pathways respond primarily to dsDNA lesions. The ATR pathway responds to ssDNA lesions, and requires the RAD9-RAD1-HUS1 (9-1-1) complex for efficient phosphorylation of downstream effector CHK1. There is significant crosstalk between these pathways, and together they signal for cell cycle arrest, DNA repair, apoptosis, and fork stabilization in response to DNA damage.

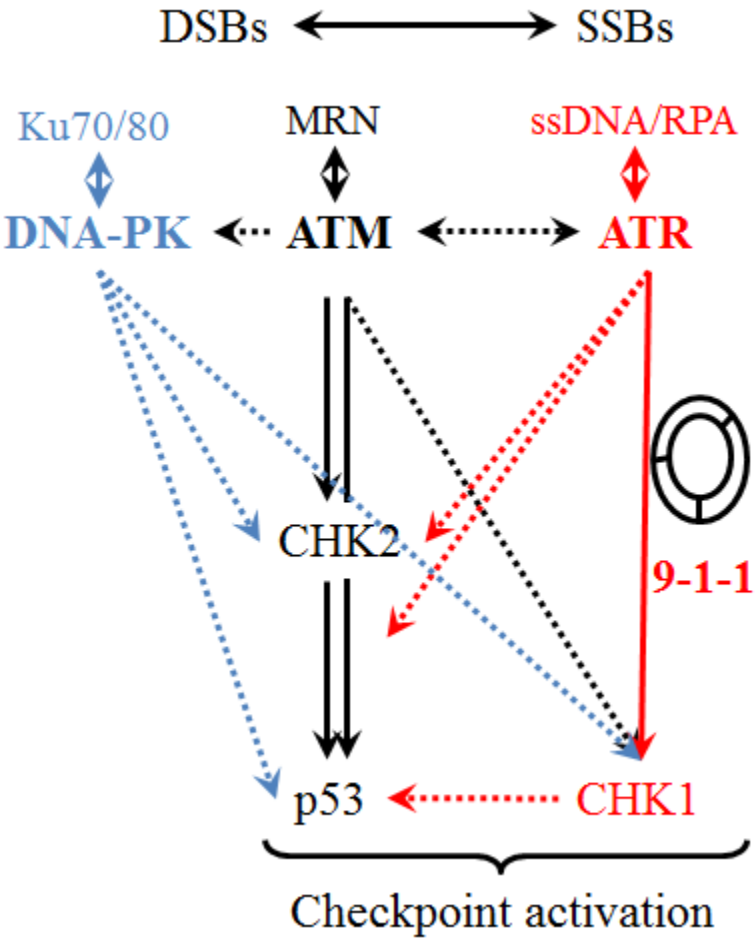
DSBs
SSBs
Ku70/80
MRN
ssDNA/RPA
DNA-PK
ATM
ATR
CHK2
9-1-1
p53
CHK1
Checkpoint activation

Table 1.1 Common DNA-damaging therapeutic agents and their consequences

Cancer treatment	Damaging agent	Lesion	Repair pathawy
Radiotherapy and radiomimetics	IR; Oxygen radicals; Bleomycin	SSBs; DSBs; base damage	Base excision repair (BER)(Fortini and Dogliotti 2007) Homologous recombination – HR Non-homologous end joining - NHEJ(O'Driscoll and Jeggo 2006)
Monofunctional alkylators	Alkylsulphonates; Nitrosourea compounds; Temozolomide	Base damage Bulky adducts Replication lesions	BER; Nucleotide-excision repair (NER)(Hoeijmakers 2001); Translesion synthesis (TLS)(Loeb and Monnat 2008; Raschle, Knipscheer et al. 2008); Fanconi anaemia repair pathway (FA); Mismatch repair (MMR)(Li 2008); RecQ-mediated repair (Rec-Q)
Bifunctional alkylators	Nitrogen mustard Mitomycin C Cisplatin	Double-strand breaks; DNA crosslinks; Bulky adducts	HR; FA; NER; Rec-Q; TLS
Antimetabolites	5-Fluorouracil (5FU) Thiopurines Folate analogues	Replication lesions; Base damage	BER
Topoisomerase inhibitors	Camptothecins Etoposide (VP16)	SSBs; DSBs; Replication lesions	Rec-Q; HR; FA; NHEJ
Replication inhibitors	Aphidicolin Hydroxyurea	Replication lesions; DSBs	HR; FA; NHEJ

Indispensable to DDR are the cell cycle checkpoints that recognize the damage and coordinate the ensuing response with the progression of the cell cycle. The cell cycle checkpoints are conserved from yeast to humans and have as central players the ATM and ATR phosphatidylinositol-3 kinase related kinase (PIKK) family (Abraham 2001). Cells that experience DNA damage during the first phase of the cell cycle (G1) activate the G1-checkpoint primarily *via* an ATM dependent mechanism (Abraham 2001; Branzei and Foiani 2008). Once activated, ATM phosphorylates p53 directly or indirectly (*via* CHK2) to upregulate the expression of the p21 cyclin-dependent kinase inhibitor and induces cell cycle arrest and promote repair.

The ATR pathway plays redundant roles in imposing this checkpoint since activation of p53 is reinforced and maintained by ATR. Once cells enter S-phase they rely mainly on the ATR pathway for imposing the intra-S checkpoint. During this phase replication stress can induce an array of DNA modifications that are kept on check by the ATR pathway. Complete and accurate DNA replication is critical to prevent mitotic catastrophe that can results from incomplete or inaccurate DNA replication. Impairment of the ATR pathway is incompatible with viability. When activated, the checkpoint leads to the proteosome-mediated degradation of CDC25A thus the failure to maintain activation of cyclin·cdk2 complexes stimulating inhibition of DNA synthesis and DNA repair through high-fidelity homologous recombination. When the pathway fails and DSBs are formed the ATM kinase participates to

reinforcing the checkpoint by phosphorylating CHK2 kinase (Abraham 2001; Branzei and Foiani 2008; Branzei and Foiani 2010).

On the other hand at the final stage of the cell cycle the G2-checkpoint relies in similar manner on ATM and ATR. When damage is produced just before the completion of S-phase, the G2-checkpoint is triggered primarily by ATR. When damage affects directly the G2-phase, the checkpoint relies mainly on ATM. No matter when or how it is activated the G2-checkpoint is imposed *via* the CDC25C phosphatase, which prevents the activation of the mitotic progression (Abraham 2001). Furthermore, another member of the PIKK protein family, DNA-PK, is also involved in DSBs damage recognition and repair through non-homologous end joining (NHEJ), but its involvement in checkpoint signaling remains elusive (Collis, DeWeese et al. 2005) (Figure 1.1). The deregulation of these pathways results in increased genomic instability (GIN) that can lead to severe human disorders including cancer. Thus, a better understanding of their joint role in DDR and their link to other homeostatic and developmental pathways represents an important step in creating molecular maps critical for establishing new therapeutic strategies.

1.2 The ATM pathway.

Following ionizing radiation (IR), ATM initiates a DDR pathway that senses DSBs formation and signals to downstream effectors to activate cell cycle

checkpoints. The role of ATM is not restricted to signaling toxic DSBs lesions, as it also plays important roles in the repair of physiological DSBs during V(D)J recombination (Lavin 2008) and oxidative stress response (Skinner 2010).

In unperturbed cells, ATM exists as a dormant dimer or high-order multimer that together with the MRE11-RAD50-NBS1 (MRN) complex monitors DNA integrity. Once DSBs are formed, the MRN complex tethers the DNA loose ends and concomitantly catalyses the activation of ATM, which undergoes rapid auto-phosphorylation at Ser1981 in humans (1987 in mouse) and phosphorylates the histone H2A variant H2AX (Bakkenist and Kastan 2003; Stracker and Petrini 2011). Phospho-H2AX (γ-H2AX) generates a chromatin microenvironment that allows and promotes the recruitment of other signaling molecules such as MDC1, 53BP1, and BRCA1, creating DNA-damage foci that act as a platform for the accumulation of damage-response and repair factors (Bonner, Redon et al. 2008). Subsequently, ATM signals to the checkpoint machinery by phosphorylating checkpoint kinase 2 (CHK2) and the transcription factor and tumor suppressor p53. Once activated p53 regulates the expression of proteins involved in regulating cell cycle progression such as the cyclin dependent kinase inhibitor p21 that arrests the cell cycle progression (Abraham, Zhou et al. 2001). However, if the repair machinery cannot resolve the damage in a timely manner the ATM pathway will cause permanent arrest

(senescence) or will induce cell death by activating the apoptotic pathway via p53-dependent or independent mechanisms (Cotter 2009).

In addition to signaling to the cell cycle checkpoint machinery, ATM is involved in DNA repair, accounting for 15-25% of the DSBs repair (Goodarzi, Noon et al. 2008). The ATM-dependent repair dynamics depend both on the phase of the cell cycle and the chromatin condensation status. Even if in the last decade the understanding of the ATM pathway has benefited from a plethora of new findings, there are still many unknowns about ATM activation and its role in signaling and repair (Lavin 2008).

1.3 ATM pathway and human pathology

In humans, mutations in the *Atm* gene lead to Ataxia-telangiectasia (A-T, OMIM #208900), an autosomal recessive syndrome characterized by early onset of cerebellar ataxia, oculocutaneous telangiectasia, immunodeficiency, sterility, chromosomal instability, increased sensitivity to IR and high risk of developing lymphoid tumors (Lavin and Shiloh 1997). Heterozygous carriers of AT mutations have been strongly linked to breast and other cancers (Angele, Romestaing et al. 2003; Thorstenson, Roxas et al. 2003; Renwick, Thompson et al. 2006). The cause of death in A-T patients is respiratory system disease or cancer (McKinnon and Caldecott 2007; McKinnon 2012).

1.3.1 ATM pathway mouse models

To better understand the role of ATM in pathology, several laboratories have created mouse models for ATM pathway impairment. *Atm* knockout mice (Barlow, Hirotsune et al. 1996; Elson, Wang et al. 1996; Xu and Baltimore 1996) and knockout mice of other members of the ATM pathway such as *Chk2, p21* or *p53* (Donehower, Harvey et al. 1992; Deng, Zhang et al. 1995; Takai, Naka et al. 2002) are viable. $Atm^{-/-}$ mice have a reduced body weight, increased GIN, hypersensitivity to IR and die between 3 to 6 months of age because of thymic lymphomas. In contrast to A-T patients, $Atm^{-/-}$ mice present mild, if any, neurological abnormalities; $Atm^{+/-}$ mice have an increased sensitivity to IR but no cancer predisposition (Barlow, Hirotsune et al. 1996; Elson, Wang et al. 1996; Xu, Ashley et al. 1996). In mice and humans failure to repair DSBs can lead to chromosomal rearrangements or translocations and thus represent a high risk of oncogene activation thus most of the phenotypes associated with A-T are due, directly or indirectly, to the incapability to respond to DSBs (Lavin 2008).

1.4 The ATR pathway

The ATR pathway responds to a variety of stresses including exogenous agents such as UV-light and endogenous replication stress (Cimprich and Cortez 2008). Once the replication machinery encounters such lesions, the polymerase stalls

and uncouples from the replicative helicase that keeps unwinding the DNA, leaving behind large stretches of single stranded DNA (ssDNA) that are immediately recognized and coated by the ssDNA-binding trimeric protein replication protein A (RPA). The ssDNA/RPA complex formation is the signaling event prerequisite for damage recognition and ATR activation.

ATR damage recognition depends on its permanent partner the ATR interacting protein (ATRIP) that recognizes and binds RPA (Zou and Elledge 2003) and its colocalization with the RAD9-RAD1-HUS1 (9-1-1) complex. The 9-1-1 complex, a proliferating cell nuclear antigen (PCNA) like clamp, is independently loaded onto the 5`DNA end adjacent to a stretch of ssDNA/RPA by the RAD17-RFC clamp loader in an ATP dependent manner (Menoyo, Alazzouzi et al. 2001) and brings together through its RAD9 tail the DNA topoisomerase II-binding protein-1 (TopBP1) (Delacroix, Wagner et al. 2007) and the RAD9-RAD1-HUS1 interacting nuclear orphan (RHINO)(Cotta-Ramusino, McDonald et al. 2011) that facilitate ATR activation (Figure 1.2).

Once activated, ATR phosphorylates checkpoint kinase 1 (CHK1) that stabilize the fork, inhibits new origin firing and initiates the cell cycle checkpoint allowing for damage repair (Cimprich and Cortez 2008). ATR is critical for cell survival (Brown and Baltimore 2000) and functions as master regulator of the intra-S

Figure 1.2. Simplified model of ATR activation at stalled replication forks. ATR activation begins when RPA binds to and stabilizes ssDNA. RPA coated single stranded DNA recruits the ATR-ATRIP complex to the site of damage. Independently, the RAD9-HUS1-RAD1 heterotrimeric clamp complex is loaded at recessed 5` DNA ends; RHINO acts to recruit and facilitate TopBP1 to the phospho-tail of RAD9 thus activating ATR. Once activated ATR phosphorylates CHK1 and other targets to prevent cell cycle progression and stop new origin firing, promote fork stability to allow for DNA repair and when damage is repaired promote fork restart.

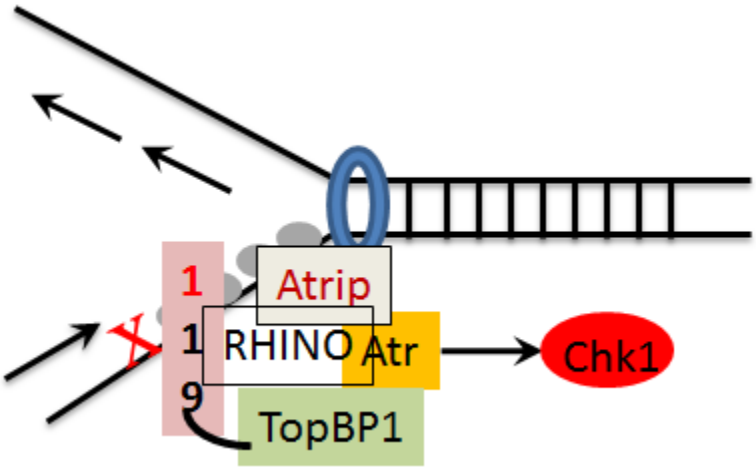
1
1
9
Atrip
RHINO
Atr
Chk1
TopBP1

cell cycle checkpoint, although its role during G1/S and G2/M checkpoints must not be disregarded (Branzei and Foiani 2008). Together, these data demonstrate that failure to initiate the ATR pathway results in damage accumulation and successive increase in genomic instability causing devastating cellular phenotypes (Brown and Baltimore 2000).

1.4.1 HUS1 is an essential component of the ATR pathway

Indispensable for the ATR pathway is the RAD9-RAD1- HUS1 complex (9-1-1). The complex was discovered screen for genes important for the response to hydroxyurea (HU) induced DNA damage and that would induce cell cycle arrest in yeast (Enoch, Carr et al. 1992). The 9-1-1 components are conserved from yeast to humans and form a clamp-like complex critical for the response to DNA damage (Volkmer and Karnitz 1999). Later it was demonstrated that 9-1-1 is the structural ortholog PCNA, a homotrimeric sliding clamp that tethers DNA polymerase (Griffith, Lindsey-Boltz et al. 2002). Analogous to PCNA that requires the replication factor C (RFC) for its loading, the 9-1-1 is loaded by RAD17-RFC complex. These observations proposed similar roles and structures for these complexes (Venclovas and Thelen 2000).

Recent crystallography data confirmed the structural hypothesis (Dore, Kilkenny et al. 2009; Sohn and Cho 2009; Xu, Bai et al. 2009) but proposed that

while PCNA and 9-1-1 share similarities they also perform distinct functions. Though both PCNA and 9-1-1 are loaded onto ssDNA, PCNA is loaded during replication at the primer-template junctions (recessed 3' end) and slides over the double stranded DNA (dsDNA). On the other hand 9-1-1 is loaded onto dsDNA at recessed 5' ends at sites of DNA damage and is expected to slide along the phosphate backbone of the DNA. Crystal structure data suggests though that the 9-1-1 complex directly interacts with DNA rather than slides off linear DNA (Sohn and Cho 2009). Thus PCNA acts as a processivity factor and moves along with the replication machinery tethering pol δ and ε, while 9-1-1 is docks at sites of DNA damage or where forks stall and acts as a landing platform for additional checkpoint and repair proteins (Shiotani and Zou 2009).

Although initial research showed that 9-1-1 and PCNA can be ubiquitinated (Majka and Burgers 2004; Fu, Zhu et al. 2008; Tsutakawa, Van Wynsberghe et al. 2011) to recruit DNA-repair factors like translesion synthesis polymerase or that they can stimulate BER (Jansen, Fousteri et al. 2007), recent evidence disputes this idea for 9-1-1 (Davies, Neiss et al. 2010; Inagaki, Sleddens-Linkels et al. 2011).

All the 9-1-1 subunits, including HUS1, are vital for structural integrity of the complex and are considered critical members of the ATR pathway (Weiss, Enoch et al. 2000; Hopkins, Auerbach et al. 2004; Han, Hu et al. 2010). In mouse, the *Hus1*

gene consists of nine exons that once transcribed give rise to a 4.2 kb cDNA transcript that is translated into to a 32-kDa HUS1 protein. HUS1 is expressed in most adult tissues and within the complex functions to promote genotoxin induced ATR activation (Weiss, Kostrub et al. 1999). Constitutive *Hus1* knock-out in mice results in mid-gestational embryonic lethality caused by widespread apoptosis (Weiss, Enoch et al. 2000). *Hus1* null cells accumulate genome damage, show increased apoptosis, and fail to proliferate, however *p53* or *p21* deletion permits them to grow (Weiss, Enoch et al. 2000; Zhu and Weiss 2007). *Hus1* is essential for fragile site stability, since in *Hus1* null cells spontaneous chromosomal abnormalities take place preferentially at common fragile sites *via* a p53 independent mechanism (Zhu and Weiss 2007). Upon genotoxic stress $Hus1^{-/-}p21^{-/-}$ cells are incapable to activate the ATR pathway (Weiss, Matsuoka et al. 2002) and display a severe intra-S checkpoint defect (Weiss, Leder et al. 2003). Since loss of HUS1 leads to increased GIN and is not compatible with life, the roles for the 9-1-1 complex *in-vivo* in both physiologic and pathologic circumstances are not fully understood.

9-1-1 has also been shown to be an integral component of the telomeres. RAD9 preserves telomere integrity and prevents chromosomal fusions in mouse and human cells (Verdun and Karlseder 2006). In both humans and mice *Hus1*-deficient MEFs and thymocytes show severe telomeric shortening. Moreover, in cell lysates, the 9-1-1 complex was demonstrated to interact with catalytically competent

telomerase and act as a positive regulator of its DNA polymerase activity providing a mechanistic link between the activity of DNA-damage-checkpoint proteins and the telomere-maintenance machinery (Francia, Weiss et al. 2006; Francia, Weiss et al. 2007)

1.4.2 HUS1 can act independently of ATR to promote repair

Cell culture systems have shown that 9-1-1 is directly involved in BER. The 9-1-1 complex interacts and stimulates the activity of the important BER members apurinic/apyrimidinic endonuclease 1 (APE 1) and DNA ligase I (Helt, Wang et al. 2005; Wang, Lindsey-Boltz et al. 2006) and that acts as a damage-specific activator of flap endonuclease 1 (FEN1) that cleaves the flap remaining following DNA repair (Friedrich-Heineken, Toueille et al. 2005 1115). Moreover, it was proposed that 9-1-1 also acts in BER by attracting POL-β to DNA damage sites, linking the checkpoint response and DNA repair (Toueille, El-Andaloussi et al. 2004). By interacting with the MYH (MutY glycosylase homologue), 9-1-1 can increase replication fidelity by removing adenines or 2-hydroxyadenine misincorporated opposite 8-oxo-G (7,8-dihydro-8-oxo-guanine)(Shi, Chang et al. 2006). This indicates that the complex is directly involved in long patch BER (LP-BER) and together with its independent role in ATR activation realizes a link between DNA damage checkpoint and repair through BER.

Since PCNA interacts with polymerase δ and ε as well as with some translesion synthesis polymerases the 9-1-1 complex has been examined for similar interactions (Jansen, Fousteri et al. 2007; Navadgi-Patil and Burgers 2009). To this extent HUS1, has been shown to physically interact with POL-K, a translesion synthesis factor (Kai and Wang 2003), and influence POL-ζ mutagenesis processes (Sabbioneda, Minesinger et al. 2005). Additionally, the 9-1-1 complex has been shown to act as a member of mismatch repair pathway following treatment with the DNA methylating agent N-methyl-N'-nitro-N-nitrosoguanidine (MNNG) when it physically interacts with MSH2, MSH3, and MSH6 mismatch recognition factors (Bai, Madabushi et al. 2010). Undoubtedly, the 9-1-1 complex is involved in a broad range of repair processes coordinating checkpoint signaling and repair through mechanisms the extent of which are not yet completely understood.

1.4.3 ATR pathway and human pathology

In humans, impairment of the ATR pathway leads to Seckel syndrome (ATR-SS) (OMIM #210600) an autosomal recessive disorder characterized by proportionate dwarfism, severe microcephaly, craniofacial abnormalities and mental retardation (Alderton, Joenje et al. 2004; O'Driscoll, Dobyns et al. 2007). Moreover subsets of these patients termed Atr-SS have an ATR splicing mutation that leads to hypomorphic *ATR* expression (O'Driscoll and Jeggo 2003).

Apart developmental defects, since GIN is a classic hallmark of cancer and defects in ATR result in chromosomal aberrations it is not unexpected that mutations of members of the ATR pathway have also been implicated in cancer development. Increased mutation frequencies in ATR and CHK1, have been found to correlate significantly with advanced tumor grade (Vassileva, Millar et al. 2002). Truncating mutations in ATR exon 10 of have been described in cancers exhibiting microsatellite instability (Menoyo, Alazzouzi et al. 2001; Lewis, Mullany et al. 2005). Additionally, truncating *ATR* mutations present in endometrial cancers are associated with aggressiveness as evidenced by reduced disease-free survival (Zighelboim, Schmidt et al. 2009). In colon cancers *ATR* status was not associated with tumor stage; however ATR mutations were associated with a trend toward improved disease-free survival suggesting that *ATR* mutations may affect clinical behavior and response to therapy in colon cancers (Lewis, Bakkum-Gamez et al. 2007). These differences in prognosis may be due to tissue-specific variances in ATR requirement, since lower levels of RAD9 in some prostate cancers acts to prevent tumor development (Wang, Hsu et al. 2004). The role of ATR pathway in tumor biology remains to be established as, to date, complete loss of any component of the ATR pathway has not been found in any human tumor, endorsing the ATR role as tumor suppressor.

1.4.4 ATR pathway mouse models

Unlike the ATM pathway the members of the ATR pathway are vital for survival. ATR (Brown and Baltimore 2000; de Klein, Muijtjens et al. 2000) , RAD17 (Budzowska, Jaspers et al. 2004), RAD9 (Hopkins, Auerbach et al. 2004), RAD1 (Han, Hu et al. 2010), HUS1(Weiss, Enoch et al. 2000), or CHK1 (Liu, Guntuku et al. 2000; Takai, Tominaga et al. 2000) constitutive knockout mice all die during early embryogenesis.

In order to understand the requirement for ATR in adults and circumvent this lethality, conditional mouse models have been created. Tamoxifen inducible ATR knockout in adult mice caused a dramatic loss of tissue-specific stem and progenitor cell populations resulting in an overt progeroid syndrome; ATR has been shown to be essential for highly proliferative tissues while no structural or degenerative phenotypes were observed in postmitotic organs such as the brain (Ruzankina, Pinzon-Guzman et al. 2007). This *Atr* mosaic mouse model suggested that most of the phenotypic characteristics of the Atr-SS are due *Atr* insufficiency during embryonic development. Surprisingly, modulating the ATR-SS A2101G synonymous mutation in mouse resulted in no phenotype (Ragland, Arlt et al. 2009); however, when the entire Atr human sequence incorporating the splicing defect was engineered, an *Atr* hypomorphic, Seckel-like mouse was created ($Atr^{s/s}$)(Murga,

Bunting et al. 2009). Surviving *Atr*$^{s/s}$ mice recapitulated the human Atr-SS and showed dwarfism, craniofacial abnormalities, brain defects and pancytopenia. Unlike human patients *Atr*$^{s/s}$ mice presented severe ageing phenotypes that caused them to die by six months of age. *Atr*$^{s/s}$ embryos showed increased level of γ-H2AX and apoptosis accumulation while the presence of GIN was not tested in the adults. The authors proposed that all the adult phenotypes were the result of intrauterine programming (O'Driscoll 2009; Fernandez-Capetillo 2010).

The caustic phenotypes associated with constitutive ATR pathway deregulation impeded the functional analysis of its role in genotoxic sensitivity and tumor development. Heterozygous mice were used for genetic analysis. By crossing the *Atr*$^{+/-}$ mice on a mismatch repair deficient background it was observed that *Atr*$^{+/-}$ */Mlh1*$^{-/-}$ double mutant mice show a haploinsufficient tumor suppressor function and are highly prone to embryonic lethality. These data suggests that MMR proteins functionally interact with ATR during the cellular response to genotoxic stress (Fang, Tsao et al. 2004; Lee, Jin et al. 2012). Application of the 7,12-dimethylbenzanthracene (DMBA) carcinogen onto the skin of animals with conditional *Rad9* deletion in the skin caused earlier onset of tumors and senile skin plaques, showing that RAD9 is critical for the prevention of skin tumors in mice (Hu, Liu et al. 2008). *Chk1*$^{+/-}$ mice show increased number of S phase arrested cells due to increased spontaneous DNA damage resulting in phenotypes that contribute

to tumorigenesis (Lam, Liu et al. 2004). Additionally, *Chk1* heterozygosity modestly accelerates the tumorigenesis seen in *Wnt1* transgenic mice, supporting the haploinsufficient tumor suppressor role of CHK1 (Liu, Guntuku et al. 2000). Taken together, these reports suggest that in mice components of the ATR pathway act as important players in tumor biology.

Our laboratory created a conditional *Hus1* allele ($Hus1^{flox}$) where exons two and three are flanked by loxP sites. When Cre was express in various tissues the conditional knockout mice were produced at unexpectedly low frequency and showed limited inactivation of the conditional allele, suggesting that *Hus1*-deficient cells were at a strong selective disadvantage in adult animals. This was not the case in the lung and mammary gland, highlighting varying requirements for *Hus1* in different tissues (Levitt, Liu et al. 2005). We ultimately made an allelic series featuring incrementally reduced *Hus1* function by using the hypomorphic allele $Hus1^{neo}$ in combination with null ($Hus1^{\Delta 1}$) or wild-type ($Hus1^{+}$) alleles (Figure 1.3). $Hus1^{neo/\Delta 1}$ mice had the lowest *Hus1* expression in the series and showed increased genomic instability and genotoxin hypersensitivity. These mice have enough *Hus1* to maintain cellular homeostasis, but not enough to respond to stress. Thus, a viable mouse model defective for the ATR pathway was created (Levitt, Zhu et al. 2007).

Figure 1.3. Alleles used to construct the Hus1 allelic series, which expresses decremental Hus1 levels. (A) Schematic representation of the *Hus1* alleles generated in systems for constitutive and conditional *Hus1* inactivation. (B) Northern blot analysis of duplicate samples of primary MEF cultures of the indicated genotypes hybridized with a ^{32}P-labeled *Hus1* or *Gapdh* cDNA probe.

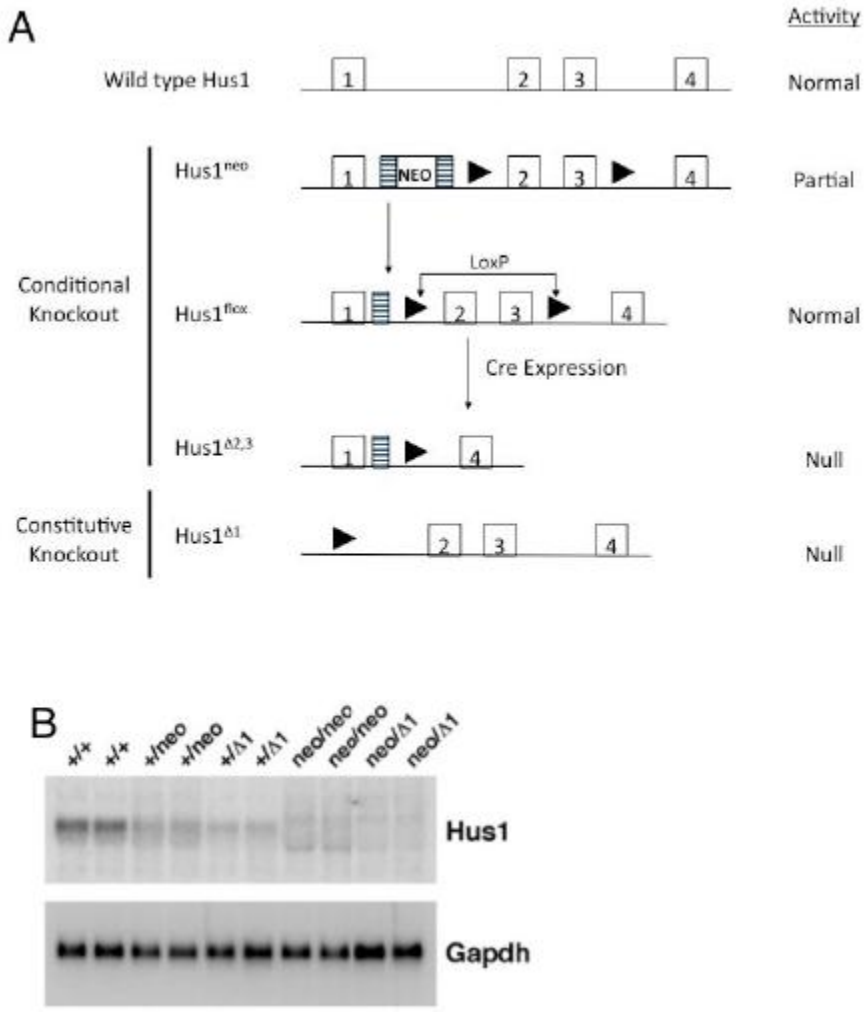

Modified From *P. Levitt et al. (2007) Mol.Cell. Biol. 27(6): 2189-2201*

1.5 The DNA-PK pathway

DSBs are the most harmful lesions that genomes can experience. Consequently cells have evolved multiple repair enzymes that in association with the cell cycle checkpoints promote repair and allow survival. Central to DSBs repair are two essentially distinct pathways: HR and NHEJ. Although the exact mechanisms that dictate the use of one over the other are not completely known the cell cycle stage has unambiguous influence on this choice (Hoeijmakers 2001; Branzei and Foiani 2008).

Under control of the RAD52 epistasis group, HR is an error-free repair mechanism that acts during the S and G2 phases of the cell cycle and allows for precise repair of the damage using the sister chromatid as a template (Moynahan and Jasin 2010). On the other hand NHEJ is an error-prone repair mechanism that acts in the G1/G0 and M phases of the cell cycle and during the development of B- and T-lymphocytes during V(D)J recombination (Weterings and Chen 2008) and class switch recombination (CSR) (Cook, Oganesian et al. 2003). Although inaccurate, NHEJ is involved in the repair of most DSBs that an adult organism experiences and is under the control of the DNA-PK, a PIKKs protein kinase containing a regulatory (KU70/80) and a catalytic subunit (DNA-PKcs) (Collis, DeWeese et al. 2005). NHEJ integrates the recognition, tethering and processing of the broken DNA-ends

with ligation. DNA-PK plays an important sheltering role at telomeres(de Lange 2002) and additionally it has been reported to phosphorylate, *in-vitro* and *in-vivo,* numerous protein substrates involved both in NHEJ and other cellular processes(Meek, Dang et al. 2008).

Humans deficient for NHEJ factors develop severe combined immunodeficiency (SCID) characterized by opportunistic infections, chronic diarrhea and failure to thrive. A subset of these patients are radiosensitive (RS-SCID) and have a greater risk of developing lymphomas (McKinnon and Caldecott 2007). Remarkable, unlike in humans, the spontaneous genetic forms of SCID in animals are DNA-PKcs mutations (mice, dogs and horses). DNA-PK knock-out mice models are viable, fertile, show increased IR sensitivity, a SCID-like phenotype and variable risk of developing lymphomas (Smith and Jackson 1999). One proposed theory is that in human DNA-PK plays additional roles that are critical for survival. This hypothesis is reinforced by the fact that primate cells express almost 50 folds more DNA-PK than rodents whereas all the other NHEJ factors are expressed at lower levels (Meek, Dang et al. 2008). Additionally, due to the identification of DNA-PK upregulation in several radio-protected cancers, it has been proposed that DNA-PK inhibitors have a great potential in enhancing the sensitivity of cancer cell to therapy. Since then several highly specific DNA-PK inhibitors have been developed and are currently tested for their efficacy (Collis, DeWeese et al. 2005).

Table 1.2. Mouse models for ATM, ATR and DNA-PK pathways deficiency

Mouse model	Phenotype
***Atm*$^{-/-}$**	Reduced body size; IR sensitivity; increased GIN ; 100% die with T-cell lymphoma (3-6 months of age)
***Chk2*$^{-/-}$**	Viable; fertile; radioresistant; apoptotic defect; increased tumor predisposition
***p53*$^{-/-}$**	Early-onset tumor incidence ; increased GIN; 100% die
***Atr*$^{-/-}$**	Embryonic lethal (< 7.5dpc)
***Atr*$^{s/s}$**	Hypomorphic; dwarfism (Igf1 dependent); senescence, craniofacial defects, brain defects; increased GIN and apoptosis at embryonic level
***Hus1*$^{-/-}$**	Embryonic lethal (9.5dpc)
***Rad1*$^{-/-}$**	Embryonic lethal (9.5dpc)
***Rad9*$^{-/-}$**	Embryonic lethal (9.5dpc)
***Chk1*$^{-/-}$**	Embryonic lethal(before implantation)
***DNA-PK*$^{-/-}$**	Immunodeficiency; increased GIN and lymphoma risk;
***Atm*$^{-/-}$*Chk2*$^{-/-}$**	p53$^{-/-}$ like phenotype in thymocites; Atm$^{-/-}$ like tumor free survival
***Atm*$^{-/-}$*p53*$^{-/-}$**	Significant increased tumor formation
***Chk2*$^{-/-}$*p53*$^{-/-}$**	p53$^{-/-}$-like phenotype
***Chk1*$^{-/-}$*p53*$^{-/-}$**	Embryonic lethal (before implantation)
***Atr*$^{s/s}$*p53*$^{-/-}$**	Rarely born; severe senescence; 100% die by 2 months of age; increased GI in MEFs
***Atm*$^{-/-}$*Atr*$^{s/s}$**	Embryonic lethal ; no data reported (no description given; no MEFs generated)
***Atm*$^{-/-}$*Hus1*$^{neo/ex}$**	Embryonic lethal (10.5dpc)
***Atm*$^{-/-}$*Hus1*$^{neo/neo}$**	Dwarfism (Igf1 independent); more than additive GIN; craniofacial abnormalities;100% T-cell lymphoma (Atm$^{-/-}$ like)
***p53*$^{-/-}$*Hus1*$^{neo/ex}$**	p53$^{-/-}$ like phenotype (Weiss Lab - unpublished)
***Atm*$^{-/-}$*DNA-PK*$^{-/-}$**	Embryonic lethal (< 11.5dpc)
***DNA-PK*$^{-/-}$*Chk2*$^{-/-}$**	Significant decreased life span due to infections; no tumors
***DNA-PK*$^{-/-}$*p53*$^{-/-}$**	Significant increased tumor formation (lymphoma)

For extensive description consult (Donehower, Harvey et al. 1992; Barlow, Hirotsune et al. 1996; Elson, Wang et al. 1996; Xu and Baltimore 1996; Brown and Baltimore 2000; Weiss, Enoch et al. 2000; Takai, Naka et al. 2002; Gatei, Sloper et al. 2003; Levitt, Liu et al. 2005; Levitt, Zhu et al. 2007; Ruzankina, Pinzon-Guzman et al. 2007; Stracker, Morales et al. 2007; Stracker, Couto et al. 2008; Murga, Bunting et al. 2009; Balmus, Zhu et al. 2012)

1.6 Phosphatidylinositol-3 kinase related kinases crosstalk

ATM, ATR and DNA-PK are serine/threonine kinases that upon DNA-injury localize to the damaged site and initiate DDR. ATM and ATR have been historically involved in signaling to the cell cycle checkpoint whereas DNA-PK`s contribution remains controversial. Throughout the cell cycle ATM and ATR are influenced by a multitude of factors that control their overlapping and redundant involvement in initiating the G1, S and G2/M checkpoints. These factors halt cell cycle progression and make life and death decisions(Abraham, Zhou et al. 2001; Branzei and Foiani 2008).

Current molecular data shows that ATM and ATR have over 700 common substrates, targeting more than 900 phosphorylation sites(Matsuoka, Ballif et al. 2007; Cimprich and Cortez 2008). DNA-PK shares many of these substrates *in-vitro;* however, only a few have been proved to be physiological significant (Weterings and Chen 2008). Moreover, DNA-PK it is itself an ATM/ATR substrate. Until recently the ATM and ATR pathways have been thought to function in parallel. The above findings are surprising and have prompted researchers to dissect specific interactions between the ATM and ATR pathways. The first level of crosstalk takes place at the DNA-breaks themselves. ssDNA can easily yield a DSB whereas the repair of DSBs comprises an intermediary, ATM dependent resection step that creates ssDNA overhangs thus activating ATR. In addition ATM can enhance ATR activation by

phosphorylating TopBP1(Yoo, Kumagai et al. 2007) whilst ATR has been reported to directly phosphorylate ATM and activate CHK2 (Stiff, Walker et al. 2006).

Once activated ATM and ATR will phosphorylate H2AX to create a chromatin microenvironment appropriate for repair. This target is shared with DNA-PK which in their absence mediates a γ-H2AX-salvage pathway (Chanoux, Yin et al. 2009). Downstream of ATM and ATR, CHK2, CHK1 and p53 can be activated by both kinases (Gatei, Sloper et al. 2003; Antoni, Sodha et al. 2007; Balmus, Zhu et al. 2012). While the crosstalk at the level of CHK1 and CHK2 kinases is still attributed to interconversion of the DNA lesions and subsequent activation of canonical activators (Cimprich and Cortez 2008), the phosphorylation of p53(Meek 2009) by ATM, ATR, CHK2 and CHK1 has been confirmed by many studies.

The functional overlap of the ATM and ATR kinases is critical for redundancy in checkpoint signaling. As previously stated the implication of DNA-PK in activating the cell cycle surveillance apparatus is disputed and remains to be proven. The possibility of crosstalk between the DNA-PK, ATM and ATR with respect to activation of CHK1, CHK2, and p53 has been described in several instances (Cimprich and Cortez 2008). In human cancerous cell lines ATR and DNA-PK have been shown to cooperate in CHK1 dependent G2 arrest in response to specific drugs (Liu, Matsuda et al. 2008). Other reports hint to a cell type or cell phase specific requirement for these interactions. B and T cells rely more on ATM and DNA-PK and have a reduced requirement for ATR; here ATM deficiency results in a DNA-PK

dependent phosphorylation of KAP1, CHK2 and p53(Wang, Guo et al. 2000; Arlander, Greene et al. 2008; Callen, Jankovic et al. 2009). On the other hand in fibroblasts exposed to IR, DNA-PK selectively regulates p53-induced apoptosis but not cell cycle arrest (Woo, McLure et al. 1998; Araki, Fukumura et al. 1999; Jimenez, Bryntesson et al. 1999).

This pattern of specific PIKKs functional redundancy turned out to be a recurrent theme in the cell cycle checkpoint signaling field and *in-vivo* models that can be used to genetically test these interactions have been developed. Mice models for the ATM pathway are viable, show increased GIN, and are predisposed to tumor development. The DNA-PK mouse models are also viable and recapitulate the human SCID syndrome. In contrast, all members of the ATR pathway are critical for survival and *in-vivo* relevant model have long been absent. Nevertheless several labs have created mouse models hypomorphic for the ATR pathway that surprisingly showed no tumor phenotypes. With these models in hand specific genetic interaction can now be tested (Table 1.2).

The genetic experiments using the ATM pathway members confirmed the known molecular data and when ATR pathway members were crossed to an ATM deficient background the double knockouts reinforced the proposed redundancy. Although *Atm*$^{-/-}$ and *DNA-PK*$^{-/-}$ mice are viable the *Atm*/*DNA-PK* double mutants show synthetic lethality emphasizing their cooperative roles in development (Sekiguchi, Ferguson et al. 2001). This relationship is critical at the kinase level since

DNA-PK$^{-/-}$*Chk2*$^{-/-}$ mice are viable due to ATM redundancy (Guidos, Williams et al. 1996). *Atr*$^{s/s}$*p53*$^{-/-}$ mice show a severe acceleration of the *Atr*$^{s/s}$ senescence phenotype while the *Atr*$^{s/s}$*Atm*$^{-/-}$ mice were reported synthetic lethal (Murga, Bunting et al. 2009). The severe phenotypes associated with the *Atr*$^{s/s}$*p53*$^{-/-}$ and *Atr*$^{s/s}$*Atm*$^{-/-}$ mice are an impediment in understanding the physiological impact of deregulated ATM/ATR pathways and their role in checkpoint signaling and pathology.

Using the *Hus1* allelic series will allow us to better understand these interactions. Because we have a stepwise deregulation model we will most likely be able to circumvent lethality and comprehend the impact of *Atm*/*Hus1* impairment at the organism level.

1.7 Cancer therapy and the non-oncogene addiction

Cancer therapy usually involves removal of the cancer cells from the affected individual (Chabner and Roberts 2005). This can be done by surgery or the use of chemical therapy (chemotherapy) that selectively marks cancer cells for cell death. Chemotherapy in combination with surgery is to date the most common treatment, although new strategies are in place to improve patient outcome.

In general, cancer therapy takes advantage of the increased replication potential of many tumors and thus directed towards impeding cell cycle progression. Cell division can be targeted by inhibition of the mitotic spindle, inhibition of the

growth signals required for cell cycle entry or, most commonly, by exploiting the effects of DNA-damaging drugs (Table 1.1). The DDR-targeted drugs can lead to cell death either directly or following replication of damaged DNA, thus affecting highly replicating tissues. Different genotoxic agents have been tested in mouse models both for understanding the effect on different cancesr and the toxicity associated with such treatments. Common types of DNA-damage that interfere with normal cell cycle progression range from DSBs that are caused by clastogens like ionizing radiations or bleomycin (Hsiang, Lihou et al. 1989) to DNA base adducts caused by alkylating agents. The alkylating agents can be monofunctional like nitrosourea, cyclophosphamide or temozolomide (modifying single bases) (Stevens, Hickman et al. 1987; Komotar, Otten et al. 2008; Minniti, De Sanctis et al. 2008) or bifunctional like mitomycin C (an antibiotic extracted from *Streptomyces caccpitosus*) or cisplatin (crosslinking two bases creating either intra- or inter- strand-links) (Lehnert 1998; Borchiellini, Etienne-Grimaldi et al. 2012; Lord and Ashworth 2012) and pose severe treats to normal cell cycle progression. Other than direct DNA-lesions, cell cycle can be affected by inhibition of DNA synthesis using DNA polymerase inhibitors (aphidicolin) (Ikegami, Taguchi et al. 1978) or affecting dNTP production by inhibiting ribonucleotide reductase – RNR (hydroxyurea) or thymidine synthase (Bianchi, Pontis et al. 1986). Moreover, since many cancers are defective for the DDR pathways, the specific sensitivity of such cancer cells to DNA-damaging agents is enhanced.

The classical example for the use of such therapies is exemplified by the successful use of the poly(ADP-ribose) polymerase (PARP) inhibitors in certain DNA repair-deficient cancers, like breast cancer. When patients with advanced triple-negative breast cancers that have *BRCA1/2* mutations were treated with DNA-damaging chemotherapy in combination with the PARP inhibitor *iniparib*®, increased cancer cell death was promoted and this translated in prolonged patient survival compared with chemotherapy treatment alone. This success was due to the fact that while normal cells would effectively repair chemotherapeutic induced DNA damage *via* a PARP dependent mechanism, BRCA1/2-deficient cells would be unable to carry out repair, ultimately leading to cell death (Ellisen 2011).

Similar strategies could be used in the context of ATM/ATR pathways. Defects in the ATM pathway result in increased sensitivity to DSB inducing agents while deficiency in the ATR pathway leads to sensitivity to replication stress inducing agents (Abraham and Halazonetis 2012). Since these compounds were giving promising results in killing cancer cells in cell culture systems, their toxicity was assessed in animal models before human use. Wild type mice treated with a 9-10Gy whole body IR suffer from a lethal hematopoietic syndrome and die 12 to 20 days later. At doses higher than 15Gy animal succumb 7 to 12 days later to a gastrointestinal syndrome (Sinclair 1973; Takai, Naka et al. 2002; Gudkov and Komarova 2003). Consistent with the idea that the ATM pathway is the main

responder to ionizing radiations, *Atm*$^{-/-}$ mice are hypersensitive to IR and at doses higher than 5Gy IR die within 4 to 8 days from a gastrointestinal syndrome (Barlow, Hirotsune et al. 1996; Gurley and Kemp 2007). The analysis of the IR pathophysiology in wild type mice revealed acute alterations in the thymus, spleen, bone marrow, spermatogonia, epithelia of the gut, hair follicles and abortion of embryos at early stages of gestation, changes that are accompanied by apoptosis. Analysis of the sensitivity to IR during development revealed that wild type embryos are most sensitive to IR during early development (Michel 1989; Gurley and Kemp 2007).

Mice treated with 8 mg/kg body weight MMC, representing the median lethal dose (LD50) in 14 days survival studies, suffer from hematopoietic, intestinal and renal toxicity (Crooke and Bradner 1976; Hamner, Verani et al. 1983; Legha 1985; Linette, McGee et al. 1992; Shirakawa, Morita et al. 1993). In humans, MMC does not cross the blood-brain barrier and is widely distributed throughout the body but is metabolised mainly in the liver with about 10% being excreted unchanged in the urine (Gangolli and Royal Society of Chemistry (Great Britain) 1999). Mice defective for the FA pathway as well as FA patients cannot deal with the cross-links induced by MMC and are hypersensitive to this reagent (Moldovan and D'Andrea 2009). HU has been shown to be highly cytotoxic cells deficient for the ATR pathway while little effect was seen in the wild type control cells. The toxicity associated with *in vivo*

administration of HU by i.p. delivery to wild type pregnant mice has shown that administration of a 1g/kg body weight dose at E8.5 results in embryo lethality if pregnancy is taken to term. Using 400mg/kg and 800mg/kg body weight doses had no effect on embryo survival but determined increased cell death in the central nervous system (CNS). The increased apoptosis in the CNS was detectable as early as 3 hours post treatment, and showed the highest levels after 12 hours, followed by recovery at 48 hours (Woo, Katayama et al. 2003; Woo, Katayama et al. 2004).

The problem with the original chemotherapeutic treatments is recurrence of tumors. Thus, a better understanding of tumor biology is needed. Because cancer is usually a highly proliferative process associated with defects in DDR the checkpoint functionality of many cancers has been studied and, different from what was expected many tumors showed an upregulation DDR components such as p53, CHK2 or CHK1 as compared to the normal surrounding tissue (Bartek, Bartkova et al. 2007). Although initially it was thought that the increased functionality of these DDR components might be due to the increased levels of replication stress that come with increased proliferation (Bartkova, Horejsi et al. 2005) current models propose that the increased DDR functions as a survival mechanism adapted by cancer cells to survive the associated replication stress, thus promoting tumor growth.

Overexpression of ATR pathway components RAD9, HUS1 and CHK1, for example, is seen in human breast tumors (Cheng, Chow et al. 2005), prostate cancers (Zhu, Zhang et al. 2008), ovarian cancers (de la Torre, Gil-Moreno et al. 2008) and colorectal cancers (Ashwell and Zabludoff 2008). While many cancer cells are defective for the G1 checkpoint (mainly due to ATM pathway mutations) they have intact S/G2 checkpoints as they need them to survive. To test this hypothesis the ATR pathway was inhibited in cancer cells and mouse models for ATR deficiency and this resulted to increased cell death (Luo, Rockow-Magnone et al. 2001) or failure to initiate spontaneous tumor formation *in-vivo* (Levitt, Zhu et al. 2007; Ruzankina, Pinzon-Guzman et al. 2007; Greenow, Clarke et al. 2009; Murga, Bunting et al. 2009; Ruzankina, Schoppy et al. 2009; Yazinski, Westcott et al. 2009; Stephanie A. Yazinsky in preparation).

For example while oncogenic RAS and p53 loss-of-function mutations are common in many cancers that present limited sensitivity to conventional chemotherapy these genetic alterations create a hypersensitivity to ATR pathway inhibition (Toledo, Murga et al. 2011). Moreover synthetic lethal phenotypes were observed at cellular level when ATR suppression was combined with oncogenic stress caused by H-Ras^{G12V}, K-Ras^{G12D}, or c-Myc overexpression (Schoppy, Ragland et al. 2012). Similarly, CHK1 inhibitors were highly effective in killing Myc-driven lymphomas and *Atr*$^{S/S}$ mice were protected from developing Myc-induced

lymphomas or pancreatic tumors (Murga, Campaner et al. 2011; Bartek, Mistrik et al. 2012).

The observations that cancer cells rely more heavily than normal cells on a functional intra-S and G2 checkpoints is currently refer to as the process of "non-oncogene addiction". While non-oncogene addiction genes, are required for preserving cancer progression, they do not undergo oncogenic mutations. The concept of non-oncogene addiction accentuates the key impact of these supporting networks to tumorigenesis highlighting points of intervention for cancer therapeutics (Luo, Solimini et al. 2009).

Taken together, these results show that ATR pathway is essential for maintaining cancer cell viability and can be exploited to sensitize cancer cells to common DNA chemotherapeutic drugs. CHK1 inhibitors are in advanced clinical trials that show very promising results (Bartek, Mistrik et al. 2012; Schoppy, Ragland et al. 2012). The current working model states that ATR pathway inhibition drives cancer cells death due to increased replication stress because cancer cells cannot recover from these insults.

1.8 Summary and remaining questions

Due to the lethality associated with complete ATR pathway deficiency and the limited mammalian models available for hypomorphic deregulation of this pathway

the *in vivo* relationship between ATM and ATR pathways remained elusive. Moreover, since ATR pathway inhibition shows such promising results for improving cancer treatment efficacy (Brooks, Oakes et al. 2012; Tang, Dai et al. 2012), it was imperative to learn more about the effect of ATR deficiency in normal tissues. Here we took advantage of the unique *Hus1* mouse model to answer these questions.

In Chapter 2 we focus on understanding the relationship between the interplay between the ATM and ATR pathway and human inborn disease. Seckel Syndrome is a debilitating disease that we don't completely understand, mainly because of a lack of suitable animal models. Moreover the characteristic Seckel phenotypes are present in many DDR syndromes, implying that they are consequence of increased GIN during development, independent of the DDR component mutated. Additionally, some A-T patients like the A-T_{Fresno} variant patients show a more severe disease most likely because other polymorphism in DDR pathway genes. By using the *Hus1* allelic series as a tool we hope to be able to understand better what is the relationship between the two main DDR pathways and development and disease, both at organism and cellular levels. The *Hus1* allelic series will be crossed on an $Atm^{-/-}$ background and the *Hus1*/*Atm* double mutant mice will be assessed. I expect that a synthetic lethal interaction will be described owing to the cooperative roles of ATM and HUS1 in DDR.

In Chapter 3 we test the role for HUS1 in DDR both in physiologic conditions as well as after genotoxin treatments. Due to the current evolving evidence that the ATR/CHK1 pathway can be used as a tool to sensitize cancer cells to chemotherapy the understanding on how ATR inhibition would affect normal organisms is essential. This kind of analysis has been impeded by the severe phenotypes associated with ATR deficiency. Our *Hus1* mouse model represents a unique tool for such approaches since the Hus1 impaired mice are born at expected frequencies, show no overt phenotype, and no increased incidence of cancer formation. The fact that they have increased GIN levels as measured by micronucleus formation prompted us to hypothesize that they have enough *Hus1* to deal with normal replication stress but will become incapable to induce a proper DDR when challenged with genotoxin induced replication stress.

By using this mouse model we will be able to dissect the relationship between the ATR and ATM pathways in response to IR treatment. We hypothesize that *Hus1* deficient mice will show no hypersensitivity to IR but will be hypersensitive to replication stress inducing reagents like MMC or HU. To test these hypotheses *Hus1* impaired mice and wild type littermate controls will be challenged with either IR or HU or MMC and the survival post treatment will be assessed. To further understand the role of *Hus1* in the different compartments treated mice will be sacrificed at 8 and 96 hour time points and the pathology of the different organ systems assessed.

Moreover to understand the ATM/HUS1 interplay in response to genotoxins Atm/Hus1 double mutant mice will be used for similar experiments.

Together these data will allow us to create a map for the role of HUS1 in development and pathology as well as for the interaction with the ATM pathway. Such information will be used in the future for the better understanding of human inborn disease and the design of better cancer therapies.

CHAPTER 2

DISEASE SEVERITY IN A MOUSE MODEL OF ATAXIA TELANGIECTASIA IS MODULATED BY THE DNA DAMAGE CHECKPOINT GENE HUS1[1]

2.1 **Abstract**

The human genomic instability syndrome Ataxia Telangiectasia (A-T), caused by mutations in the gene encoding the DNA damage checkpoint kinase ATM, is characterized by multisystem defects including neurodegeneration, immunodeficiency, and increased cancer predisposition. ATM is central to a pathway that responds to double strand DNA breaks, while the related kinase ATR leads a parallel signaling cascade that is activated by replication stress. To dissect the physiological relationship between the ATM and ATR pathways, we generated mice defective for both. Because complete ATR pathway inactivation causes embryonic lethality, we weakened the

1 The data in this chapter has been published: Gabriel Balmus, Min Zhu, Sucheta Mukherjee, Amy M Lyndaker, Kelly R Hume, Jaesung Lee, Mark L Riccio, Anthony P Reeves, Nathan B Sutter, Drew M Noden, Rachel M Peters, Robert S Weiss (2012) - Disease severity in a mouse model of Ataxia Telangiectasia is modulated by the DNA damage checkpoint gene Hus1 – *Human Molecular Genetics 21 (15), 3408-3420*

ATR mechanism to different degrees by impairing HUS1, a member of the 9-1-1 complex that is required for efficient ATR signaling. Notably, simultaneous ATM and HUS1 defects caused synthetic lethality. *Atm/Hus1* double mutant embryos showed widespread apoptosis and died mid-gestationally. Despite the underlying DNA damage checkpoint defects, increased DNA damage signaling was observed, as evidenced by H2AX phosphorylation and p53 accumulation. A less severe *Hus1* defect together with *Atm* loss resulted in partial embryonic lethality, with the surviving double mutant mice showing synergistic increases in genomic instability and specific developmental defects including dwarfism, craniofacial abnormalities, and brachymesophalangy, phenotypes that are observed in several human genomic instability disorders. In addition to identifying tissue-specific consequences of checkpoint dysfunction, these data highlight a robust, cooperative configuration for the mammalian DNA damage response network and further suggest *HUS1* and related genes in the ATR pathway as candidate modifiers of disease severity in A-T patients.

2.2 **Introduction**

Ataxia-telangiectasia (A-T, OMIM #208900) is a hereditary genomic instability syndrome caused by loss of function mutations in *ATM*, which encodes a protein kinase involved in cellular DNA damage responses (DDR) (McKinnon 2012). A-T is

characterized by progressive cerebellar ataxia, oculocutaneous telangiectasias, immunodeficiency, infertility, increased cancer incidence, and radiation hypersensitivity. These clinical manifestations are the consequence of failed responses to DNA double strand breaks (DSB) that arise spontaneously or as programmed developmental events. Rare patients with atypical manifestation of the disease have been described and referred to as "A-T variants". One such variant, termed A-T_{Fresno}, combines typical A-T phenotypes with microcephaly and mental retardation making it among the most severe A-T forms known (Gilad, Chessa et al. 1998).

ATM normally functions as the principal component of one of the cellular DNA damage checkpoint pathways that detect aberrant DNA structures and coordinate DNA repair with cell cycle progression. Checkpoint mechanisms are part of a broader DDR that protects genomic integrity and ensures normal development, tissue homeostasis, and cancer-free survival (Jackson and Bartek 2009). In response to DSB, the ATM kinase undergoes a transition from inactive dimer to active, auto-phosphorylated monomer and then phosphorylates numerous substrates involved in signaling transduction and downstream effector functions, including H2AX, CHK2, and p53. A second checkpoint pathway, organized around the related kinase ATR, responds to a wide variety of lesions, including bulky DNA adducts and DNA crosslinks, as well as processed DSB. Activated ATR phosphorylates CHK1 and other targets, promoting fork stabilization, inhibition of late origin firing, and stimulation of

DNA repair (Cimprich and Cortez 2008). Critical for ATR activation is the RAD9-RAD1-HUS1 (911) complex, a PCNA-like clamp that is loaded onto damage sites and recruits the ATR activator TOPBP1 (Kemp and Sancar 2009). Importantly, the 911 complex additionally has direct roles in regulating base excision repair, translesion DNA synthesis, and apoptotic signaling (Helt, Wang et al. 2005). The genes encoding the 911 complex, like all ATR pathway core components, are essential for organismal survival (Weiss, Enoch et al. 2000; Hopkins, Auerbach et al. 2004; O'Driscoll 2009). Partial *ATR* impairment in humans leads to Seckel syndrome (SCKL1, OMIM #210600) an autosomal recessive disorder characterized by proportional dwarfism, microcephaly, craniofacial abnormalities and mental retardation (O'Driscoll 2008).

Due to their distinct componentry and activation by different types of genome damage, the ATM and ATR pathways initially were thought to function as independent, separable mechanisms. However, aberrant DNA structures often engage both pathways to some extent, and there is substantial biochemical crosstalk between the pathways (Cimprich and Cortez 2008). A full appreciation of these interactions in vertebrates has been hampered by a lack of suitable genetic tools. While *Atm*-deficient mice are viable and show many A-T phenotypes (Barlow, Hirotsune et al. 1996; Elson, Wang et al. 1996; Xu, Ashley et al. 1996), the severe phenotypes associated with ATR pathway impairment have been an impediment to understanding the biological significance of the interplay between the ATM and ATR pathways. In this

study, we overcome this limitation with a *Hus1* allelic series in which null ($Hus1^{\Delta 1n}$) or wild-type ($Hus1^{+}$) alleles are used in combination with a hypomorphic ($Hus1^{neo}$) allele that expresses *Hus1* at approximately 20% of the wild-type level (Levitt, Zhu et al. 2007). $Hus1^{neo/\Delta 1n}$ mice, which have the lowest *Hus1* expression in the series, are born at expected frequencies and appear grossly normal but are incapable of proper genome maintenance as evidenced by increased spontaneous GIN and hypersensitivity to exogenous genotoxins (Levitt, Zhu et al. 2007). By combining the *Hus1* allelic series with targeted *Atm* deletion, we identify an essential cooperative relationship between ATM and HUS1 during embryonic development and in specific adult tissues.

2.3 **Material and methods**

Animals. All animals used in this study were handled in accordance with federal and institutional guidelines, under a protocol approved by the Cornell University Institutional Animal Care and Use Committee (IACUC). $Hus1^{neo}$ and $Hus1^{\Delta 1n}$ mice were maintained on the 129S6 background (Weiss, Enoch et al. 2000; Levitt, Zhu et al. 2007). *Atm* knockout mice were maintained on the FVB background (Elson, Wang et al. 1996). These strains were interbred to create *Atm*/*Hus1* double mutant mice. Mice were genotyped by PCR analysis of genomic DNA isolated from tail snip biopsies as previously described (Weiss, Enoch et al. 2000). Images of live mice and skulls were

taken using a Canon EOS Digital Rebel XTi digital camera equipped with a Canon EF-S 18-55mm lens. For analysis of embryonic development, timed matings were performed. Noon of the day of vaginal plug detection was defined as embryonic day E0.5. For analysis of tumor-free survival, a cohort of mice was maintained for up to 18 months of age or until the appearance of visible neoplasms or signs of clinical disease, including weight loss, hunched posture, labored breathing, poor grooming, or wasting, at which point they were euthanized by carbon dioxide asphyxiation and necropsied. For analysis of radiation sensitivity, mice were subjected to 4Gy or 5Gy doses of γ-irradiation using a Mark I Model 68 sealed ^{137}Cs source gamma irradiator (JL Shepherd & Associates) and monitored for up to 30 days or until reaching humane endpoint criteria based on the clinical disease signs noted above.

Histology and Immunohistochemistry. Following euthanasia, isolated tissues were weighed and then fixed in 10% formalin. Embryos were fixed in 4% paraformaldehyde. Histological sections of paraffin-embedded tissues were stained with hematoxylin and eosin and subjected to pathological assessment. For assessment of nuclear morphology, Feulgen-Schiff staining was carried out using a standard protocol (Weiss, Enoch et al. 2000). For immunohistochemistry, E10.5 embryos were embedded in paraffin and serial 5 μm sections were collected on Superfrost Plus slides (Fisher) and processed for immunohistochemistry using citric acid for p53 or EDTA for γ-H2AX

-based antigen retrieval. Sections were incubated with anti-γ-H2AX (Upstate #05-636) or p53 (Cell Signalling #2524) antibodies followed by a secondary biotinylated anti-mouse antibody (Invitrogen, Histostain SP 95-6543B). DAB (DAKO) was used as chromogen and hematoxylin as a counter-stain. TUNEL staining was performed using the Apoptag (Chemicon International) system according to the manufacturer's instructions. More than 1000 cells from at least three 100X fields were counted per embryo. Histology images were obtained using an Aperio Scanscope (Aperio Technologies, USA). The quantitation was done by counting the distribution of DAB positive cells (brown stain) as depicted in Figure S1 D.

Skeletal morphology and measurements. Micro-computed tomography (CT) scans were done on both living mice and isolated specimens using GE CT120 micro-CT (GE Healthcare, London, Ontario, Canada) and Xradia VersaXRM-500 (Xradia, Pleasanton, CA, USA) scanners. Standard micro-CT scan parameters were used and are available upon request. For isolated skull preparations, mice were euthanized and decapitated, and heads were de-skinned and boiled in tap water for 20 minutes. Skulls were then mechanically cleaned using forceps while the brain was removed by flushing with water. Skulls were dried before being stored. For live imaging, mice were anesthetized with isoflurane and scanned. In order to accurately measure the distance between two points of interest, we developed a tool for marking points on the skull

surface in three dimensional (3D) image space. For every marked point, a surface coordinate location was computed in mm for x, y, and z 3-D coordinates. The distance between any two surface points was computed by using the Euclidean distance of the mapped image coordinates. Statistical analysis of the resulting morphometry data was performed by a principal component (PC) analysis using the princomp() function and a covariance matrix in R 2.6.0. Limbs were isolated after euthanasia and subjected to micro-CT imaging as described above. Analysis of the resulting data and 3D reconstructions were done using OsiriX software (Rosset, Spadola et al. 2004). Skeletal staining with Alcian Blue and Alizarin Red was performed as previously described (Kaufman 1992). Briefly, embryos were eviscerated, fixed in 80% ethanol for at least 24 hours, dehydrated in 95% ethanol, and stained overnight with Alcian Blue (Sigma A3157) in 95% ethanol: 1% glacial acetic acid solution. Bone was counterstained with Alizarin Red (Sigma A5533) in 2% KOH for 3 hours. Embryos were cleared in a decreasing 2% KOH/glycerol series (80:20; 60:40; 40:60) for 24 hours each and stored indefinitely in 2% KOH: glycerol (20:80). The stained embryos were imaged using a Leica MZ125 inverse microscope equipped with a RT Slider camera (Diagnostic Instruments).

Micronucleus assay. Analysis of micronucleus (MN) formation in peripheral blood cells was performed as previously described (Shima, Hartford et al. 2003; Levitt, Zhu et al.

2007). Briefly, peripheral blood was collected from the mandibular vein, fixed in methanol, and incubated in bicarbonate buffer containing RNase A and anti-CD71: FITC antibody (Biodesign International). After washing and staining with propidium iodide, the cells were analyzed on a FACSCalibur flow cytometer (Becton-Dickinson, San Jose, CA).

Cell culture and proliferation measurements. Mouse embryonic fibroblasts (MEFs) were prepared from E13.5 embryos following timed matings between $Hus1^{+/neo}Atm^{+/-}$ and $Hus1^{neo/neo}Atm^{+/-}$ mice. Briefly, embryos were dissected from the deciduum, mechanically disrupted, and cultured in DMEM supplemented with 10% fetal bovine serum, 1.0 mM L-glutamine, 0.1 mM minimal essential medium nonessential amino acids, 100 μg/ml streptomycin sulfate, and 100 U/ml penicillin. The initial plating was defined as passage zero (p0), and cells were subsequently maintained on a 3T3 protocol (Todaro and Green 1963). Clonogenic potential was assessed by plating MEFs in 6 well dishes at 5×10^2 or 3×10^3 cells per well and changing the media every 3 days. After 11 days in culture, cells were washed with PBS and fixed in methanol for one hour at room temperature, stained overnight with a 5% crystal violet solution in 70% ethanol, and washed with tap water. Immortalized $Hus1^{+/+}p21^{-/-}$ and $Hus1^{-/-}p21^{-/-}$ MEFs were described previously (Weiss, Enoch et al. 2000). For IR treatment, cells at passage 2 or 3 were exposed to γ-irradiation using a Mark I Model 68 sealed ^{137}Cs

source gamma irradiator (JL Shepherd & Associates) at a dose rate of 123.1 Rad/min. For UV treatment, the medium was removed from the cells, cells were washed with PBS, the top of the culture dish was removed, and the cells were exposed to 254 nm UV light using a XL-1000 UV Crosslinker (Spectro Linker).

Metaphase chromosome preparation. Chromosome preparation from mouse embryonic fibroblasts (MEFs) from the first passage (P1) followed standard procedures that included a 1 hour colcemid treatment (10 μg/ml; Invitrogen) followed by 6 minutes hypotonic incubation (0.075M KCl) and fixation in 3:1 methanol: glacial acetic acid (Rens, Fu et al. 2006). At this point cells were dropped onto slides, dried and stained with 1:50 Giemsa (Original Azure Blend, Harleco) in Gurr buffer, pH 7. Metaphase chromosomes were scored under a 100 (1.6X) oil objective lens according to standard guidelines (International Standing Committee on Human Cytogenetic Nomenclature., Shaffer et al. 2009).

Northern blotting and real-time PCR. Total RNA was prepared from E10.5 embryos and from liver using RNA STAT-60 reagent (Tel-Test, Friendswood, TX) and then resolved on a 1% agarose/formaldehyde gel, transferred to a nylon membrane, and hybridized with ^{32}P-labeled cDNA probes. Quantification of signal intensity was done

using a Storm 860 phosphorimager (Molecular Dynamics , Sunnyvale, USA). Total RNA was used for reverse transcription using the SuperScript III kit (Invitrogen) according to the manufacturer`s instructions. Quantitative real-time PCR (Q-PCR) was performed on an ABI 7500 System (PE Applied-Biosystems) using cDNA as a template in the presence of SYBR-green (Quanta Biosciences PerfeCTa SYBR Green FastMix). Primer pairs were designed using the Integrated DNA Technologies RealTime PCR Assay Design tool (www.idtdna.com) to generate intron-spanning products of 150-200bp as follows: *Ghr*: 5'- AGCCTCGATTCACCAAGTG-3' and 5'-AATTCTTGCAGCTTGTCGTTG -3'; *Igf1*: 5'-GAGACTGGAGATGTACTGTGC-3' and 5'- CTCCTTTGCAGCTTCGTTTTC-3'; *Gstt2*: 5'-TGCCCAAGTCCACGAATAC-3' and 5'-CCAGGACCATTCTATCTCTGTTC-3'; *Bax*: 5'-TTGGAGATGAACTGGACAGC -3' and 5'-CAGTTGAAGTTGCCATCAGC-3'; *Puma*: 5'-CTGGAGGGTCATGTACAATCTC-3' and 5'-GGTGTCAGAAGGCGGAG-3'; *p21*: 5'-CTTGCACTCTGGTGTCTGAG-3' and 5'-GCACTTCAGGGTTTTCTCTTG-3'; *beta-actin*: 5'-ACCTTCTACAATGAGCTGCG -3' and 5'CTGGATGGCTACGTACATGG-3'. The generation of specific PCR products was confirmed by melting curve analysis and gel electrophoresis. Each primer pair was tested with a logarithmic dilution of cDNA mix to generate a linear standard curve, which was used to calculate the primer pair efficiency (Dean Fraga,

Tea Meulia et al. 2008).

Western blotting. Cells were harvested and solubilized in RIPA buffer as described previously (Harlow and Lane 2006) or protein was extracted using a high-salt extraction procedure (Achari and Lees-Miller 2000). Total protein was quantified by Bradford assay, resolved on 6% to 14% SDS-PAGE gels, and subjected to immunoblotting using antibodies from Millipore (anti-γ-H2AX, #05-636 and anti-CHK2, #05-649), Santa Cruz (anti-CHK1, G-4; sc-8408 and anti-p53, FL-393; sc-6243), Cell Signaling (anti-phospho-CHK1, Ser345, #2341), Rockland (anti-ATM, pSer1981, 200-310-400) and Sigma (anti-beta actin, #A5441). Western-blot imaging and quantification was performed using a Versa Doc Imaging System (Bio-Rad Laboratories).

2.4 **Results**

2.4.1 **Combined inactivation of *Atm* and *Hus1* results in synthetic lethality.**

To elucidate the genetic relationships between the ATM- and ATR-mediated DNA damage checkpoint pathways, we generated mice defective for both. Interbreeding of mice bearing targeted *Atm* and *Hus1* alleles was performed in order to produce *Atm*-deficient mice with incremental reductions in *Hus1* gene dosage

(*Hus1*$^{+/+}$ > *Hus1*$^{+/neo}$ > *Hus1*$^{+/\Delta 1n}$ > *Hus1*$^{neo/neo}$ > *Hus1*$^{neo/\Delta 1n}$). *Hus1*$^{+/neo}$ cells and mice are phenotypically normal and frequently used as wild-type equivalents in this study (Levitt, Zhu et al. 2007). Of 1753 weaned offspring analyzed, no *Hus1*$^{neo/\Delta 1n}$*Atm*$^{-/-}$ mice were obtained, and only 84 *Hus1*$^{neo/neo}$*Atm*$^{-/-}$ mice were obtained while 259 were expected (Table 2.1; $p<0.001$ Chi-square test). The nature of the lethal phenotype associated with combined *Atm* and *Hus1* inactivation was determined by analyzing double mutant and control embryos from embryonic day E8.5 to birth (Table 2.2). While *Hus1*$^{neo/\Delta 1n}$*Atm*$^{-/-}$ embryos appeared normal at E8.5, they were smaller relative to their littermates at E9.5 and all died between E10.5 and E11.5 (Figure 2.1A-D). A less severe *Hus1* defect in *Hus1*$^{neo/neo}$*Atm*$^{-/-}$ embryos resulted in no gross abnormalities prior to E13.5, at which point the double mutant embryos were smaller than their littermates. Approximately 30% of *Hus1*$^{neo/neo}$*Atm*$^{-/-}$ embryos were abnormal at E14.5 and died by E15.5 (Figure 2.1E-H). *Hus1*$^{neo/neo}$*Atm*$^{-/-}$ mice that survived beyond this mid-gestational period were significantly smaller than control littermates

Table 2.1. Synthetic lethality following combined impairment of *Hus1* and *Atm* in mice[a].

Hus1 genotype	*Atm* genotype	Number expected	Number observed
+/+		3	5
+/*neo*		95	108
+/⊿*1n*	+/+	12	9
neo/*neo*		259	286
neo/⊿*1n*		69	58
+/+		6	5
+/*neo*		190	208
+/⊿*1n*	+/-	24	31
neo/*neo*		518	659
neo/⊿*1n*		138	190
+/+		3	4
+/*neo*		95	93
+/⊿*1n*	-/-	12	13
neo/*neo*		259	84
neo/⊿*1n*		69	0
		1753	1753

[a] Mice were genotyped by PCR analysis of tail DNA at 3 weeks of age. Expected values represent the combined Mendelian ratios from several crosses involving different parental genotypes ($p<0.001$; Chi-square test)

Table 2.2. Genotype and phenotype analysis of embryos from interbreedings of *Hus1 and Atm* mutant mice [a]

Genotype		E8.5			E9.5			E10.5			E11.5			E12.5			E13.5		
Hus1	*Atm*	**E**	**O**	**P**	E	O	P	**E**	**O**	**P**	E	O	P	**E**	**O**	**P**	E	O	P
+/+																			
+/neo					2	1								**1**	**0**		7	5	
+/Δ1n	+/+				2	2											1	1	
neo/neo		**6**	**5**	**2a**	20	21		**19**	**21**	**2a**	8	7		**5**	**2**		7	8	
neo/Δ1n		**6**	**3**		8	13		**13**	**13**		8	7		**4**	**2**		1	0	
+/+																			
+/neo					4	5								**2**	**2**		15	15	
+/Δ1n	+/-				4	4											1	2	
neo/neo		**12**	**15**	**1a**	40	37	3a	**37**	**32**		15	16		**10**	**14**		15	15	
neo/Δ1n		**12**	**10**		15	17		**27**	**38**	**4a**	15	19		**8**	**14**	**1a**	1	1	
+/+																			
+/neo					2	5								**1**	**1**		7	8	
+/Δ1n	-/-				2	0											1	1	
neo/neo		**6**	**6**	**1a**	20	14	2a	**19**	**13**	**2a**	8	5		**5**	**4**		7	7	
neo/Δ1n		**6**	**9**		8	7	7a	**13**	**10**	**10a**	8	6	6d	**4**	**0**		1	0	
TOTAL		**30**	**30**		126	126	1r	**127**	**127**		60	60	4r	**39**	**39**	**9r**	63	63	4r

Genotype		E14.5			E15.5			E16.5			E17.5			E18.5			P1		
Hus1	*Atm*	**E**	**O**	**P**	E	O	P	**E**	**O**	**P**	E	O	P	**E**	**O**	**P**	E	O	P
+/+																			
+/neo		**8**	**7**		2	3		**3**	**1**		3	3		**7**	**6**		9	10	1d
+/Δ1n	+/+							**1**	**0**		1	2							
neo/neo		**15**	**13**		9	8		**9**	**11**		9	9		**9**	**13**		26	25	
neo/Δ1n		**3**	**3**		5	6		**4**	**6**		7	11		**2**	**2**		5	7	
+/+																			
+/neo		**15**	**19**		5	2		**5**	**5**		5	6		**14**	**15**	**1a**	19	22	1a
+/Δ1n	+/-							**1**	**0**		1	1							
neo/neo		**30**	**30**		18	18		**17**	**19**		18	21		**18**	**20**		53	59	1d
neo/Δ1n		**6**	**8**		11	17		**8**	**7**		14	14		**5**	**4**		11	13	
+/+																			
+/neo		**8**	**5**		2	3		**3**	**5**	**2a**	3	3		**7**	**7**		9	8	
+/Δ1n	-/-							**1**	**1**	**a**	1	0							
neo/neo		**15**	**17**	**9a 5d**	9	10	7a 2d	**9**	**8**	**4a 4d**	9	5	5a	**9**	**6**	**6a**	26	20	8a 12d
neo/Δ1n		**3**	**0**		5	0		**4**	**0**		7	0		**2**	**0**		5	0	
TOTAL		**102**	**102**	**5r**	67	67	5r	**63**	**63**	**4R**	75	75	4r	**73**	**73**	**2r**	164	164	

[a] Embryos from timed matings were isolated at the indicated time post coitum and genotyped by PCR analysis of yolk sac DNA. The observed (O) values were compared to expected (E) values based on the normal Mendelian ratios for several crosses involving different parental genotypes. Any abnormal phenotypes (P) were noted. Embryos that were small in size, developmentally delayed, or morphologically aberrant but had a beating heart was classified as abnormal (a), while embryos without a heartbeat were classified as dead (d). The rows marked 'TOTAL' also indicate the number resorbed embryos that could not be genotyped (r).

Figure 2.1. Embryonic lethality upon simultaneous deregulation of *Atm* and *Hus1*. Embryos from timed matings were isolated at the indicated stage of embryonic development, imaged for morphological assesment and genotyped by PCR. (A-D) Representative images of *Hus1*$^{neo/\Delta 1n}$*Atm*$^{-/-}$ embryos and control littermates from E8.5 to E11.5. (E-F) Representative images of *Hus1*$^{neo/neo}$*Atm*$^{-/-}$ embryos and control littermates from E13.5 to E16.5. Note that at E14.5 some *Hus1*$^{neo/neo}$*Atm*$^{-/-}$ embryos are dead whereas others are smaller than control littermates but otherwise normal.

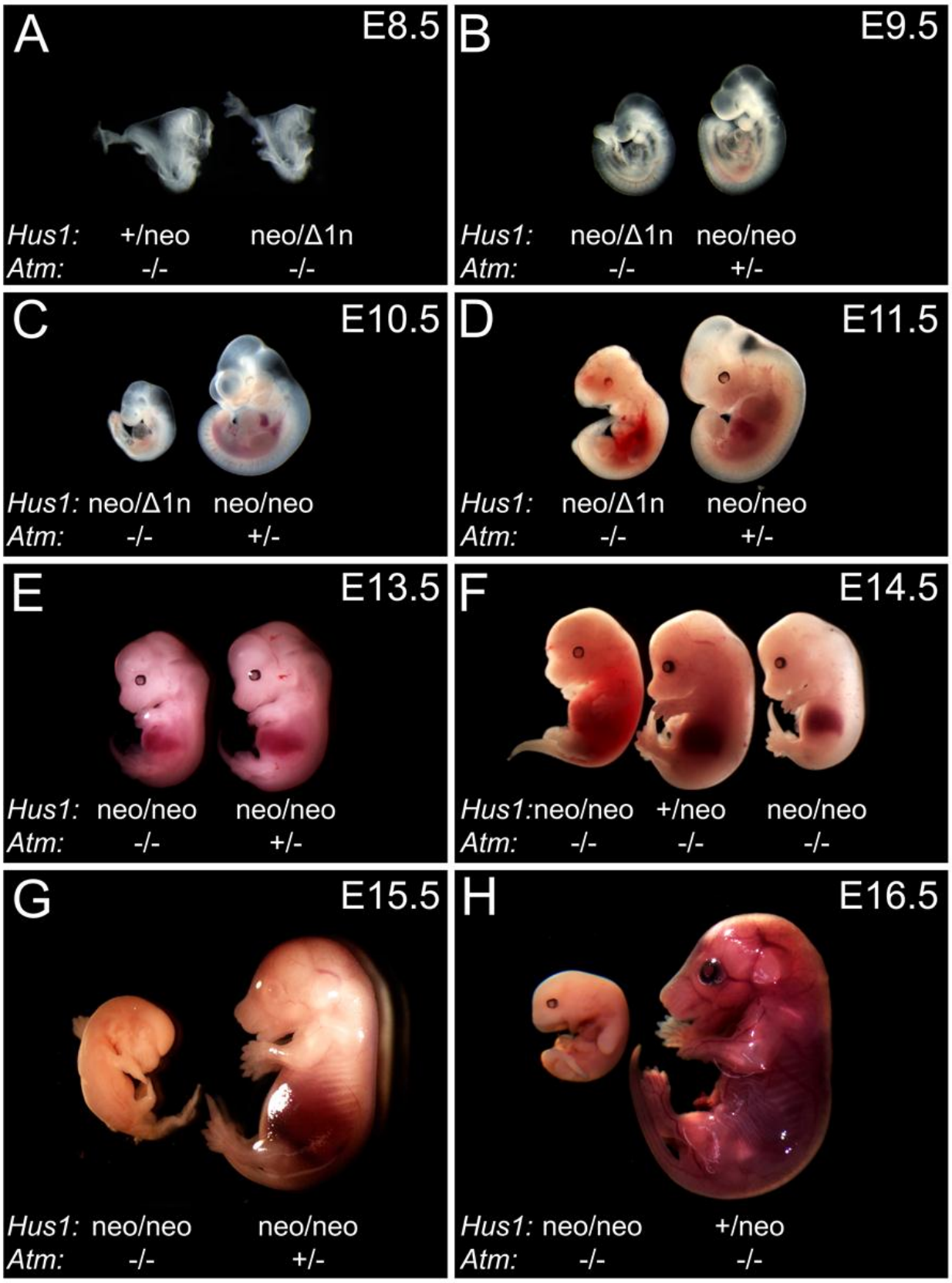
A
E8.5
Hus1: +/neo neo/Δ1n
Atm: -/- -/-
B
E9.5
Hus1: neo/Δ1n neo/neo
Atm: -/- +/-
C
E10.5
Hus1: neo/Δ1n neo/neo
Atm: -/- +/-
D
E11.5
Hus1: neo/Δ1n neo/neo
Atm: -/- +/-
E
E13.5
Hus1: neo/neo neo/neo
Atm: -/- +/-
F
E14.5
Hus1:neo/neo +/neo neo/neo
Atm: -/- -/- -/-
G
E15.5
Hus1: neo/neo neo/neo
Atm: -/- +/-
H
E16.5
Hus1: neo/neo +/neo
Atm: -/- -/-

(Figure 2.4 A,B; $p<0.05$ Student's t test), and 30-40% of mice of this genotype died on the first day of life (P1) (Table S1), while the remainder survived beyond weaning (Table 2.1). Together, these data indicate that although defects in *Atm* or *Hus1* individually are compatible with grossly normal development and organismal viability, simultaneous defects in *Atm* and *Hus1* cause synthetic lethality in a *Hus1* gene dosage dependent manner.

2.4.2 **Increased genomic instability and cell death in Atm/Hus1-deficient embryos.**

The failure of cells to deal with replication stress and spontaneous DNA lesions can lead to impaired cell proliferation and/or survival (Bartek, Lukas et al. 2004). To evaluate these outcomes in *Atm*/*Hus1* mutant embryos, we initially performed Feulgen-Schiff staining on E10.5 embryos and quantified the frequency of pyknotic and mitotic nuclei. There was a significant increase in pyknotic nuclei indicative of apoptosis in $Hus1^{neo/\Delta 1n}Atm^{-/-}$ and $Hus1^{neo/neo}Atm^{-/-}$ embryos as compared to the $Hus1^{+/neo}Atm^{+/+}$ control group (Figure 2.2, $p<0.001$; Student's t test). By contrast, cell proliferation was unaffected. We reasoned that the apparent increase in apoptosis in the *Atm*/*Hus1* double mutants could be due to checkpoint activation and therefore monitored the accumulation of phosphorylated H2AX (γ–H2AX) and total p53, markers of an activated DDR (Jackson and Bartek 2009). Terminal uridine deoxynucleotidyl transferase dUTP nick-end labeling (TUNEL) staining also was

Figure 2.2. Significant increase in apoptosis but no change in proliferation in *Atm/Hus1* double mutant embryos. Representative sections of Feulgen-Schiff staining of A) $Hus1^{+/neo}Atm^{+/+}$ and B) $Hus1^{neo/\Delta 1n}Atm^{-/-}$ embryos at E10.5. Right panels: higher magnification view of neural tube showing representative apoptotic (red arrow head) and mitotic (black arrow head) figures. Scale bar represents 25μm. C) Values indicate the percent of apoptotic and mitotic cells (± standard deviation) as determined from Feulgen-Schiff stained sections of embryos of the indicated genotypes. Student's t-test identified a significant increase in apoptosis ($p<0.001$) in both $Hus1^{neo/\Delta 1n}Atm^{-/-}$ (n=3) and $Hus1^{neo/neo}Atm^{-/-}$ (n=5) but no change in proliferation when compared to $Hus1^{+/neo}Atm^{-/-}$ (n=3). D) Representative γ-H2AX immunohistochemistry images for E8.5 $Hus1^{+/+}$ embryos with no treatment or after 5Gy IR treatment. Read arrows point to positive staining.

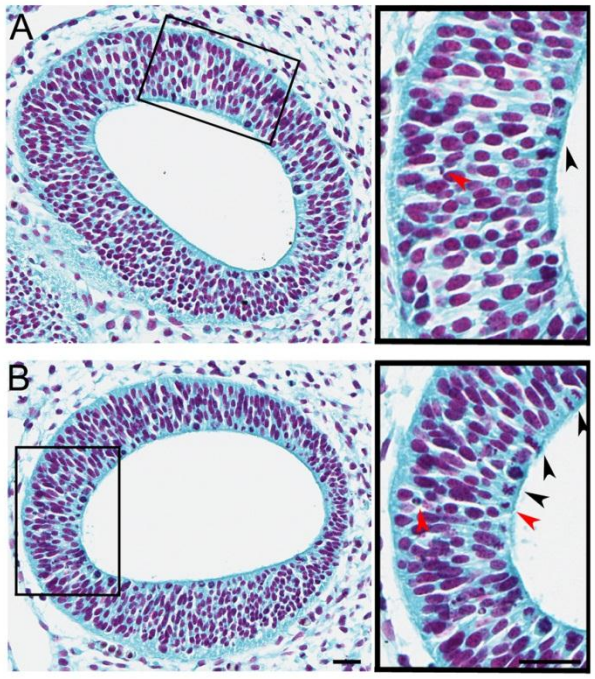

C

Genotype	Apoptotic	Mitotic
Hus1 $^{+/neo}$ *Atm* $^{+/+}$	0.44±0.45	1.16±0.91
Hus1 $^{neo/neo}$ *Atm* $^{+/+}$	0.55±0.36	0.98±0.49
Hus1 $^{neo/\Delta 1n}$ *Atm* $^{+/+}$	0.67±0.63	0.60±0.44
Hus1 $^{+/neo}$ *Atm* $^{-/-}$	0.86±0.88	0.82±0.66
Hus1 $^{neo/neo}$ *Atm* $^{-/-}$	3.37±1.15†	1.53±1.25†
Hus1 $^{neo/\Delta 1n}$ *Atm* $^{-/-}$	13.76±4.91‡	1.35±1.43‡
†p-value vs. *Hus1* $^{+/neo}$ *Atm* $^{-/-}$	0.00001	0.41358
‡p-value vs. *Hus1* $^{+/neo}$ *Atm* $^{-/-}$	0.00005	0.32515

D

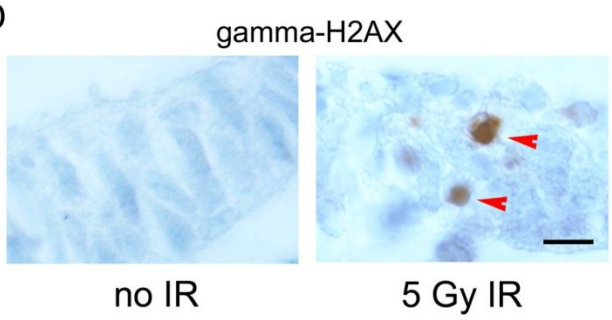

Figure 2.3. Significantly increased apoptosis and DDR activation in *Atm/Hus1* double mutant embryos. Sections of E10.5 *Atm/Hus1* embryos of the indicated genotypes were stained for γ-H2AX, p53, or by TUNEL assay. A) Representative images of embryo neural tube sections stained for γ-H2AX, p53 and TUNEL are shown. Scale bar represents 25μm. B) Percentage of γ-H2AX, TUNEL or p53 positive cells. Values are the mean of at least three embryos per genotype; error bars indicate standard deviation. Quantification was performed in neural ectoderm to ensure that equivalent cell populations were compared between genotypes; however similar staining patterns were observed throughout the embryos, irrespective of cell type. The percentage of positively stained cells in $Hus1^{neo/\Delta 1n}Atm^{-/-}$ and $Hus1^{neo/neo}Atm^{-/-}$ embryos was significantly different from each other ($p<0.05$; Student's t-test) and when each was compared to all the other genotypes ($p<0.01$, Student's t-test). C) Bar graph representing the fold increase in expression level of *p21*, *Bax*, and *Puma* for embryos of the indicated genotype relative to $Hus1^{+/neo}Atm^{+/+}$ as measured by qPCR. *p21* expression was significantly increased in $Hus1^{neo/\Delta 1n}Atm^{+/+}$, $Hus1^{+/neo}Atm^{-/-}$, $Hus1^{neo/neo}Atm^{-/-}$, and $Hus1^{neo/\Delta 1n}Atm^{-/-}$ embryos ($p<0.05$; Student's t-test) and was significantly greater in $Hus1^{neo/\Delta 1n}Atm^{-/-}$ embryos as compared to all other genotypes ($p<0.05$; Student's t-test).

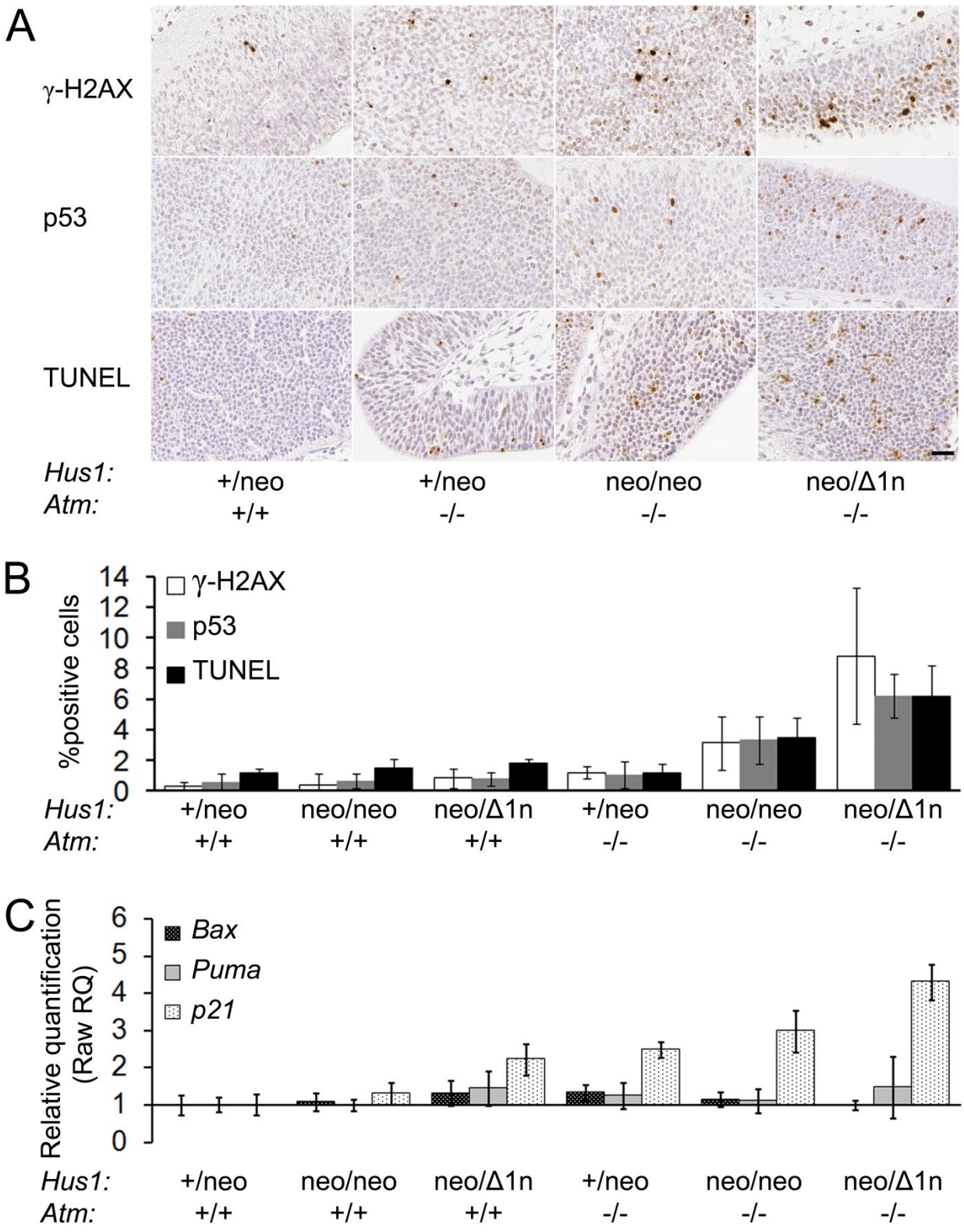
A
γ-H2AX
p53
TUNEL
Hus1:
Atm:
+/neo
+/+
+/neo
-/-
neo/neo
-/-
neo/Δ1n
-/-
B
%positive cells
γ-H2AX
p53
TUNEL
Hus1:
Atm:
+/neo
+/+
neo/neo
+/+
neo/Δ1n
+/+
+/neo
-/-
neo/neo
-/-
neo/Δ1n
-/-
C
Relative quantification (Raw RQ)
Bax
Puma
p21
Hus1:
Atm:
+/neo
+/+
neo/neo
+/+
neo/Δ1n
+/+
+/neo
-/-
neo/neo
-/-
neo/Δ1n
-/-

performed to directly measure apoptosis. While almost no γ-H2AX, p53, or TUNEL-positive cells were detected in *Hus1* or *Atm* single mutant embryos, *Hus1*$^{neo/neo}$*Atm*$^{-/-}$ and to an even greater extent *Hus1*$^{neo/\Delta 1n}$*Atm*$^{-/-}$ littermates showed significantly increased positive staining (Figure 2.3A, B; $p<0.05$; Student's t test). Because p53 can induce cell cycle arrest through transcriptional activation of *p21* or apoptosis by upregulating *Bax* and *Puma*, we used real-time PCR to measure the expression level of these genes in E10.5 embryos. Consistent with the observation of p53 accumulation in *Atm*/*Hus1* double mutant embryos, there was a corresponding significant increase in *p21* expression (Figure 2.3 C; $p<0.05$ Student's t test). Interestingly, there were no detectable changes in *Bax* or *Puma* expression, raising the possibility of a p53-independent apoptotic mechanism. Similar results were observed by Northern blot analysis (data not shown). Altogether, these findings suggest that the embryonic lethality following combined deregulation of *Atm* and *Hus1* is associated with a generalized accumulation of genome damage, activation of a DDR, and ultimately widespread apoptosis.

2.4.3 **Dwarfism in adult *Hus1*$^{neo/neo}$*Atm*$^{-/-}$ mice.**

Approximately one-third of *Hus1*$^{neo/neo}$*Atm*$^{-/-}$ mice survived to adulthood, and without exception these animals exhibited a striking dwarfism that became apparent at approximately E13.5 and persisted through adulthood (Figure 2.4 A-D). Consistent

Figure 2.4. Relative brain size in *Hus1*$^{neo/neo}$*Atm*$^{-/-}$ and littermate control mice. A) Brains dissected from 6-week old littermate male mice of the indicated genotypes are shown. Scale bar represents 5 mm. B) Box plot shows the percent weight of the brain relative to total body weight for mice of the indicated genotypes at 6 weeks of age. The brain weight of *Hus1*$^{neo/neo}$*Atm*$^{-/-}$ mice (n=5) was significantly different from that of *Hus1*$^{+/neo}$*Atm*$^{+/+}$ (n=3) (*$p<0.009$; Student's t-test), *Hus1*$^{neo/neo}$*Atm*$^{+/+}$ (n=3) (*$p<0.001$; Student's t-test) and *Hus1*$^{+/neo}$*Atm*$^{-/-}$ (n=4) (*$p<0.03$; Student's t-test) mice. C) Representative Hematoxylin and Eosin (upper panels) and Bielschowsky silver (lower panels) stained sequential sections of corpus callosum from mice of the indicated genotypes. Scale bar represents 50μm.

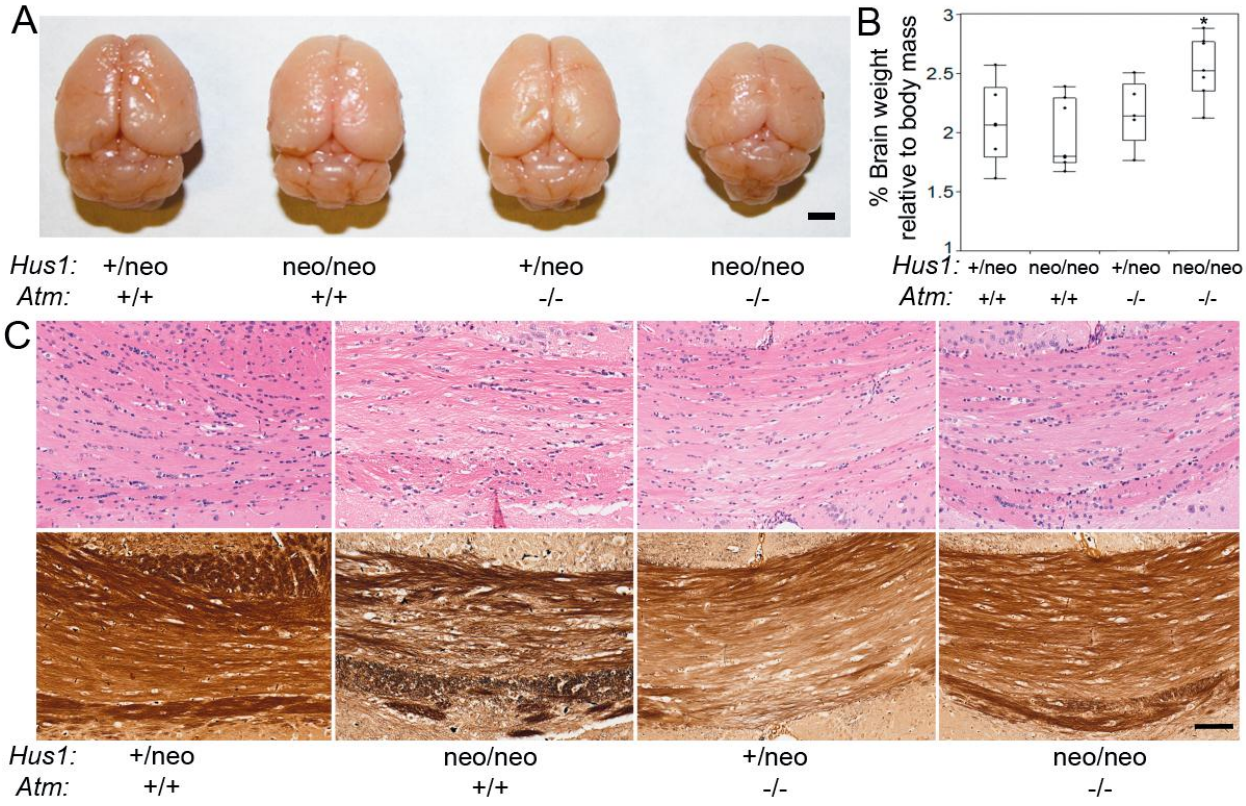
A
Hus1: +/neo neo/neo +/neo neo/neo
Atm: +/+ +/+ -/-
-/-
B
% Brain weight relative to body mass
3
2.5
2
1.5
1
*
Hus1: +/neo neo/neo +/neo neo/neo
Atm: +/+ +/+ -/- -/-
C
Hus1: +/neo neo/neo +/neo neo/neo
Atm: +/+ +/+ -/- -/-

Figure 2.5. Dwarfism in *Hus1*$^{neo/neo}$*Atm*$^{-/-}$ embryos and adult mice. A) Box plot indicates the body weight of E18.5 embryos of the indicated genotypes (n≥4 per group). *Hus1*$^{neo/neo}$*Atm*$^{-/-}$ embryos were significantly smaller than their littermates ($p<0.001$, Student's t-test). B) Representative image of newborn (P1) littermates of the indicated genotypes is shown. Scale bar represents 5 mm. C) Photograph of 6-week old male littermates of the indicated genotypes. D) Body weight analysis of *Hus1*$^{neo/neo}$*Atm*$^{-/-}$ mice and control littermates. The average body weights of female mice (n≥5) of the indicated genotypes, from weaning to 9 weeks of age, are shown. The mean body weight was significantly lower for *Hus1*$^{+/neo}$*Atm*$^{-/-}$ mice as compared to the *Atm*$^{+/+}$ groups (*$p<0.05$; Mixed Model Analysis); *Hus1*$^{neo/neo}$*Atm*$^{-/-}$ mice had significantly lower mean body weight as compared to all other groups (**$p<0.01$; Mixed Model Analysis). E) Northern blot analysis of transcript levels of *Igf1* and *Ghr* in total RNA from liver. *Gapdh* was used as a loading control.

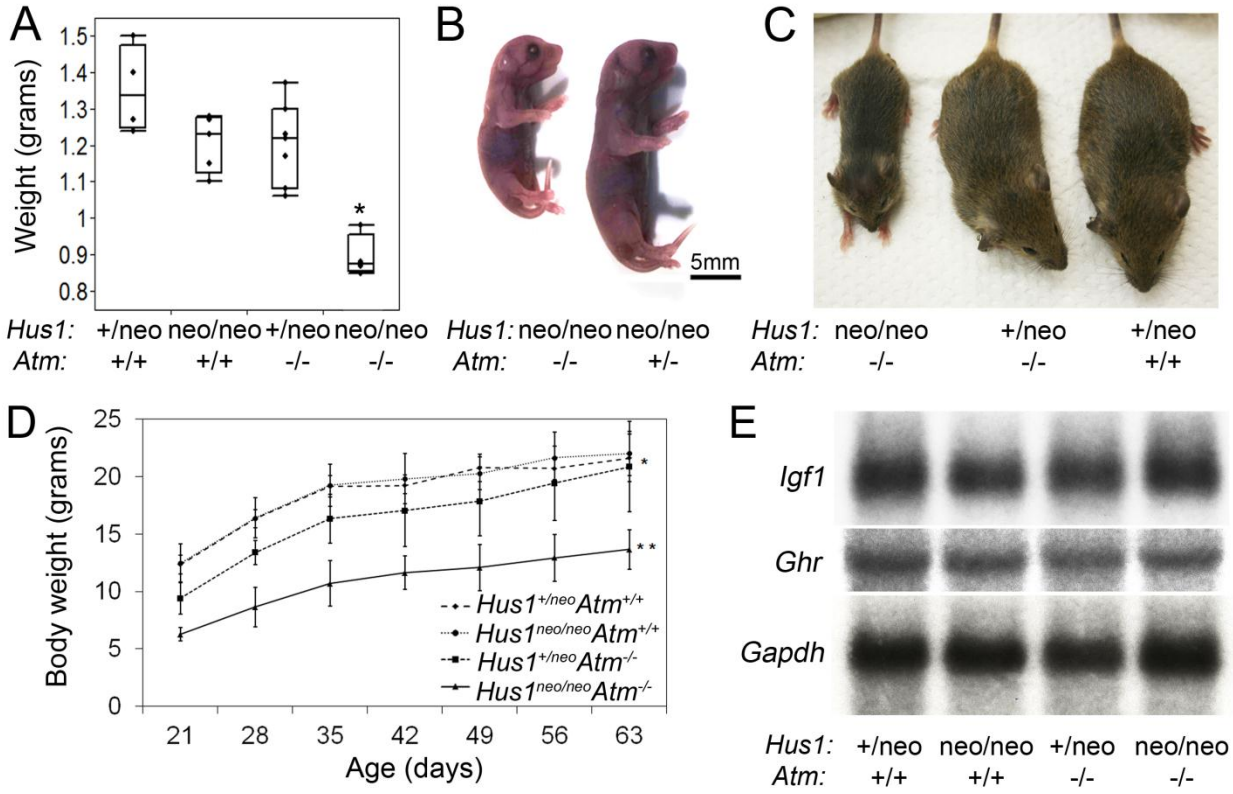
A
Weight (grams)
1.5
1.4
1.3
1.2
1.1
1
0.9
0.8
*
Hus1: +/neo neo/neo +/neo neo/neo
Atm: +/+ +/+ -/- -/-
B
5mm
Hus1: neo/neo neo/neo
Atm: -/- +/-
C
Hus1: neo/neo +/neo +/neo
Atm: -/- -/- +/+
D
Body weight (grams)
25
20
15
10
5
0
21 28 35 42 49 56 63
Age (days)
*
**
Hus1+/neoAtm+/+
Hus1neo/neoAtm+/+
Hus1+/neoAtm-/-
Hus1neo/neoAtm-/-
E
Igf1
Ghr
Gapdh
Hus1: +/neo neo/neo +/neo neo/neo
Atm: +/+ +/+ -/- -/-

Table 2.3. Organ weight in *Hus1*$^{neo/neo}$*Atm*$^{-/-}$ and littermate control mice [a]

Genotype	Relative organ weight (%) [b]			
	Hus1$^{+/neo}$*Atm*$^{+}$ [c] (n=6)	*Hus1*$^{neo/neo}$*Atm*$^{+/+}$ (n=7)	*Hus1*$^{+/neo}$*Atm*$^{-/-}$ (n=5)	*Hus1*$^{neo/neo}$*Atm*$^{-/-}$ (n=7)
Total Brain	2.1 ± 0.3%	2.0 ± 0.3%	2.2 ± 0.3%	2.6 ± 0.3%*
Cerebrum	1.4 ± 0.2%	1.4 ± 0.2%	1.5 ± 0.2%	1.8 ± 0.2%†
Cerebellum	0.6 ± 0.1%	0.5 ± 0.1%	0.7 ± 0.2%‡	0.7 ± 0.1%‡
Spleen	0.5 ± 0.2%	0.4 ± 0.1%	0.4 ± 0.1%	0.3 ± 0.1%
Liver	5.4 ± 0.1%	5.6 ± 0.4%	5.6 ± 0.8%	6.1 ± 0.5%
Kidney	0.7 ± 0.1%	0.8 ± 0.1%	0.7 ± 0.1%	0.8 ± 0.1%
Thymus	0.5 ± 0.2%	0.5 ± 0.2%	0.4 ± 0.1%	0.5 ± 0.1%
Testis	0.4 ± 0.1%	0.4 ± 0.1%	0.1 ± 0.1%$^{\#}$	0.2 ± 0.1%$^{\#}$

[a] Mice were sacrificed at 6 weeks of age and the indicated organs were weighed.

[b] Values represent percent organ weight relative to total body weight ± standard deviation. Relative brain mass was greater in the *Hus1*$^{neo/neo}$*Atm*$^{-/-}$ mice ($^{*}p<0.05$) as compared to all other groups. A significant difference also was apparent for cerebrum alone ($^{\dagger}p<0.005$), whereas the cerebellum was relatively larger in both *Hus1*$^{neo/neo}$*Atm*$^{-/-}$ ($^{\ddagger}p<0.006$) and *Hus1*$^{+/neo}$*Atm*$^{-/-}$ ($^{\ddagger}p<0.03$) mice as compared to *Hus1*$^{neo/neo}$*Atm*$^{+/+}$ animals. Testis weight was relatively lower for both *Hus1*$^{+/neo}$*Atm*$^{-/-}$ and Hus1$^{neo/neo}$Atm$^{-/-}$ mice as compared to all other genotypes ($^{\#}p<0.001$). Statistical analysis was performed by Student's t-test.

[c] *Hus1*$^{+/neo}$*Atm*$^{+}$ refers to the mean for *Hus1*$^{+/neo}$*Atm*$^{+/+}$ (n=3) and *Hus1*$^{+/neo}$*Atm*$^{+/-}$ (n=3) control littermates.

with previous reports (Barlow, Hirotsune et al. 1996; Elson, Wang et al. 1996; Xu, Ashley et al. 1996), modestly reduced body size was observed in *Hus1*$^{+/neo}$*Atm*$^{-/-}$ mice defective for *Atm* alone ($p<0.05$; Mixed model analysis). This phenotype was significantly enhanced in *Hus1*$^{neo/neo}$*Atm*$^{-/-}$ animals, which on average were 40% smaller by weight than control littermates at 6 weeks of age (Figure 2.5 D; $p<0.01$; Mixed model analysis). Most organs were proportionally smaller in both *Hus1*$^{+/neo}$*Atm*$^{-/-}$ and *Hus1*$^{neo/neo}$*Atm*$^{-/-}$ mice as compared to *Hus1*$^{+/neo}$*Atm*$^{+/+}$ controls (Table 2.3). *Hus1*$^{neo/neo}$*Atm*$^{-/-}$ mice showed a slight increase in relative brain size as compared to mice of all other genotypes, but this was not associated with any apparent histopathological abnormalities (Figure 2.4).

It is well established that the somatotroph axis that includes growth hormone (GH) and insulin-like growth factor 1 (IGF1) plays important roles in somatic growth and aging (Lupu, Terwilliger et al. 2001). Deficiencies in the GH/IGF1 somatotroph axis are observed in some mouse mutants that display dwarfism in conjunction with underlying DDR defects (Niedernhofer 2008). In order to understand the molecular basis for the dwarfism in *Atm*/*Hus1* mutant mice we analyzed the expression levels of *Igf1* and *Ghr* and found no difference in their transcript levels in livers of 6-week old mice of representative genotypes (Figure 2.5E), findings that were confirmed by qPCR (data not shown). Furthermore, preliminary analyses revealed no differences in circulating IGF1 levels in *Hus1*$^{neo/neo}$*Atm*$^{-/-}$ mice relative to controls (data not shown). Overall these results demonstrate that combined *Hus1* and *Atm* deficiency has a

Figure 2.6. Skeletal abnormalities in *Hus1*$^{neo/neo}$*Atm*$^{-/-}$ embryos and adult mice. A) Shown is a representative image of Alizarin red-Alcian blue stained skulls from E18.5 littermates of the indicated genotypes. Dotted lines outline the region where the skull plates have yet to fill in and fuse. The arrowhead indicates the fenestrations present in the *Hus1*$^{neo/neo}$*Atm*$^{-/-}$ skull. B) Skulls were prepared from 6-week old littermates of the indicated genotypes and photographed. The arrowhead indicates the fenestrations present in the parietal bone. The arrow indicates abnormal sutures of the mutant. Lower panels: higher magnification view of sutures in the *Hus1*$^{neo/neo}$*Atm*$^{-/-}$ (left) and *Hus1*$^{+/neo}$*Atm*$^{-/-}$ (right) skulls. C) A representative image of the skulls from 6 week old littermates of the indicated genotypes is shown. The outline was generated in Photoshop to illustrate the doming of the skull. D, E) 3D reconstructions based on micro-CT data for forelimbs (D) or hindlimbs (E) from *Hus1*$^{neo/neo}$*Atm*$^{-/-}$ and *Hus1*$^{+/neo}$*Atm*$^{-/-}$ mice, and bar graphs of the corresponding measurement data (n=3 per genotype). Red arrowheads point to the mesophalanx of digit V. The relative length of mesophalanx V in both forelimbs and hindlimbs was significantly shorter in *Hus1*$^{neo/neo}$*Atm*$^{-/-}$ mice as compared to all other genotypes (*$p<0.001$; Student's t-test).

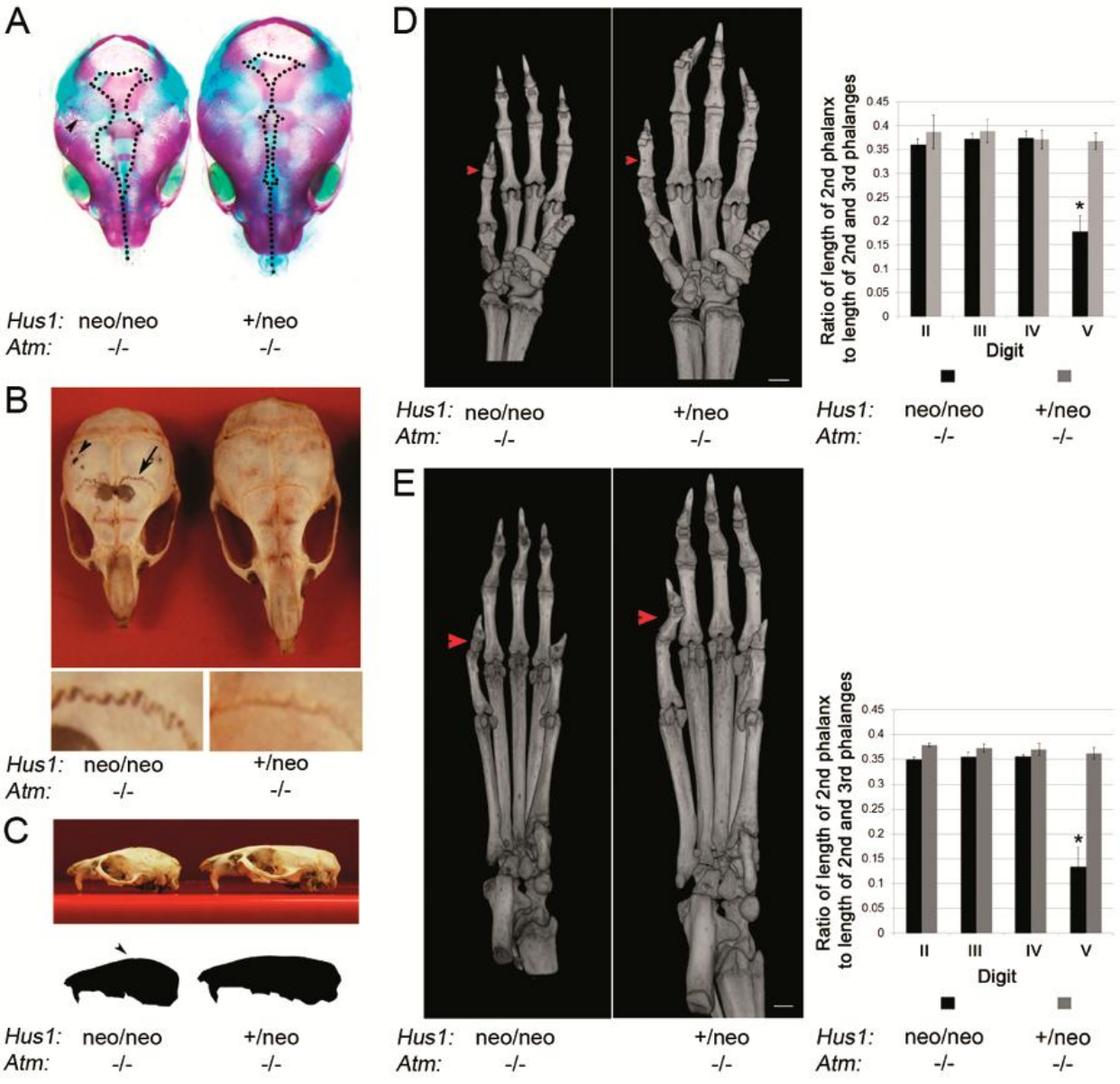
A
Hus1: neo/neo +/neo
Atm: -/- -/-
B
Hus1: neo/neo +/neo
Atm: -/- -/-
C
Hus1: neo/neo +/neo
Atm: -/- -/-
D
Hus1: neo/neo +/neo
Atm: -/- -/-
Ratio of length of 2nd phalanx to length of 2nd and 3rd phalanges
0.45
0.4
0.35
0.3
0.25
0.2
0.15
0.1
0.05
0
*
II III IV V
Digit
Hus1: neo/neo +/neo
Atm: -/- -/-
E
Hus1: neo/neo +/neo
Atm: -/- -/-
Ratio of length of 2nd phalanx to length of 2nd and 3rd phalanges
0.45
0.4
0.35
0.3
0.25
0.2
0.15
0.1
0.05
0
*
II III IV V
Digit
Hus1: neo/neo +/neo
Atm: -/- -/-

Figure 2.7. Skeletal abnormalities in *Hus1*$^{neo/neo}$*Atm*$^{-/-}$ mice. A) Littermate embryos of the indicated genotypes at E15.5 were stained with Alizarin Red and Alcian Blue. Arrow heads indicate the incomplete closure of the head bones and the presence of fenestrations. The dotted lines outline the head bones and highlight the incomplete development in *Hus1*$^{neo/neo}$*Atm*$^{-/-}$ as compared to *Hus1*$^{+/neo}$*Atm*$^{-/-}$ embryos. B) Limbs of littermate embryos of the indicated genotypes at E15.5 were stained with Alizarin Red and Alcian Blue. Red arrow heads indicate the mesophalanx of the fifth digit. Insets show magnified views of the fifth digit in black and white. C) Limbs of littermate embryos of the indicated genotypes at P10 were stained with Alizarin Red and Alcian Blue. Red arrow heads indicate the mesophalanx of the fifth digit. D) A schematic of the dorsal aspect of the mouse skull is shown (top). The landmark points used for the analysis are numbered. Representative measurements were chosen for the analysis as follows: 1-2 Nose length; 1-6 Skull length; 2-4 Naso-parietal length; 2-6 Naso-occipital length; 4-5 Interparietal length; 7-12 Skull width; 8-13 Intersquamosal distance; 9-14 Interzygomatic distance; 10-15 Intercanthal distance; 11-16 Face width; 13-14 Zygomatic length; 14-15 Premaxilo-zygomatic distance; 15-16 Premaxili-maxilo distance; 16-18 Maxilo-frontal length; 17-18 Frontal width. Image modified from (Cook 1965) with permission from Elsevier. Visualization of the marked surface points is shown on a 3D reconstruction of micro-CT images of a *Hus1*$^{+/neo}$*Atm*$^{+/+}$ mouse skull (bottom). The distance between any two surface points was then computed using Euclidean distance of the mapped image coordinates as described in

Material and Methods. E) Principal component 1 (PC1) scores for each individual mouse (filled circles) shown as boxplots by genotype ($n \geq 5$ for each genotypic class). The *Hus1*$^{neo/neo}$*Atm*$^{-/-}$ skulls differed significantly from all other genotypes along the PC1 axis ($p<0.0001$; Student's t-test). *Hus1*$^{+/neo}$*Atm*$^{-/-}$ skulls were significantly smaller than those of *Hus1*$^{neo/neo}$*Atm*$^{+/+}$ mice ($p<0.05$, Student's t-test). F) Factor loadings for principal component one. Bars indicate the correlations and inverse correlations (17-18, 4-5) between individual measurements and PC1. The pattern of variation captured by PC1 is a combination of both change in overall skull size and shape: the skulls of the *Hus1*$^{neo/neo}$*Atm*$^{-/-}$ were smaller overall but their interparietal lengths (4-5) and frontal widths (17-18) are larger. The PC analysis was repeated excluding the *Hus1*$^{neo/neo}$*Atm*$^{-/-}$ samples and no differences were observed.

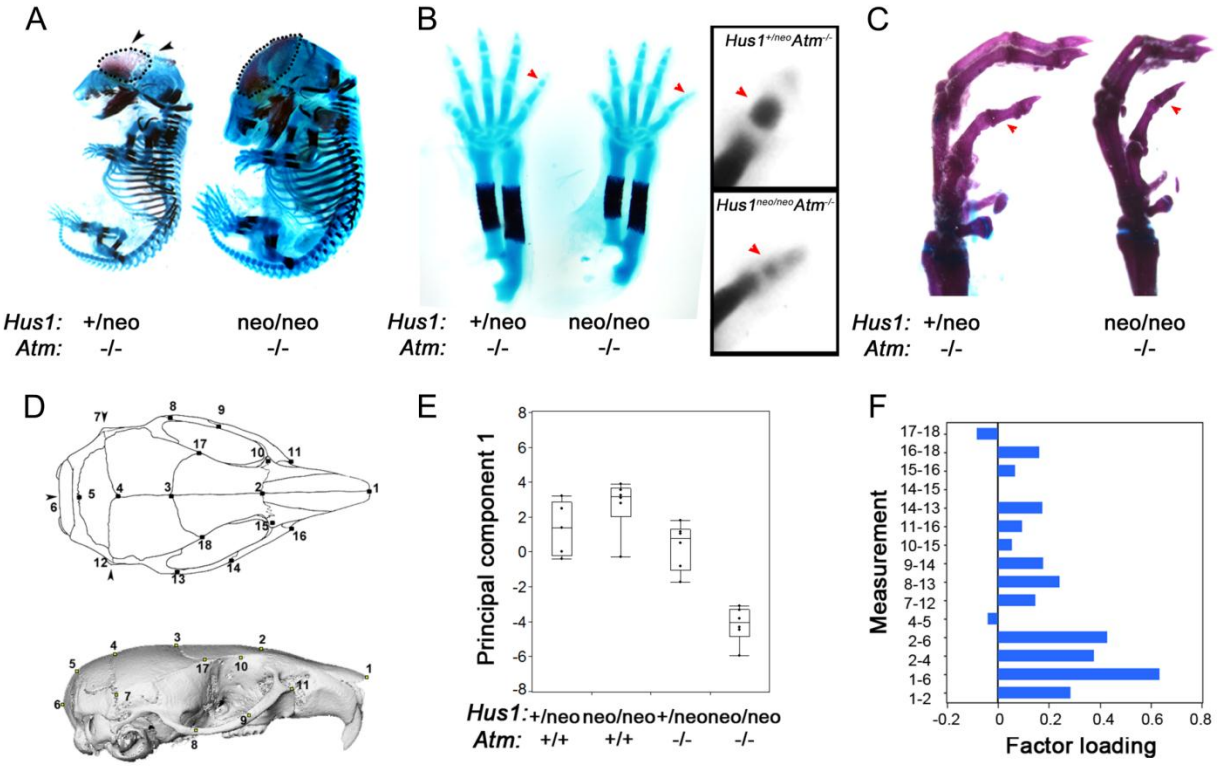
A
Hus1: +/neo neo/neo
Atm: -/- -/-
B
Hus1: +/neo neo/neo
Atm: -/- -/-
Hus1+/neoAtm-/-
Hus1neo/neoAtm-/-
C
Hus1: +/neo neo/neo
Atm: -/- -/-
D
E
Principal component 1
Hus1: +/neo neo/neo +/neo neo/neo
Atm: +/+ +/+ -/- -/-
F
Measurement
17-18
16-18
15-16
14-15
14-13
11-16
10-15
9-14
8-13
7-12
4-5
2-6
2-4
1-6
1-2
-0.2 0 0.2 0.4 0.6 0.8
Factor loading

severe impact on body size from mid-gestation to adulthood and that this proportional dwarfism arises independently of detectable abnormalities in the somatotroph axis.

2.4.4 **Skeletal abnormalities in Hus1$^{neo/neo}$Atm$^{-/-}$ mice.**

Visual inspection of *Hus1$^{neo/neo}$Atm$^{-/-}$* mice also revealed fronto-parietal alopecia and an abnormal facial morphology (Figure 2.5C). To understand the origins of these abnormalities, we performed Alizarin-red/Alcian-blue staining of embryos. At E18.5, *Hus1$^{neo/neo}$Atm$^{-/-}$* embryos had widely open sagittal (midline) sutures and presented an array of fenestrations primarily in the parietal bone (Figure 2.6A) that also were apparent as early as E15.5 (Figure 2.7A). In order to characterize the craniofacial defects in adult animals, we first produced isolated skull preparations from mice at 6 week of age. Grossly, *Hus1$^{neo/neo}$Atm$^{-/-}$* skulls showed a domed morphology with incomplete closure of the sagittal sutures and reduced bone thickness in the fronto-parietal region, multiple fenestrations in the parietal bone and jagged coronal (fronto-parietal) sutures (Figure 2.6 B, C). To identify and quantify patterns in skull morphology, we analyzed high resolution three-dimensional images generated by micro-computed tomography (micro-CT) (Figure 2.7 D). A series of measurements were then subjected to principal component (PC) analysis to identify suites of changes in skull morphology. The first PC by itself explained 83.6% of the variance in the 23 skull measurements and therefore in a single number captured the significant variation

between *Hus1*$^{neo/neo}$*Atm*$^{-/-}$ samples and those of *Hus1*$^{+/neo}$*Atm*$^{+/+}$, *Hus1*$^{neo/neo}$*Atm*$^{+/+}$, and *Hus1*$^{+/neo}$*Atm*$^{-/-}$ genotypes (Figure 2.7 E). The correlations or factor loadings between the PC1 score and each distance measured for each mouse further resolved the pattern of variation: the skulls of *Hus1*$^{neo/neo}$*Atm*$^{-/-}$ mice were smaller overall and differed in shape, with an elongated inter-parietal bone and a wider frontal bone, which increased the inter-orbital distance (Figure 2.7 F).

Detailed analysis of the embryonic skeletal preparations also revealed brachymesophalangy of the fifth digit (Figure 2.7 B, C). Interestingly, this and the related phenotype of clinodactyly are associated with several hereditary GIN syndromes, other congenital disorders, and fetal teratogen exposure (Rypens, Dubois et al. 2006). Further inspection of micro-CT images indicated that the phalangeal defect was fully penetrant in adult *Hus1*$^{neo/neo}$*Atm*$^{-/-}$ mice and affected both the forelimbs and hindlimbs (Figure 2.6 D, E). Quantitative measurements showed that the mesophalanx of the fifth digit was less than one-half of the expected size in *Hus1*$^{neo/neo}$*Atm*$^{-/-}$ mice relative to controls, whereas the remaining digits were unaffected ($p<0.001$; Student`s t test). Considered together with the craniofacial defects described above, these results demonstrate an essential dual function for *Atm* and *Hus1* in the development of the skeleton and suggest a potential elevated sensitivity of particular bone progenitor cells to checkpoint impairment and genomic instability.

2.4.5 **Increased genomic instability in adult mice defective for both Atm and Hus1.**

HUS1 and ATM are integral components of DNA damage signaling pathways that function to protect genomic integrity. We therefore tested the impact of combined *Atm* and *Hus1* defects on GIN in adult mice by measuring micronucleus (MN) formation in peripheral blood cells using a flow cytometry based assay. MN are entire chromosomes or fragments of chromosomes that have not been incorporated in the main nuclei at cell division and are a hallmark of GIN. Consistent with previous findings (Shima, Hartford et al. 2003; Levitt, Zhu et al. 2007), a moderate *Hus1* defect alone in $Hus1^{neo/neo}Atm^{+/+}$ mice caused no significant change in MN formation relative to $Hus1^{+/neo}Atm^{+/+}$ littermate controls, whereas *Atm* deficiency alone was associated with significantly increased MN formation in $Hus1^{+/neo}Atm^{-/-}$ mice (Figure 2.8 A; $p<0.001$; Student's t test). Notably, $Hus1^{neo/neo}Atm^{-/-}$ mice had more than an additive increase in MN formation when compared to $Hus1^{neo/neo}Atm^{+/+}$ and $Hus1^{+/neo}Atm^{-/-}$ animals ($p=0.002$; Univariate Analysis of Variance). By contrast, expression of damage inducible genes such as *p21* was unaltered in adult liver, a relatively quiescent tissue (Figure 2.9). These observations suggest that phenotypes associated with combined *Atm* and *Hus1* defects in adult mice may be more pronounced in proliferating cell populations such as blood cell precursors and highlight a potential role for replication stress as a key factor in the observed genetic interaction.

Figure 2.8. Increased genomic instability with no change in tumor predisposition in *Hus1*$^{neo/neo}$*Atm*$^{-/-}$ mice. A) Bar graph shows the average percentage of peripheral blood cells with micronuclei in mice of the indicated genotypes. *Hus1*$^{neo/neo}$*Atm*$^{+/+}$ and *Hus1*$^{+/neo}$*Atm*$^{+/+}$ mice showed similar levels of GIN while *Hus1*$^{+/neo}$*Atm*$^{-/-}$ mice had a significant increase in micronucleus formation ($p<0.001$; Student's t test). The combined effect of *Hus1* impairment in an *Atm* null background (*Hus1*$^{neo/neo}$*Atm*$^{-/-}$) resulted in a greater than additive increase in GIN ($p=0.002$; Univariate Analysis of Variance). B) Bar graph shows the relative number of thymocytes in 6-week old mice of the indicated genotypes ($n\geq3$ per group) expressed as a percentage of the value for *Hus1*$^{+/neo}$*Atm*$^{+/+}$ control littermates. Error bars indicate standard deviation. The entire thymus from each mouse was harvested and mechanically disrupted, and viable trypan blue negative thymocytes were counted using a hemocytometer. The relative number of thymocytes was significantly lower for both *Hus1*$^{+/neo}$*Atm*$^{-/-}$ and *Hus1*$^{neo/neo}$*Atm*$^{-/-}$ mice (*$p<0.001$; Student's t-test). C) Representative Hematoxylin and Eosin stained sections of thymic lymphomas from *Hus1*$^{+/neo}$*Atm*$^{-/-}$ (left) and *Hus1*$^{neo/neo}$*Atm*$^{-/-}$ (right) mice. Scale bar represents 50μm. D) Cohorts of *Hus1*$^{neo/neo}$*Atm*$^{-/-}$ ($n=41$) and *Hus1*$^{+/neo}$*Atm*$^{-/-}$ ($n=43$) mice were monitored for tumor development as described in Material and Methods. A Kaplan-Meier survival curve is shown. Overall survival was not significantly different between genotypes ($p=0.644$, log-rank test)

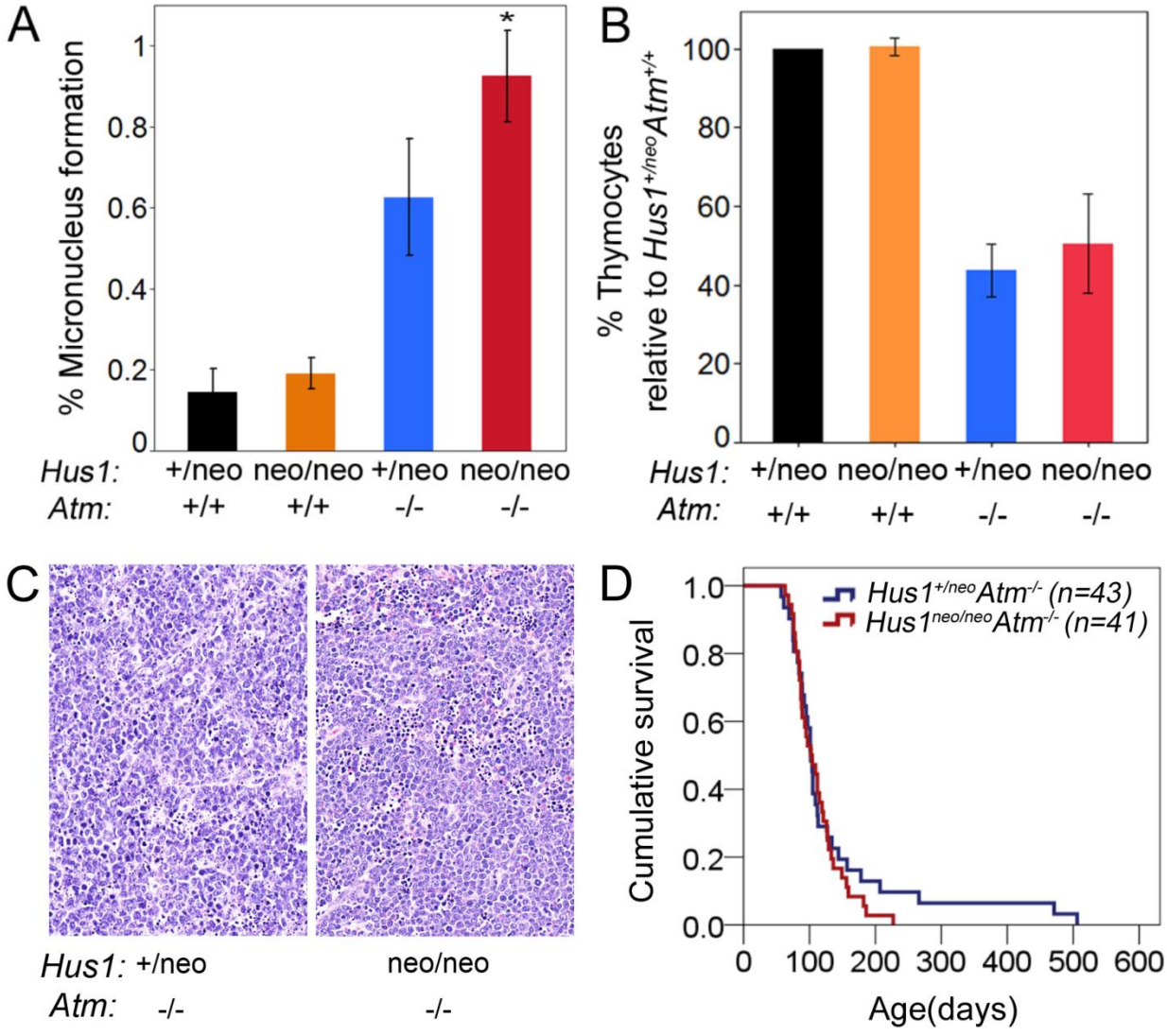
A
% Micronucleus formation
0
0.2
0.4
0.6
0.8
1
*
Hus1: +/neo neo/neo +/neo neo/neo
Atm: +/+ +/+ -/- -/-
B
% Thymocytes relative to Hus1+/neoAtm+/+
0
20
40
60
80
100
Hus1: +/neo neo/neo +/neo neo/neo
Atm: +/+ +/+ -/- -/-
C
Hus1: +/neo neo/neo
Atm: -/- -/-
D
Cumulative survival
0.0
0.2
0.4
0.6
0.8
1.0
Hus1+/neoAtm-/- (n=43)
Hus1neo/neoAtm-/- (n=41)
0 100 200 300 400 500 600
Age(days)

Figure 2.9. Liver transcript analysis in *Hus1/Atm* double mutant and control mice. Bar graph shows the fold expression level of *p21*, *Bax*, and *Gstt2* in liver samples (n=3) from mice of the indicated genotypes relative to $Hus1^{+/neo}Atm^{+/+}$. No significant differences were detected.

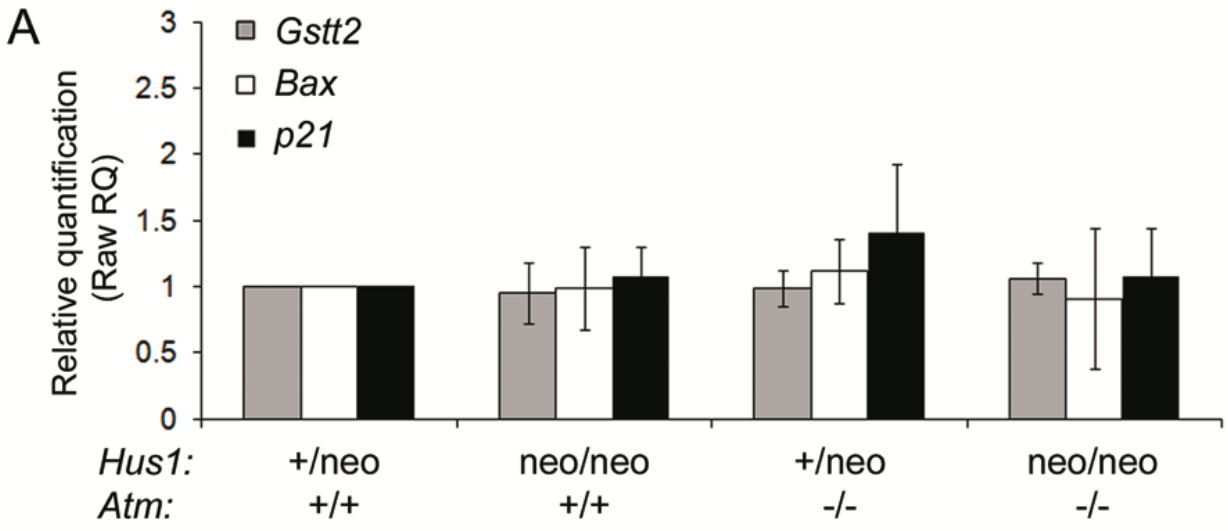
A
Gstt2
Bax
p21
Relative quantification
(Raw RQ)
3
2.5
2
1.5
1
0.5
0
Hus1:
Atm:
+/neo
+/+
neo/neo
+/+
+/neo
-/-
neo/neo
-/-

Table 2.4. Blood composition in *Hus1*$^{neo/neo}$*Atm*$^{-/-}$ and littermate control mice [a]

Test	*Hus1*$^{+}$*Atm*$^{+}$ [b] (n=5)	*Hus1*$^{+/neo}$*Atm*$^{-/-}$ (n=4)	*Hus1*$^{neo/neo}$*Atm*$^{-/-}$ (n=4)	Units
Hematocrit	49.2 ± 3.6	48.0 ± 3.9	45.3 ± 7.8	%
Hemoglobin	14.7 ± 0.8	15.1 ± 1.2	13.7 ± 2.0	g/dL
Red Blood Cells (RBC)	9.0 ±1.9	9.4 ± 0.7	8.9 ± 1.5	mill/μL
Mean cell volume (MCV)	51.4 ± 3.4	51.0 ± 1.6	51.0 ± 1.4	fL
Mean corpuscular hemoglobin (MCH)	15.6 ± 0.5	16.0 ± 0	15.5 ± 0.6	pg
Mean corpuscular hemoglobin concentration (MCHC)	30.2 ± 2.3	31.8 ± 0.5	30.5 ± 1.0	g/dL
Red blood cell distribution width (RDW)	13.0 ± 0.7	12.9 ± 0.6	13.5 ± 0.8	%
White Blood Cells (WBC)	6.7 ± 0.3	4.7 ± 3.2	5.1 ± 2.8	thou/μL
Platelet Count	1477 ± 193.5	1368.3 ± 509.2	1149.7 ± 516.1	thou/μL
Mean Platelet Volume (MPV)	8.2 ± 1.0	8.7 ± 1.0	8.5 ± 1.6	fL
Segmented Neutrophil(s)	0.7 ± 0.4	1.7 ± 2.0	1.8 ± 1.8	thou/μL
*Lymphocyte(s)	5.6 ± 0.2	2.3 ± 0.9[c]	2.5 ± 1.1[c]	thou/μL
Monocyte(s)	0.2 ± 0.1	0.2 ± 0.1	0.3 ± 0.2	thou/μL
Eosinophil(s)	0.2 ± 0.1	0.3 ± 0.1	0.3 ± 0.1	thou/μL
Basophil(s)	0.1 ± 0.1	0.1 ± 0.1	0.1 ± 0.1	thou/μL
Large Unstained Cell(s)	0.1 ± 0.1	0.2 ± 0.2	0.3 ± 0.1	thou/μL

[a] Blood was collected from 6-week old mice by mandibular bleeding into EDTA containing tubes (Hoff 2000) and sent to Cornell Animal Health Diagnostic Center.

[b] *Hus1*$^{+}$*Atm*$^{+}$ refers to the mean for *Hus1*$^{+/neo}$*Atm*$^{+/+}$ (n=1), *Hus1*$^{+/neo}$*Atm*$^{+/-}$ (n=2), *Hus1*$^{neo/neo}$*Atm*$^{+/+}$ (n=1) and *Hus1*$^{neo/neo}$*Atm*$^{+/-}$ (n=1) mice.

[c] The only statistically significant differences observed were between *Atm*$^{-/-}$ (both *Hus1*$^{+/neo}$*Atm*$^{-/-}$ and *Hus1*$^{neo/neo}$*Atm*$^{-/-}$) and *Atm*$^{+}$ mice ($p < 0.05$; Student's t-test). Values are consistent with previously reported blood composition data for wild-type and Atm-deficient mice (Barlow, Hirotsune et al. 1996; Elson, Wang et al. 1996; Xu, Ashley et al. 1996; Wirth-Dzieciolowska, Karaszewska et al. 2009).

Increased GIN may influence different steps *en-route* to carcinogenesis, including tumor initiation and progression, and in *Atm*-null mice contributes to the development of thymic lymphoma with near complete penetrance (Barlow, Hirotsune et al. 1996; Elson, Wang et al. 1996; Xu, Ashley et al. 1996). Prior to tumor development, $Hus1^{neo/neo}Atm^{-/-}$ and $Hus1^{+/neo}Atm^{-/-}$ mice contained similar numbers of lymphocytes in the thymus (Figure 2.8 B) and circulating blood (Table 2.4) and subsequently showed no significant difference in tumor-free survival as determined by Kaplan-Meier survival analysis (Figure 2.8 D). Furthermore, the resulting neoplasms were indistinguishable histopathologically (Figure 2.8 C). Together, these results reveal that combined defects in *Atm* and *Hus1* result in synergistic increases in GIN in adult mice but without major consequences on thymic tumorigenesis.

2.4.6 **Partial *Hus1* impairment synergizes with *Atm* deficiency to accelerate senescence without detectably altering key DNA damage checkpoint signaling events or radiation sensitivity.** The strong genetic interaction observed between *Atm* and *Hus1* raised the possibility of overlapping roles for these checkpoint proteins in DNA damage signaling. Complete *Hus1* inactivation results in impaired activation of the ATR substrate CHK1 but does not diminish induction of the ATM substrates CHK2 or p53 (Weiss, Matsuoka et al. 2002). Consistent with the prevailing view that ATM activation occurs independently of the 911 complex, we observed that IR- or UV-induced ATM phosphorylation occurred to a similar or greater extent in *Hus1*-

null cells as compared to *Hus1*-proficient controls (Figure 2.10A). To better understand the relationship between *Hus1* and *Atm* at the cell and molecular levels, we isolated primary mouse embryonic fibroblasts (MEFs) from the *Atm*/*Hus1* mouse model and analyzed their behavior in culture. Consistent with previous results (Xu and Baltimore 1996; Levitt, Zhu et al. 2007), *Atm*-deficient $Hus1^{+/neo}Atm^{-/-}$ MEFs underwent senescence prematurely whereas $Hus1^{neo/neo}Atm^{+/+}$ MEFs doubled in a manner similar to $Hus1^{+/neo}Atm^{+/+}$ control cells. The combination of *Atm* and *Hus1* defects in $Hus1^{neo/neo}Atm^{-/-}$ MEFs resulted in extremely rapid senescence after just a few doublings (Figure 2.11A). Chromosome analysis at the first passage revealed increased frequency of chromosomal abnormalities in $Hus1^{neo/neo}Atm^{+/+}$ single mutant cells when compared to $Hus1^{+/neo}Atm^{+/+}$ cells ($p<0.05$; Student's t test). ATM deficiency in $Hus1^{+/neo}Atm^{-/-}$ and $Hus1^{neo//neo}Atm^{-/-}$ cell lines resulted in increased number of abnormalities ($p<0.05$ Student's t test) with the *Hus1*/*Atm* double mutants having a significant increase in extensive chromosomal damage ($p<0.01$; Student's t test) as well as an increased frequency in radial figures ($p<0.05$; Student's t test) when compared to $Atm^{-/-}$ single mutant alone (Figure 2.12). Nevertheless, cells of all genotypes were capable of undergoing spontaneous immortalization, after which they doubled at similar rates when maintained under standard 3T3 culture conditions, both in low (3%) (data not shown) and normal (20%) O_2 levels (Figure 2.11A). The proliferative capacity of the spontaneously immortalized *Atm*/*Hus1* MEFs was analyzed under more stringent conditions by plating cells at low density and assessing

Figure 2.10. DNA damage signaling in *Atm/Hus1* double mutant mouse embryonic fibroblasts. A) Immortalized MEFs of the indicated genotypes were treated with 20Gy IR or 65J/m^2 UV, and total protein lysates were prepared at 0, 2 and 8 hours post-treatment. Samples were immunoblotted using antibodies specific for phospho-Ser1981-ATM, or Beta actin as a loading control. Similar results were obtained with an independent set of $Hus1^{-/-}p21^{-/-}$ and matched control $Hus1^{+/+}p21^{-/-}$ MEFs (data not shown). B) Primary MEFs at passage 1 or 2 were treated with 30Gy IR or 65J/m^2 UV and total cell protein lysates were prepared at 0, 2, 8 and 24 hours post-treatment and immunoblotted for CHK1, phosphoSer345-CHK1, CHK2 and p53. Arrow indicates the position of phosphorylated CHK2. Beta-actin was used as a loading control. C) Kaplan-Meier survival curves show the radiation sensitivity of mice of the indicated genotypes following exposure to 4Gy (left) or 5Gy (right) IR. The cohort treated with 4Gy included $Hus1^{+/neo}Atm^{+}$ (n=7; Atm^{+} is a combination of $Atm^{+/+}$ and $Atm^{+/-}$), $Hus1^{neo/neo}Atm^{+/+}$ (n=6), $Hus1^{+/neo}Atm^{-/-}$ (n=9) and $Hus1^{neo/neo}Atm^{-/-}$ (n=12) mice. The cohort treated with 5Gy included $Hus1^{+/neo}Atm^{+}$ (n=4), $Hus1^{neo/neo}Atm^{+/+}$ (n=6), $Hus1^{+/neo}Atm^{-/-}$ (n=6) and $Hus1^{neo/neo}Atm^{-/-}$ (n=4) mice. There were no significant differences in survival between $Hus1^{+/neo}Atm^{-/-}$ and $Hus1^{neo/neo}Atm^{-/-}$ mice after 4Gy (p=0.295) or 5Gy (p=0.366) as determined by log-rank test.

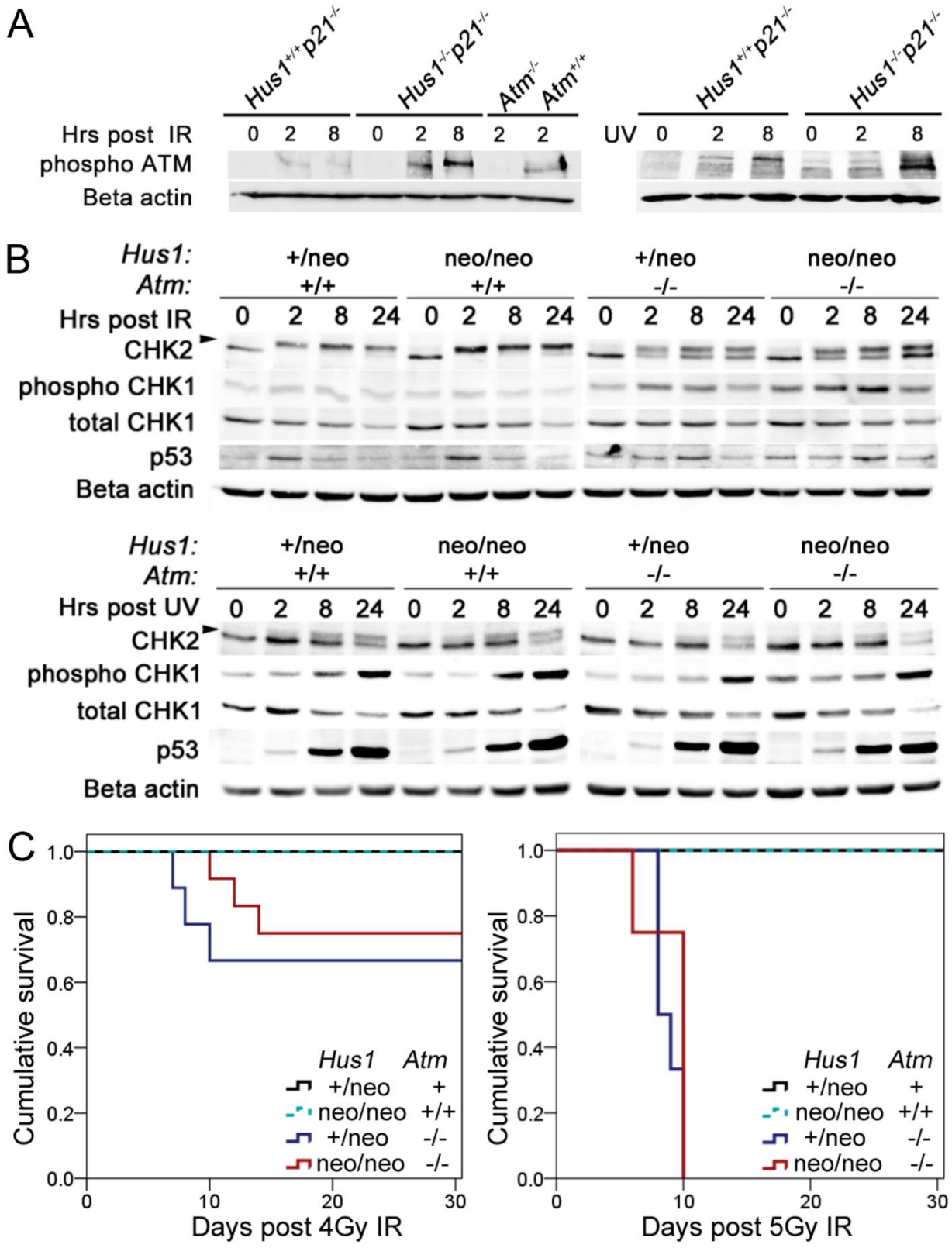
A
Hus1+/+p21-/-
Hus1-/-p21-/-
Atm-/-
Atm+/+
Hus1+/+p21-/-
Hus1-/-p21-/-
Hrs post IR
0 2 8 0 2 8 2 2
UV
0 2 8 0 2 8
phospho ATM
Beta actin
B
Hus1:
Atm:
+/neo
+/+
neo/neo
+/+
+/neo
-/-
neo/neo
-/-
Hrs post IR
0 2 8 24 0 2 8 24 0 2 8 24 0 2 8 24
CHK2
phospho CHK1
total CHK1
p53
Beta actin
Hus1:
Atm:
+/neo
+/+
neo/neo
+/+
+/neo
-/-
neo/neo
-/-
Hrs post UV
0 2 8 24 0 2 8 24 0 2 8 24 0 2 8 24
CHK2
phospho CHK1
total CHK1
p53
Beta actin
C
Cumulative survival
1.0
0.8
0.6
0.4
0.2
0.0
0 10 20 30
Days post 4Gy IR
Hus1 Atm
+/neo +
neo/neo +/+
+/neo -/-
neo/neo -/-
Cumulative survival
1.0
0.8
0.6
0.4
0.2
0.0
0 10 20 30
Days post 5Gy IR
Hus1 Atm
+/neo +
neo/neo +/+
+/neo -/-
neo/neo -/-

Figure 2.11. Rapid senescence and defective colony formation in *Hus1/Atm* double mutant MEFs. A) Primary mouse embryonic fibroblasts (MEFs) were isolated and maintained on a standard 3T3 culture protocol. Cumulative population doublings were calculate over time and plotted. B) Spontaneously immortalized *Atm/Hus1* MEFs were plated at 5 x 10^2 or 3 x 10^3 cells per well of 6 well dishes, and the colony forming potential of each cell line was assessed.

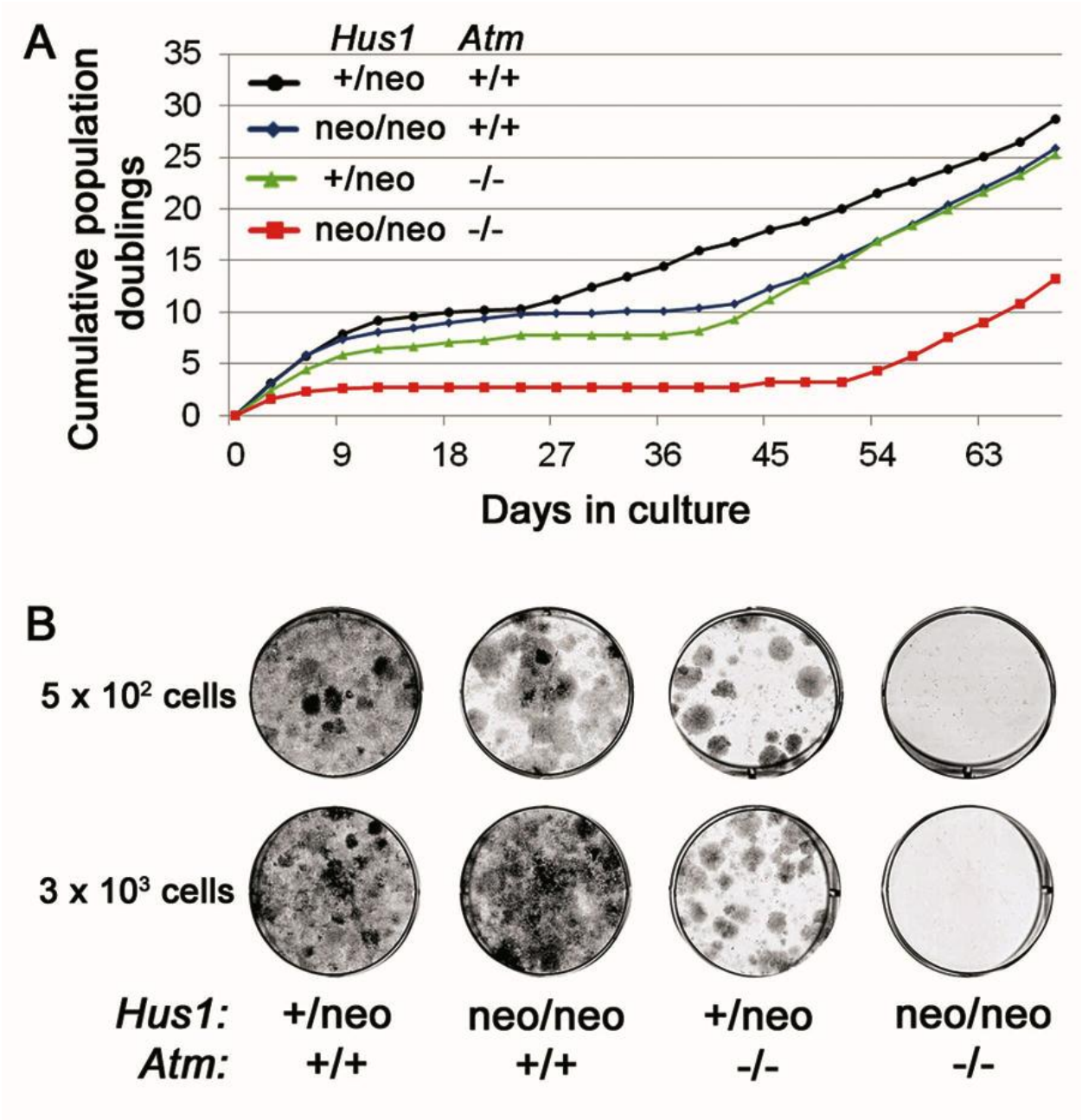
A
Hus1 Atm
+/neo +/+
neo/neo +/+
+/neo -/-
neo/neo -/-
Cumulative population doublings
0
5
10
15
20
25
30
35
0
9
18
27
36
45
54
63
Days in culture
B
5 x 10² cells
3 x 10³ cells
Hus1: +/neo neo/neo +/neo neo/neo
Atm: +/+ +/+ -/- -/-

the colony forming potential of each cell line. Colony formation was reduced in immortalized *Hus1*$^{neo/neo}$*Atm*$^{+/+}$ cells and impaired to an even greater degree in *Hus1*$^{+/neo}$*Atm*$^{-/-}$ MEFs. Remarkably, *Hus1*$^{neo/neo}$*Atm*$^{-/-}$ MEFs were completely defective for colony formation, under either atmospheric (Figure 1.11B) or low (data not shown) oxygen conditions, despite the fact that these cells showed normal proliferation when cultured at higher densities. Thus, simultaneous defects in *Atm* and *Hus1* result in accelerated senescence and, despite being compatible with spontaneous immortalization, cause profound impairment of the capacity of single cells to grow out as colonies.

To further understand the cooperative relationship between HUS1 and ATM in DNA damage signaling, we next treated the *Atm*/*Hus1* primary MEFs with UV or IR and assessed the activation of canonical ATR and ATM downstream targets. Untreated *Hus1*$^{neo/neo}$*Atm*$^{-/-}$ MEFs had slightly higher basal levels of p53 and phospho-CHK1 (Figure 2.10B), suggestive of increased spontaneous DNA damage accumulation. Moderate *Hus1* impairment alone had no detectable effect on DNA damage signaling upon IR treatment, with comparable levels of CHK2 phosphorylation and p53 accumulation occurring in *Hus1*$^{+/neo}$*Atm*$^{+/+}$ and *Hus1*$^{neo/neo}$*Atm*$^{+/+}$ cells. The slight accumulation of phosphorylated CHK1 following IR also was unchanged in *Hus1*$^{neo/neo}$*Atm*$^{+/+}$ cells. Lacking ATM alone, *Hus1*$^{+/neo}$*Atm*$^{-/-}$ cells showed delayed induction of both CHK2 and p53 following IR and a slight increase in CHK1 phosphorylation. Interestingly, *Hus1*$^{neo/neo}$*Atm*$^{-/-}$ MEFs showed the same IR-

Figure 2.12. Increased chromosomal abnormalities in *Hus1/Atm* double mutant MEFs. Metaphases from passage 1 (P1) cells lines of the following genotypes were utilized: $Hus1^{+/neo}Atm^{+/+}$ (n=3), $Hus1^{neo/neo}Atm^{+/+}$ (n=3), $Hus1^{+/neo}Atm^{-/-}$ (n=4), $Hus1^{neo/neo}Atm^{+/+}$ (n=4). Chromosome preparations were stained with Giemsa and imaged at 160X magnification. A) Images of *Hus1/Atm* MEFs of the indicated genotypes are shown. Red arrowheads point to chromosomal breaks/gaps. The panel for $Hus1^{neo/neo}Atm^{-/-}$ genotype exemplifies a typical metaphase with extensive chromosomal abnormalities. B) Quantification of the frequency of chromosomal abnormalities per metaphase spread in *Hus1/Atm* MEFs of the indicated genotypes. Extensive damage refers to metaphases that contained too many chromosome abnormalities to be counted. C) Table of occurrence of the different types of gross chromosomal abnormalities. The total number of breaks/gaps, fusions, radial chromosomes and acentric chromosomes was quantified for cells of each genotype.

A

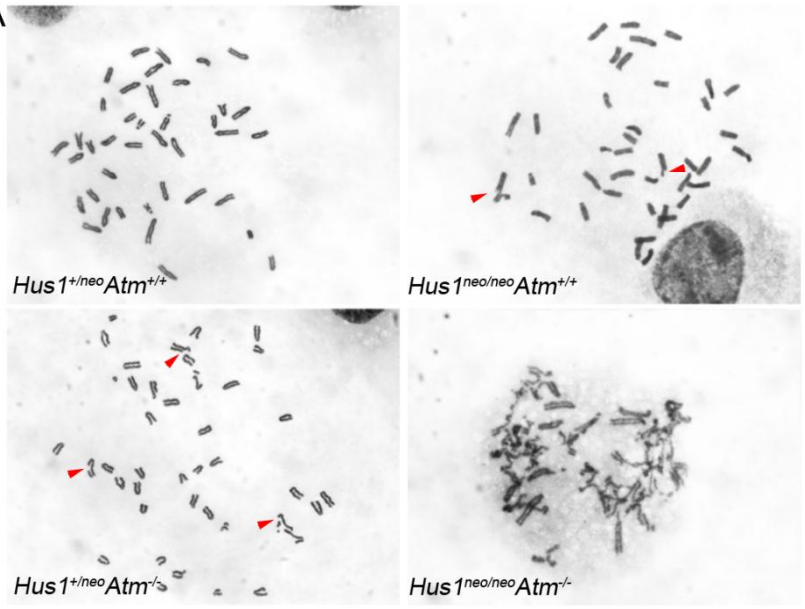

B

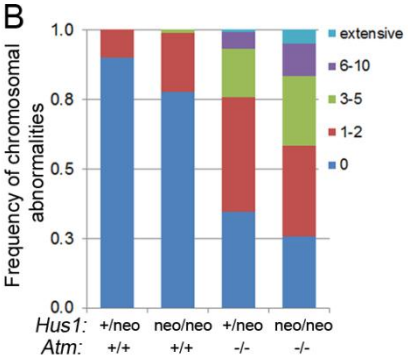

C

Genotype	Total metaphases	Breaks/Gaps	Fusions	Radials	Acentrics
Hus1 $^{+/neo}$ *Atm* $^{+/+}$ *(n=3)*	90	9	0	0	0
Hus1 $^{neo/neo}$ *Atm* $^{+/+}$ *(n=3)*	90	19	1	1	3
Hus1 $^{+/neo}$ *Atm* $^{-/-}$ *(n=4)*	120	146	9	5	41
Hus1 $^{neo/neo}$ *Atm* $^{-/-}$ *(n=4)*	120	211	8	11	59

induced DDR kinetics as *Hus1*$^{+/neo}$*Atm*$^{-/-}$ cells, and the magnitude of the response was similar with the exception that CHK1 activation after IR was even greater in cells defective for both *Atm* and *Hus1*. In response to UV, CHK2 and CHK1 phosphorylation as well as p53 accumulation were unaffected by *Atm* inactivation, partial *Hus1* impairment, or both (Figure 2.10B). Although defects in other signaling events not analyzed here cannot be ruled out, these data suggest that primary *Atm*/*Hus1* double mutant cells can trigger key DNA damage checkpoint signaling events as well as the single mutants. As a final measure of how interactions between *Atm* and *Hus1* affect DNA damage responses, we compared the radiation sensitivity of mice with individual or combined defects in *Atm* and *Hus1*. Consistent with the lack of detectable synergistic effects on IR-induced checkpoint signaling in MEFs, *Atm*/*Hus1* double mutant mice showed an equivalent sensitivity to whole body IR exposure as *Atm* single mutant mice, which are hypersensitive to IR (Figure 2.10C). Thus, the defective DSB response in *Atm*-deficient mice is not substantially worsened by additional partial *Hus1* impairment.

2.5 **Discussion**

The ATM and ATR DNA damage checkpoint pathways initially were viewed as separable, parallel signaling cascades that respond to distinct DNA lesions. However, recent biochemical evidence indicating significant crosstalk between the two pathways has led to the concept of a broad, integrated DDR network (Matsuoka, Ballif et al.

2007). Nevertheless, the genetic relationship between these pathways in vertebrates has been difficult to investigate due to the lethality associated with complete inactivation of ATR pathway components. Here we used a system for partial *Hus1* inactivation to show for the first time that ATM and HUS1 cooperate in genome maintenance *in vivo*. Whereas mice defective for either *Atm* or *Hus1* alone are viable, simultaneous dysfunction of both genes resulted in synthetic lethality. The ability to finely tune *Hus1* expression levels further revealed tissue-specific phenotypes, such as craniofacial and limb defects, associated with moderate *Hus1* impairment in an *Atm*-deficient background. This was unexpected, as the two main mammalian DDR pathways are often considered ubiquitously important, and suggests that there is significant tissue-specific variation in the level of endogenous DNA damage and/or the activity of additional pathways that respond to DNA lesions. Mapping out these specificities will be critical for understanding the etiology of many inborn diseases as well as the nature of organismal responses to chemotherapeutics and other genotoxic agents.

The most striking phenotype in $Hus1^{neo/neo}Atm^{-/-}$ mice was their significantly reduced overall size, which was apparent prior to birth. In mice and humans there are several reports of dwarfism associated with DDR defects, but the underlying mechanisms are still poorly understood in many cases. Most theories for how DDR dysfunction causes dwarfism center on either cell-autonomous defects or systemic growth axis perturbations. In particular, impairment of nucleotide excision repair in

mouse models of Cockayne syndrome results in dwarfism that is associated with suppression of the growth hormone/insulin-like growth factor (GH/IGF1) axis in what is believed to represent a homeostatic feedback response to GIN (Niedernhofer 2008). Likewise, SIRT6 deficiency in mice results in genomic instability, reduced *Gh*/*Igf1* expression, and dwarfism (Mostoslavsky, Chua et al. 2006). Conversely, other mouse models in which inactivation of genome maintenance mechanisms leads to dwarfism maintain an intact somatotroph axis. For instance, *Atm*-null mice are slightly smaller than their littermates (Barlow, Hirotsune et al. 1996; Elson, Wang et al. 1996; Xu, Ashley et al. 1996) but show no differences in the circulating levels of GH or free IGF1 (Schubert, Schmitz et al. 2009). Similarly, mice lacking KU80, a subunit of the DNA-PK complex, are smaller than their littermates but have an intact somatotroph axis (Nussenzweig, Chen et al. 1996; van de Ven, Andressoo et al. 2006).

Notably, proportional dwarfism is a characteristic of humans with Seckel Syndrome. Clinical reports indicate that the GH/IGF1 axis is normal in Seckel patients, although an *Atr*-Seckel mouse model shows reduced *Igf1* and *Ghr* expression (Kjaer, Hansen et al. 2001; Murga, Bunting et al. 2009). Interestingly, Seckel Syndrome also can be caused by mutations in genes encoding centrosomal proteins, including *PCNT*, *CEP152* and *CENPJ* (Griffith, Walker et al. 2008; Rauch, Thiel et al. 2008; Al-Dosari, Shaheen et al. 2010; Kalay, Yigit et al. 2011). In these cases, defective cell division has been hypothesized to drive the cell loss that underlies the reduced body size. The apparently normal GH/IGF1 axis in *Atm*/*Hus1* mice suggests that a cell

autonomous defect also might be responsible for the proportional dwarfism reported here and raises the possibility that DNA damage accumulation upon combined *Atm* and *Hus1* impairment leads to small size through defective expansion of key cell populations, either throughout the body or in specific compartments that impact body size, such as stem cell pools or developing bone growth plates (Klingseisen and Jackson 2011; Lui and Baron 2011).

In addition to their small size, *Atm*/*Hus1* double mutant animals showed skeletal abnormalities that included incomplete ossification and aberrant architecture of the skull, as well as significant shortening of the mesophalanx of the fifth digit (brachymesophalangy V) in both forelimbs and hindlimbs. Craniofacial defects are common in patients suffering from GIN-related disorders, including Seckel Syndrome (Goodship, Gill et al. 2000), Nijmegen Breakage Syndrome (due to *NBS1* mutations) (Digweed and Sperling 2004) and Williams-Beuren Syndrome (caused by a micro-deletion at 7q11.23 that includes *RFC2*) (Osborne 1999). Digit abnormalities, including brachymesophalangy and clinodactyly, are frequently observed in patients with Seckel Syndrome as well as another GIN disorder, Fanconi Anemia (De Kerviler, Guermazi et al. 2000). In addition to their association with hereditary disease, craniofacial defects and brachymesophalangy V also are present following fetal exposure to teratogens such as alcohol (Manning and Eugene Hoyme 2007) and may be hallmarks of excessive DNA damage during development (Holmes, Kleiner et al. 1987) (Table 4.1). Why GIN is frequently associated with these particular

developmental phenotypes is largely unknown, but may reflect a heightened stress sensitivity in certain cell types. Such a mechanism has been identified in Treacher Collins Syndrome, in which the occurrence of craniofacial abnormalities has been attributed to a lower threshold of neural crest cells for stress induced p53-dependent apoptosis (Jones, Lynn et al. 2008). In *Atm*/*Hus1* mice, cell death triggered by increased genomic instability could potentially impact crest-derived cells required for suture maintenance, possibly explaining the retarded dorsal expansion of these roofing bones. The lateral fenestrations in *Atm*/*Hus1* skull bones beginning at the initial stages of bone formation suggest that early ossification is disrupted, but do not provide clues as to why these specific sites are affected. The mouse model described here will be a powerful tool for understanding cell-type specific responses to GIN and their roles in the developmental defects observed in patients with instability syndromes.

Increased GIN in *Atm*/*Hus1* double mutant mice was readily apparent during embryogenesis as well as in a tissue specific pattern in adults, as evidenced by increased MN formation in hematopoietic cells without detectable upregulation of DNA damage responsive genes in liver. HUS1 loss causes chromosomal instability specifically during S-phase (Zhu and Weiss 2007), and the observations reported here are consistent with a model in which the phenotypes associated with combined *Atm* and *Hus1* defects are due primarily to the failure of actively dividing cells to deal with replication stress. Surprisingly, the elevated GIN in *Atm*/*Hus1* mice did not

significantly change the onset or histological characteristics of thymic lymphomas relative to those arising in mice lacking *Atm* alone. It may be that the rapid onset of lymphomas in *Atm*-null mice obscures effects associated with partial *Hus1* impairment. Alternatively, a greater level of genomic instability in *Atm*/*Hus1* double mutant mice may have opposing consequences that neutralize each other, both fueling the accumulation of cancer promoting mutations and interfering with the ability of cancer cells to withstand stresses associated malignant transformation. Finally, the absence of a difference in tumor-free survival may reflect a limited requirement for *Hus1* in this compartment. Previous studies have shown that thymocytes rely more on ATM and DNA-PK than ATR (Callen, Jankovic et al. 2009), and our own work suggests that lymphocytes can tolerate *Hus1* loss better than other cell types (Levitt, Liu et al. 2005; Francia, Weiss et al. 2006; Yazinski, Westcott et al. 2009).

Unexpectedly, although we deregulated the two primary DNA damage checkpoint pathways in the *Atm*/*Hus1* mouse model and observed clear phenotypic consequences, we detected only limited alterations in canonical ATM/ATR-mediated DNA damage signaling events as compared to those in *Atm* mutants alone. Indeed, for some of the factors analyzed, DNA damage signaling was increased in *Atm*/*Hus1* embryos and MEFs. There are several possible explanations for these observations. First, upon deregulation of the ATM and ATR pathways, an overlapping DDR kinase could become activated. Among the several possible factors that could serve such a role, the best candidate may be the PIKK DNA-PK, which is known to cooperate

with ATM and ATR in H2AX phosphorylation and is capable of phosphorylating an array of DDR proteins *in vitro*, including CHK2 and p53 (Meek, Dang et al. 2008). However, CHK1 activation was readily apparent in *Atm*/*Hus1* double mutants and there is limited evidence that DNA-PK phosphorylates CHK1 (Jazayeri, Falck et al. 2006). Alternatively, ATR could mediate the checkpoint signaling either in a 911 independent manner (Navadgi-Patil and Burgers 2009) or via residual HUS1 expression from the hypomorphic *Hus1* allele. Although *Atm*/*Hus1* defective cells can sense and mount signaling responses to DNA damage, this response clearly is ineffective, resulting in GIN followed by massive apoptosis and embryonic lethality. The observed accumulation of genome damage could be due to a repair defect, an elevated damage load that overwhelms the repair machinery, or both. *Hus1* impairment did not further worsen the radiation sensitivity of *Atm*-null mice, indicating that the synthetic phenotypes in *Hus1*/*Atm* double mutant mice are unlikely to originate from more severe DSB response defects relative to those in *Atm* single mutants. Given that the 911 complex has been directly implicated in several DNA repair processes, including base excision repair and translesion synthesis, we favor the model that defective DNA repair following HUS1 deregulation leads to an increased number of DNA lesions that are normally resolved efficiently in an ATM-dependent manner, resulting in the observed synthetic lethality when both pathways are defective simultaneously (Figure 2.12).

The strong genetic interaction between *Atm* and *Hus1* in mice also has

implications for human disease. First, the synergistic increases in genome damage and apoptosis observed here following combined *Atm* and *Hus1* impairment suggest that therapeutic targeting of HUS1 or the broader ATR pathway may be effective for some malignancies that arise due to ATM pathway mutations, which may be as many as 30% of all cancers (Shiloh 2003; Reaper, Griffiths et al. 2011). However, the efficacy of such a strategy may depend on the cell of origin or other factors like the particular initiating oncogenic events in the tumor, as the impact of simultaneous *Atm* and *Hus1* defects varied between tissues. Another implication of this work relates to the basis for variant forms of A-T, like A-T_{Fresno}, which is associated with *ATM* mutations but combines typical A-T phenotypes with microcephaly and mental retardation (Gilad, Chessa et al. 1998). This variation has been attributed to genetic modifiers outside of *ATM*. The findings presented here suggest that polymorphisms in *HUS1* or other ATR pathway genes could significantly impact the onset and severity of A-T phenotypes.

2.6 **Acknowledgements**

The experiments described here represent a collaborative project from the Weiss Lab. Min Zhu started this project set up all the crosses necessary to produce the representative genotypes and participated to the embryo analysis; Sucheta Mukherjee did most of the Alizarin red/Alcian blue staining of embryo and adults and with the quantification of the growth factors transcript levels both by Northern blot and Q-

PCR; Amy M. Lyndaker repeated the western blot analysis for Chk1 and p53; Kelly R. Hume performed and quantified the TUNEL analysis on the embryos; Jaesung Lee and Anthony P. Reeves created a tool that allowed me to measure the skulls of our mutant mice; Mark L. Riccio performed the micro-CT scans; Nathan Sutter performed the principal component analysis; Drew M. Noden helped with the analysis of craniofacial defects; Rachel M. Peters realized the pathologic assessment of our mutants; Robert S. Weiss directed the research and had major impact on the design and writing of this entire chapter. Additionally Eric Alani, Sylvia Lee, and Yolanda Sanchez had helpful discussions and comments on the manuscript we published in Human Molecular Genetics, Yves Boisclair measured the circulating IGF1 levels.

CHAPTER 3

GENOTOXIN-SPECIFIC IN VIVO REQUIREMENT FOR HUS1 AND ATM FOLLOWING DNA-DAMAGE

3.1 Abstract

Cells are under constant attack from DNA-damaging agents from both endogenous and exogenous sources and protect genomic integrity through DNA-damage response (DDR) pathways that recognize lesions and promote repair, senescence or apoptosis. Central to the DDR are the ATM and ATR kinases. ATM responds mainly to double strand DNA breaks whereas ATR orchestrates the cellular response to replication stress. Because complete ATR pathway inactivation causes embryonic lethality, we created an allelic series in which the expression of *Hus1*, a member of the 911 complex that is required for efficient ATR signaling, is incrementally reduced by combining the wild-type allele ($Hus1^{+}$) with either hypomorphic ($Hus1^{neo}$) or null ($Hus1^{-/n}$) alleles. $Hus1^{neo/\Delta 1n}$ mice, which have the lowest levels of *Hus1* in this series, are born at expected frequency and appear grossly normal but show increased genomic instability and no increased cancer predisposition. Since little is known about the *in vivo* roles of the ATR pathway following genotoxic stress, we defined the tissue- and cell type-specific actions of the *Hus1*-mediated DDR.

Hus1$^{neo/\Delta 1n}$ mice showed significant hypersensitivity to agents that cause replication stress, including MMC and HU, but not to IR, which causes DSBs. Analysis of cell proliferation and apoptosis in IR sensitive tissues such as the small intestine and skin showed that partial *Hus1* inactivation had no detectable effect on radiation induced cell cycle arrest or apoptosis. Together our data shows that in response to genotoxic stress there is a clear separation of the two pathways supporting the hypothesis that the overlap between the two pathways occurs because DNA lesions conversion. Our current research focuses on understanding the cellular and molecular mechanisms that are the basis of this sensitivities and the relationship between the ATM and ATR pathways in responding to genotoxic agents. A better understanding of how checkpoint signaling impacts the responsiveness of normal tissues as well as tumors to genotoxins will give us insights into how inhibitors of checkpoint signaling pathways may interact with traditional cancer therapies.

3.2 Introduction

DNA stands at the core of life as we know it. In order to perform its function each cell of our organism relies on DNA for the execution of vital functions such as transcription or replication. Thus, to protect its integrity and the integrity of its future progeny, cells have to deal with a plethora of agents that damage the DNA. DNA damage originates from both endogenous and exogenous sources and can cause an array of lesions spanning from a base mismatch to the most toxic DSBs

(Jackson and Bartek 2009; Abraham and Halazonetis 2012). To deal with these threats cells have evolutionary developed a series of cell cycle checkpoints that allow for DDR. Central to the DDR lays a series of signal transduction pathways that sense the damage and transduce the signal to effector molecules that execute the appropriate response, being it repair or apoptosis. The main pathways involved in cellular protection from DNA damage are the ATM and ATR pathways (Cimprich and Cortez 2008; McKinnon 2012). ATM and ATR are large protein kinases of the phosphatidylinositol 3-kinase-related kinases (PIKKs) family that initiate each of these pathways. ATM responds mainly to DSBs while ATR responds to the presence of RPA coated single stranded DNA (RPA-ssDNA) as a result of replication stress.

ATM is the principal responder to DSBs and once activated phosphorylates, through others, the downstream effectors CHK2 and p53. These steps activate the DDR checkpoint and promote DNA repair. The important role of the ATM kinase is underlined by the phenotypes associated with loss of function mutations in this gene. In humans these mutations are associated with Ataxia-Telangiectasia (AT; OMIM 208900) a genomic instability syndrome characterized by extreme sensitive to IR, ataxia, telangiectasias, immune deficiency, sterility and an increased risk of lymphoma formation (McKinnon and Caldecott 2007; McKinnon 2012). An *Atm* mouse model for A-T has been engineered, that recapitulates many of the human

phenotypes (Barlow, Hirotsune et al. 1996; Elson, Wang et al. 1996; Xu, Ashley et al. 1996). *Atm*$^{-/-}$ mice have been subjected to extensive genotoxin analyses that strengthened the concept that ATM is the main responder to IR but not replication stress. At sub-lethal doses of IR, Atm$^{-/-}$ mice are immediately affected and die rapidly due to gastrointestinal toxicity (Barlow, Hirotsune et al. 1996). In *Atm*$^{-/-}$ mice the CNS is resistant to apoptosis after 14 Gy ionizing radiation including in the cerebellum, which is markedly affected in AT. In wild-type, but not *Atm*$^{-/-}$ mice, p53 was activated, suggesting that *Atm*-dependent apoptosis in the CNS is mediated by p53 (Herzog, Chong et al. 1998).

The ATR pathway responds to lesions caused by genotoxins like UV-light, HU or MMC, which create a physical barrier for the replication fork progression. When the replication machinery encounters such a lesion and the DNA-polymerases are unable to bypass it, the MCM helicases associated with the fork continue to unwind the DNA creating long stretches of ssDNA. This ssDNA, immediately protected by RPA, represents the major signal for recruitment of ATR, through its partner ATRIP and the RAD9-RAD1-HUS1 clamp (9-1-1). The 9-1-1 complex recruits to the lesion site TopBP1 and RHINO which then activate ATR kinase activity (Delacroix, Wagner et al. 2007; Cotta-Ramusino, McDonald et al. 2011). Upon activation, ATR phosphorylates the downstream effector CHK1 to promote cell cycle arrest and allows for repair.

In humans rare syndromes are associated with ATR deficiency (O'Driscoll 2008). One such disease is Seckel Syndrome (SKL1; OMIM) caused by a hypomorphic loss of function mutation in ATR. Seckel patients present with dwarfism, microcephaly and mental retardation, but no cancer predisposition (Goodship, Gill et al. 2000; O'Driscoll, Ruiz-Perez et al. 2003). In order to better study the importance of the ATR pathway for human physiology mice models for deficiency in the ATR pathway have been created. Knocking out any member of the ATR pathway resulted in severe embryonic lethality, consistent with the notion that ATR is a critical factor for replication stress (O'Driscoll 2009). Thus hypomorphic alleles were created to deregulate the ATR pathway. A transgenic mouse model bearing the humanized ATR allele (*Atr*^{S}) exhibits partial ATR expression, with Atr$^{S/S}$ homozygous mice showing severe phenotypes including dwarfism and craniofacial defects. These mice succumb rapidly to the severity of their disease. Thus, analysis of the *in vivo* response to genotoxins is impossible (Murga, Bunting et al. 2009).

A different tactic was employed by our group that used HUS1 to deregulate the ATR pathway. A *Hus1* knockout allele where *Hus1* exon 1 was removed (*Hus1*$^{\lrcorner 1n}$) was combined with either the wild type allele (Hus1^{+}) or a hypomorphic allele (*Hus1*^{neo}) to create a *Hus1* allelic series where Hus1 expression was incrementally decreassed (*Hus1*$^{+/+}$ > *Hus1*$^{+/neo}$ > *Hus1*$^{+/\lrcorner 1n}$ > *Hus1*$^{neo/neo}$ > *Hus1*$^{neo/\lrcorner 1n}$). While *Hus1*$^{+/neo}$ and *Hus1*$^{+/\lrcorner 1n}$ mice are indistinguishable from *Hus1*$^{+/+}$ mice, and in

our studies were used as wild type controls, *Hus1*$^{neo/\Delta 1n}$ mice show the lowest *Hus1* expression in the series, are viable and born at expected frequencies, show a grossly normal phenotype, no increase in cancer predisposition but an increase in micronucleus formation in the peripheral blood, indicating that the reduced *Hus1* expression is insufficient for proper genome maintenance. Hus1$^{neo/neo}$ mice with intermediate *Hus1* expression show medium GIN phenotypes (Levitt, Liu et al. 2005; Levitt, Zhu et al. 2007).

The two DDR pathways have been thought to act as parallel pathways (Cimprich and Cortez 2008; Shiotani and Zou 2009). and any cross-talk seen in checkpoint activation and DNA repair has been attributed to DNA lesion conversion: unrepaired stalled replication forks can eventually collapse in DSBs while in the repair of DSBs, ssDNA intermediates are formed. This concept has been recently challenged by cellular and biochemical assays where the two pathways have been shown to act as an integrated mechanism. ATM and ATR have been shown to have more than 700, highly interconnected, phosphorylation substrates (Matsuoka, Ballif et al. 2007). Moreover, cellular analysis of the ATR pathway deficiency has shown that ATR pathway defective cells are sensitive to IR as well as replication stress reagents. Concomitant inhibition of both ATM and ATR pathways resulted in synthetic lethality (Weiss, Matsuoka et al. 2002; Weiss, Leder et al. 2003; Murga, Bunting et al. 2009). Due to a lack of available genetic tools, the analysis of the

relationship between these two pathways in live organisms has been difficult due to the lethality associated with the knockout of any member of the ATR pathway. By combining the *Hus1* allelic series on $Atm^{-/-}$ background we showed that *in vivo*, like *in vitro Hus1*/*Atm* double mutant mice showed a synthetic lethal phenotype (Chapter 2). Contrary to our expectation, the synthetic lethality associated with *Hus1*/*Atm* impairment did not further accentuate the sensitivity to DSB formation, since *Hus1*/*Atm* double mutant mice were no more sensitive to IR as *Atm* single mutants. This suggests that all the phenotypes associated with *Hus1*/*Atm* deficiency are due to a replication stress problem (Balmus, Zhu et al. 2012).

While the role of the ATM pathway in tumor progression is well understood, the importance of the ATR pathway remained elusive and contradictory, with some studies proposing that the ATR pathway is critical for tumor suppression while others suggested a role in tumor growth (Smith, Tho et al. 2010). Whereas tumor susceptible mice showed an increased in tumor incidence when heterozygous mutations in members of the ATR pathway were included, humans suffering from ATR deficient syndromes are not prone to tumor development (Goodship, Gill et al. 2000). Moreover, data from human patients showed that members of the ATR pathway were upregulated in tumors (Maniwa et al., 2005; Zhu et al., 2008). Increased expression of DDR proteins including HUS1 were also detected in mammary tumors in mice (Zhang et al., 2008). These observations suggest that the

ATR pathway is critical for tumor development. Indeed, in mice, loss of HUS1 or ATR synergize with p53 loss to promote cell death and not tumorigenesis (Ruzankina et al., 2009; Yazinski et al., 2009). Furthermore ATR pathway inhibitors induce increased sensitivity to chemotherapeutics in several cancer cell lines (Ma, Cai et al. 2012; Origanti, Cai et al. 2012). These inhibitors are believed to represent an Achilles' heel of cancer (Bartek, Mistrik et al. 2012). Less is known though about the effect of ATR pathway inhibition in a normal organism.

Here we used the *Hus1* deficient mice to test the *in vivo* requirement for the ATR pathway under physiological and genotoxin treatment conditions. We show that in response to genotoxin stress *in vivo* the ATM and ATR pathways act as separate parallel pathways. $Hus1^{neo/\Delta 1}$ mice are no more sensitive to the DSB inducing clastogen IR than wild type controls but are hypersensitive to the replication stress inducing reagents MMC and HU. We show that the intercross between the two pathways is most likely due to an interconversion of the DNA lesions and that the fine tuning of ATR pathway inhibition will be critical for successful combined cancer therapies.

3.3 Materials and methods

Animals. All animals used in this study were handled in accordance with federal and institutional guidelines, under a protocol approved by the Cornell University

Institutional Animal Care and Use Committee (IACUC). *Hus1*^{neo} and *Hus1*$^{-/-n}$ mice were maintained on the 129S6 background. *Atm* knockout mice were maintained on the FVB background. These strains were interbred to create *Atm*/*Hus1* double mutant mice. Mice were genotyped by PCR analysis of genomic DNA isolated from tail snip biopsies as previously described.

Hydroxyurea treatment. For analysis of hydroxyurea (HU) sensitivity during embryonic development timed matings using *Hus1* allelic series mice were performed. Noon of the day of vaginal plug detection was defined as embryonic day E0.5. Pregnant females at E8 were injected via intraperitoneal delivery (IP) 400 mg/kg body weigh HU and embryos were dissected at 12 hours later for analysis. Embryos were genotyped by PCR analysis of genomic DNA isolated from by laser microdissection of embryonic tissues using a Leica LMD6000 microscope.

Ionizing radiation and mytomycin C treatment. For analysis of survival upon ionizing radiation, mice were subjected to 9Gy or 15Gy doses of γ-irradiation using a Mark I Model 68 sealed 137Cs source gamma irradiator (JL Shepherd & Associates), injected with a single IP dose of 8mg/kg or 4mg/kg body weigh mitomycin C (MMC - Sigma). Subsequently mice were monitored by daily weighing for up to 30 days or until reaching humane endpoint criteria based on the clinical disease signs. Kaplan-Meier survival analysis was performed using IBM SPSS software.

Histology. At the indicated time points after the specified genotoxin treatment, all major organs were isolated following euthanasia and then fixed in 10% formalin overnight. The second day the fixed organs were transferred to 70% ethanol, were placed in cassettes, embedded in paraffin and serial 5 μm sections were collected on Superfrost Plus slides (Fisher) using a Leica microdissection system (LMD7000). Histological sections of paraffin-embedded tissues were stained with hematoxylin and eosin using a standard protocol. Upon staining specimens were subjected to pathological assessment.

Immunohistochemistry staining. To quantify cell proliferation bromodeoxyuridine (5-bromo-2'-deoxyuridine, BrdU), a synthetic thymidine analog was used. Two hours prior to euthanasia mice were injected i.p. with an 8mg/kg dose of BrdU using a 50μg/μl stock solution. To quantify the proliferation potential the slides were analyzed using the BrdU kit (Invitrogen) according with the manufacturer's directions. Apoptosis quantitation was done using the Apoptag (Millipore) TUNEL detection system according to the manufacturer's instructions. In the case of the small intestine, individual, morphological intact crypts were identified and more than five crypts per mouse were counted. For the skin, intact hair follicles were used for quantitation by counting the distribution of DAB positive cells. Histology images were obtained using an Aperio Scanscope (Aperio Technologies, USA). Statistical analysis was performed using SPSS's (IBM) Mixed Model Analysis.

Effect of genotoxin treatment on micronucleus formation. Analysis of micronucleus (MN) formation in peripheral blood cells was performed as previously described (Shima, Hartford et al. 2003; Levitt, Zhu et al. 2007). Briefly, peripheral blood was collected from the mandibular vein at 0, 24, 48 and 76 hours post 07Gy IR, fixed in methanol, and incubated in bicarbonate buffer containing RNase A and anti-CD71: FITC antibody (Biodesign International). After washing and staining with propidium iodide, the cells were analyzed on a FACSCalibur flow cytometer (Becton-Dickinson, San Jose, CA).

3.4 RESULTS

3.4.1 *Hus1* impairment does not alter survival upon ionizing radiation treatment.

Due to their deficiency in DDR factors many cancer types are selectively sensitive to radiation based therapy (Mellor and Callaghan 2008). Targeting cancer with clastogens like ionizing radiation represents one of the most effective forms of treatment being used for many malignant tumors at various developmental stages (Gudkov and Komarova 2003).

Although a main DDR response pathway, due to the lethality associated with ATR pathway deficiency, the role of ATR pathway in the response to DSB formation *in vivo* remained unexplored. Because *in vitro* experimental data hinted for a requirement for this pathway in response to DSBs, with *Hus1* null cells being significantly more sensitive to IR than their wild type controls (Weiss, Matsuoka et al. 2002), we hypothesized that *Hus1* defective animals like the cells would show a specific higher sensitivity to IR.

To test this hypothesis we treated $Hus1^{neo/\Delta 1n}$ mice and control littermates with 9Gy and 15Gy IR doses respectively. Upon treatment, Kaplan Meyer analysis showed that independent of the dose used, $Hus1^{neo/\Delta 1n}$ mice showed no significant difference in survival when compared to *Hus1* controls, while the $Atm^{-/-}$ control group was hypersensitive (Figure 3.1). As previously reported (Bunz, Hwang et al. 1999; Takai, Naka et al. 2002), hematoxilin and eosin (HE) histopathological examination of tissues from the wild type treated groups showed, acute modifications in the thymus, spleen, bone marrow, spermatogonia, epithelia of the gut and hair follicles. In comparison to the $Hus1^{+}$ control group, tissues from $Hus1^{neo/\Delta 1n}$ mice showed no specific signatures (Table 3.1), suggesting that similar to the response at organismal level, at cellular level, there is no specific requirement for *Hus1* in response to IR. These observations indicate that *in vivo* the ATR pathway is not required for the organismal response to IR induced stress..

Figure 3.1. *Hus1* hypomorphic mice show no differential sensitivity to IR. Mice of the indicated genotypes were exposed to 6Gy, 9Gy or 15Gy respectively of IR from a sealed source cesium irradiator. Animals were monitored for survival and a chi-square statistical analysis was performed. Control *Hus1*$^{+}$ genotypes include *Hus1*$^{+/+}$, *Hus1*$^{+/neo}$, and *Hus1*$^{+/\Delta 1}$. Kaplan-Meyer survival analysis shows that while *Atm*$^{-/-}$ mice are hypersensitive to IR, Hus1$^{neo/\Delta 1}$ mice shows no significant hypersensitivity to IR at both 9Gy (B) and 15Gy (C) doses when compared to the *Hus1*$^{+}$ littermate controls.

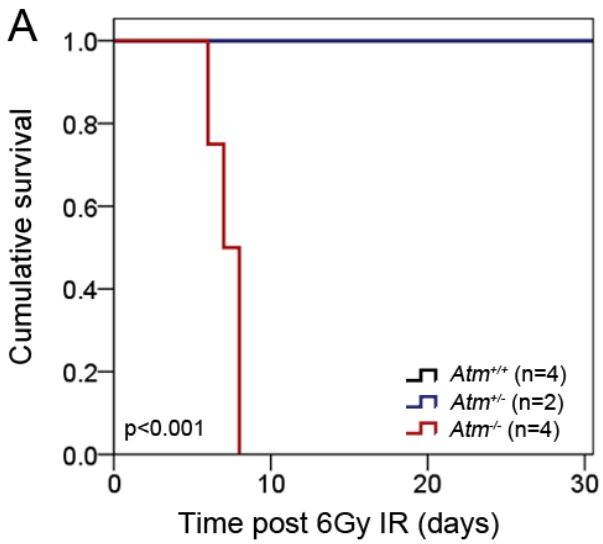
A
Cumulative survival
1.0
0.8
0.6
0.4
0.2
0.0
0
10
20
30
Time post 6Gy IR (days)
p<0.001
Atm+/+ (n=4)
Atm+/- (n=2)
Atm-/- (n=4)

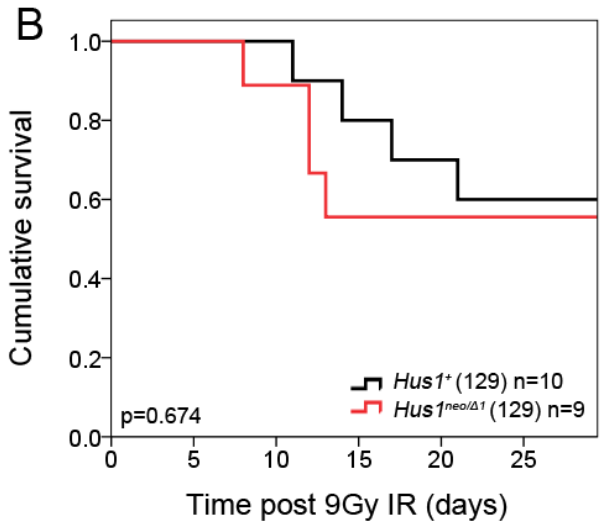
B
Cumulative survival
1.0
0.8
0.6
0.4
0.2
0.0
0
5
10
15
20
25
Time post 9Gy IR (days)
p=0.674
Hus1+ (129) n=10
Hus1neo/Δ1 (129) n=9

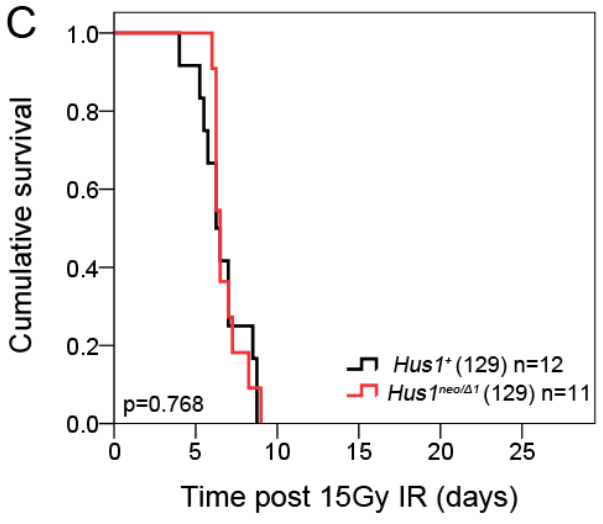
C
Cumulative survival
1.0
0.8
0.6
0.4
0.2
0.0
0
5
10
15
20
25
Time post 15Gy IR (days)
p=0.768
Hus1+ (129) n=12
Hus1neo/Δ1 (129) n=11

3.4.2 **Similar IR induced responses in the tissues of the *Hus1* mutant mice**.

Most of the phenotypes associated with the clinical signs of radiation intoxication, for either the hematopoietic or gastrointestinal lethal syndromes, are caused by an increased cell death in the respective compartments associated with changes in cell proliferation (Norimura, Nomoto et al. 1996). Because some of the *Hus1* specific changes might have been hidden by the accumulating secondary effects caused by radiation exposure, analysis of cell proliferation and apoptosis was performed at 8 hours and 96 hours post 15Gy IR, before the emergence of severe clinical signs. While at 8 hours post IR little changes were noted in the tissues examined, histopathological examination of tissues harvested 96 hours post IR showed a primary response in the skin and the epithelia of the gut represented by a cell loss in the hair follicle and hyperplasia in the intestinal crypt epithelia (Figure 3.2).

To specifically examine cellular proliferation and apoptosis in the small intestine and skin of our mice apoptosis was measured using TUNEL while cell proliferation was measured using a BrdU incorporation assay as described in Material and Methods. The examination of the apoptosis in the hair follicle of the 15 Gy treated mice revealed a mild increase in cell death at the level of the hair follicle. These differences were present and similar at both 8 and 96 hours post 15 Gy IR and were independent of the Hus1 status (Figure 3.3A). Following the exposure to a DNA damaging agent the proliferation at the level of the hair follicle arrested progressively at 8 and 96 hours post treatment. These changes were again

independent of the *Hus1* status (Figure 3.3B). Consistent with the survival data, deregulation of the ATR pathway in the *Hus1* mutant mice has no significant effect on the cell proliferation and apoptosis of the hair follicle cells, suggesting that at this level the ATR pathway is not required for the response to IR.

To further investigate the *Hus1* requirement following IR, we next evaluated the response to IR in a highly proliferative tissue, the small intestine. The cells in the small intestinal crypt proliferate continuously with all the cells being completely renewed in 24 hours (Crosnier, Stamataki et al. 2006). Analysis of the cell survival status in the small intestine revealed that at 8 hours post 15-Gy IR a significant proportion of the cells from the small intestinal crypt underwent cell death while at 96 hours post-treatment the small intestinal crypts had numbers of apoptotic cells similar to the untreated groups, implying that they have a checkpoint defect. 8 hours post-treatment, the $Hus1^{neo/\Delta 1n}$ mice showed an increased apoptosis trend compared to $Hus1^{+}$ controls. 96 hours post-treatment the difference was indistinguishable (Figure 3.4A). Proliferation analysis showed that in the untreated group the $Hus1^{neo/\Delta 1n}$ show a significant reduction in the proliferative capacity of the small intestinal crypts compared to the $Hus1^{+}$ controls. 8 hours post 15 Gy treatment the $Hus1^{neo/\Delta 1n}$ shows almost no change in the proliferation potential compared to representative untreated mice. The $Hus1^{+}$ control group showed a significant drop in proliferation. 96 hours

Figure 3.2. Tissue morphology in mice with partial *Hus1* impairment following 15Gy ionizing radiation. Following euthanasia, isolated tissues were fixed in 10% formalin. Histological sections of paraffin-embedded tissues were stained with hematoxylin and eosin (HE) and subjected to pathological assessment. (A) Representative images depicting tissue morphology in the skin from $Hus1^{neo/\Delta 1}$ mice compared to littermate controls upon 15 Gy IR. The hair follicles are grossly normal 8hrs post IR but loss of cellularity is observed at 96hrs post treatment. No difference in cellularity of the hair follicles was observed between the two genotypic groups (B) Representative images depicting tissue morphology in the small intestine of $Hus1^{neo/\Delta 1}$ mice as compared to littermate controls upon 15 Gy IR. The small intestine crypts are grossly normal 8hrs post IR but enlarged 96hrs post treatment. No difference in cellularity in the small intestine was observed between the two genotypic groups post 15Gy IR. Size bar corresponds to 50 microns. Control $Hus1^{+}$ genotypes include $Hus1^{+/+}$, $Hus1^{+/neo}$, and $Hus1^{+/\Delta 1}$.

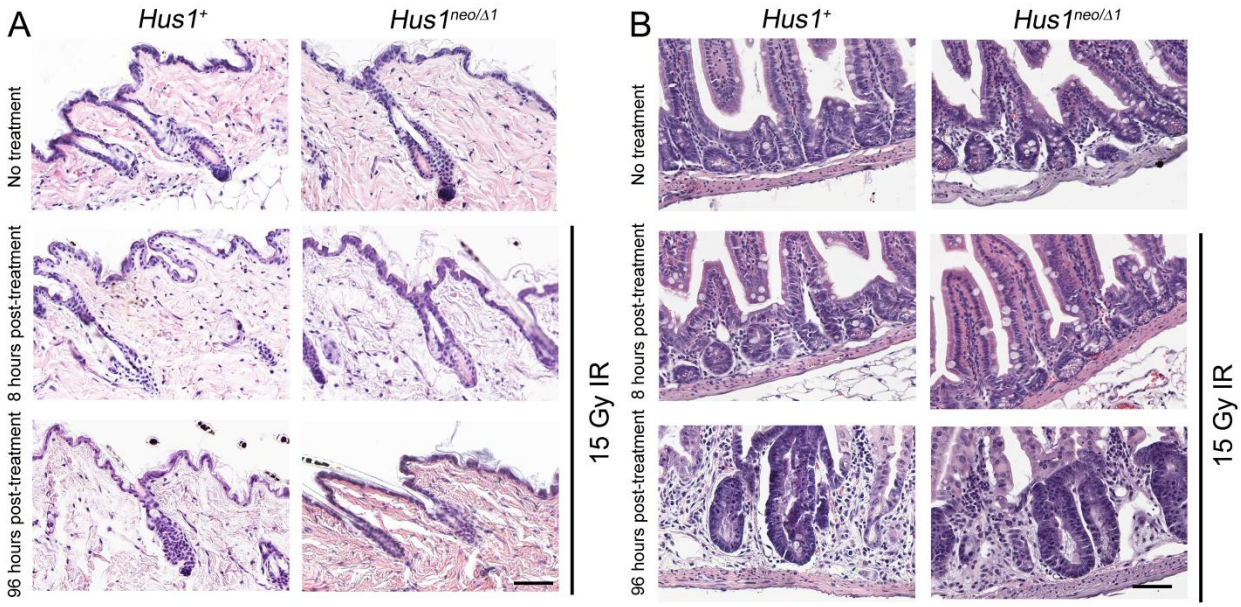
A
Hus1+
Hus1neo/Δ1
No treatment
8 hours post-treatment
96 hours post-treatment
15 Gy IR
B
Hus1+
Hus1neo/Δ1
No treatment
8 hours post-treatment
96 hours post-treatment
15 Gy IR

Figure 3.3. Analysis of cell proliferation and apoptosis in the skin from *Hus1*$^{neo/\Delta 1}$ as compared to *Hus1*$^{+}$ mice following 15Gy ionizing radiation. Immunohistochemical staining of TUNEL positive cells and BrdU positive cells in paraffin embedded skin from experimental mice. (A) Representative images depicting TUNEL positive cells, indicative of apoptosis, in the skin from *Hus1*$^{neo/\Delta 1}$ mice as compared to littermate controls after no treatment or the indicated time points after 15Gy IR. (B) Quantification of TUNEL positive cells in the skin at 0, 8, and 96 hrs post 15Gy. Significant increased levels of apoptosis were observed 8 hrs post 15Gy IR ($p<0.05$; Student's t test) at similar levels in both genotypic groups. (C) Representative images depicting BrdU positive cells, indicative of proliferation, in the skin of *Hus1*$^{neo/\Delta 1}$ mice as compared to littermate controls after no treatment or the indicated time points after 15Gy IR. (D) Quantification of BrdU positive cells in the skin at 0, 8, and 96 hrs post 15Gy. Significantly decreased levels of proliferation were observed at 8 hrs ($p<0.05$; Student's t test) and 96 hrs ($p<0.01$; Student's t test) post 15Gy IR when compared to the untreated groups or when the 8 hrs and 96 hrs time point were compared ($p<0.05$; Student's t test). No significant difference between the *Hus1*$^{neo/\Delta 1}$ mice and littermate controls was noted at any time point. Quantification was done using Size bar corresponds to 50 microns. Control *Hus1*$^{+}$ genotypes include *Hus1*$^{+/+}$, *Hus1*$^{+/neo}$, and *Hus1*$^{+/\Delta 1}$. $n\geq 3$ mice for each genotype and time point were used for quantitation; $n\geq 3$ fields of view per mouse were counted. Error bars represent $\pm$ standard deviation.

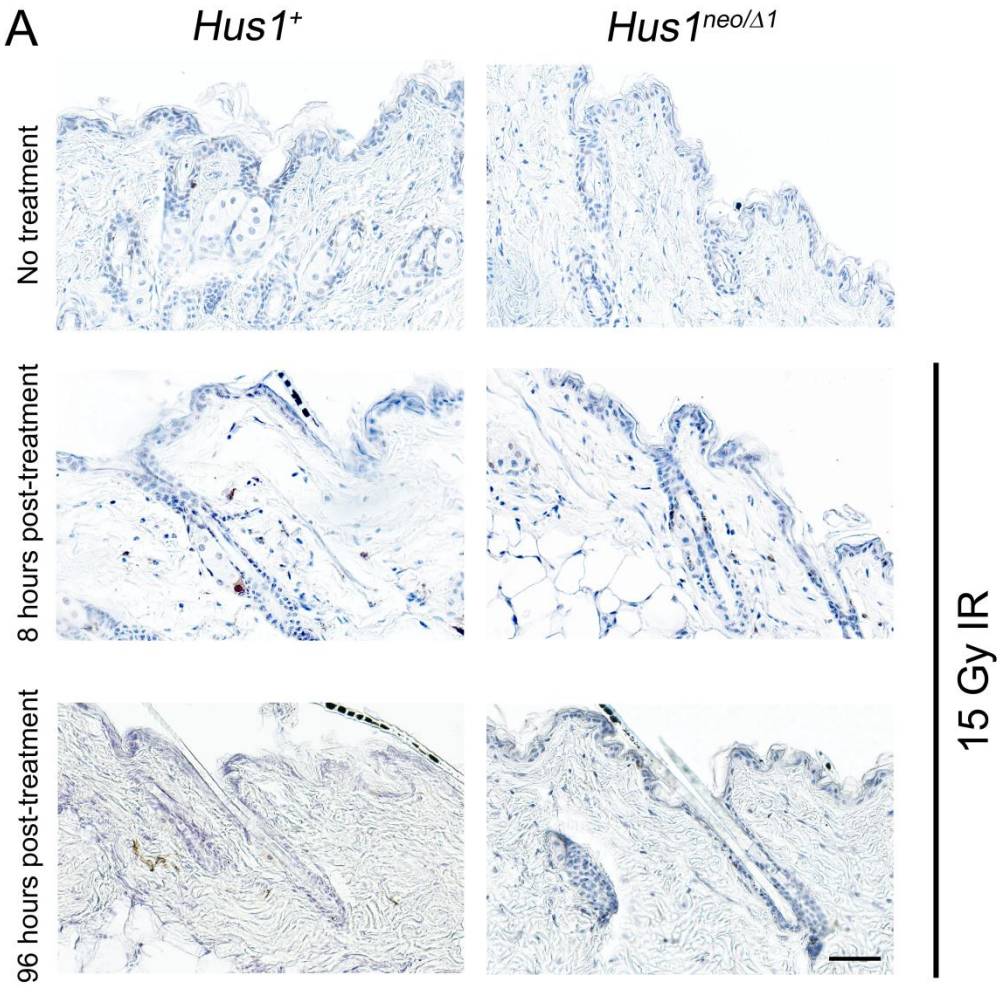
A
Hus1+
Hus1neo/Δ1
No treatment
8 hours post-treatment
96 hours post-treatment
15 Gy IR

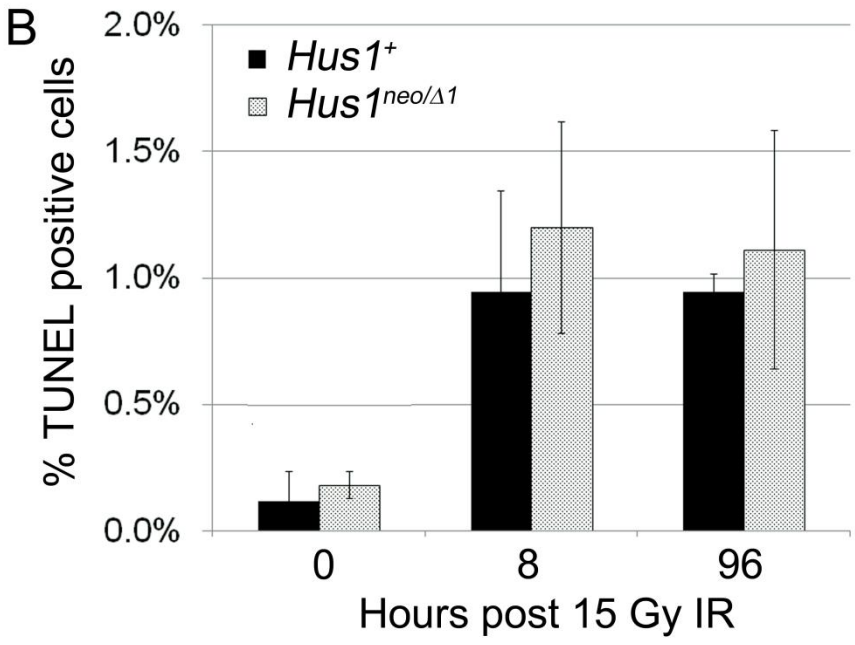
B
% TUNEL positive cells
2.0%
1.5%
1.0%
0.5%
0.0%
Hus1+
Hus1neo/Δ1
0
8
96
Hours post 15 Gy IR

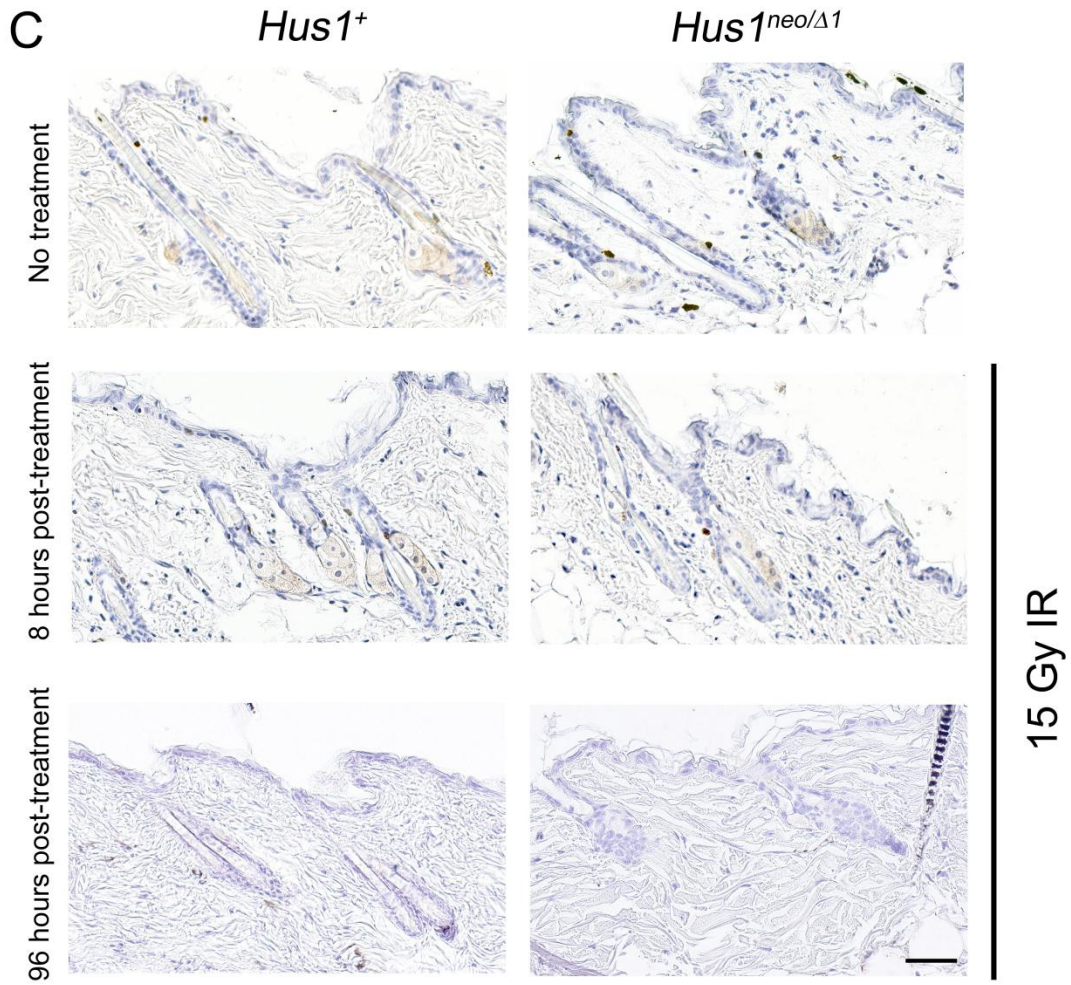
C
Hus1+
Hus1neo/Δ1
No treatment
8 hours post-treatment
96 hours post-treatment
15 Gy IR

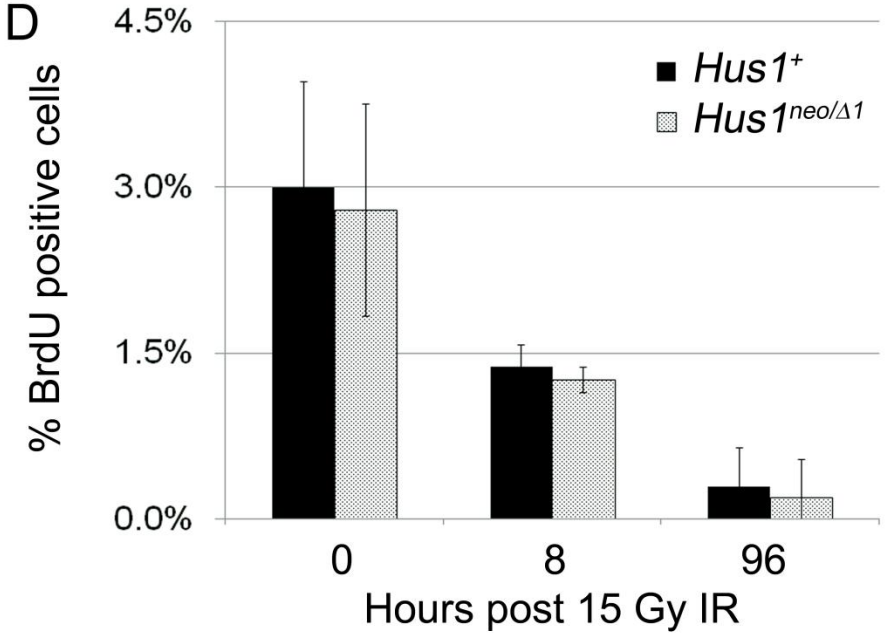
D
% BrdU positive cells
4.5%
3.0%
1.5%
0.0%
Hus1+
Hus1neo/Δ1
0
8
96
Hours post 15 Gy IR

Figure 3.4. Analysis of cell proliferation and apoptosis in the small intestine from *Hus1*$^{neo/\Delta 1}$ as compared to *Hus1*$^{+}$ mice following 15Gy ionizing radiation. Immunohistochemical staining of TUNEL positive cells and BrdU positive cells in paraffin embedded small intestine sections. (A) Representative images depicting TUNEL positive cells, indicative of apoptosis, in the small intestinal crypts from *Hus1*$^{neo/\Delta 1}$ mice compared to littermate controls after no treatment or the indicated time points after 15Gy IR. (B) Quantification of TUNEL positive cells in the small intestinal crypts at 0, 8, and 96 hrs post 15Gy. 8 hours post 15Gy IR both genotypic groups showed significant increased levels of apoptosis when compared to the untreated group ($p<0.001$; Student's t test). No significant difference between the *Hus1*$^{neo/\Delta 1}$ mice and littermate controls was noted. At 96 hrs the crypts showed severe morphology changes, but apoptosis levels returned to the untreated level. (C) Representative images depicting BrdU positive cells, indicative of proliferation, in the small intestinal crypts from *Hus1*$^{neo/\Delta 1}$ mice as compared to littermate controls after no treatment or the indicated time points after 15Gy IR. (D) Quantification of BrdU positive cells in the small intestinal crypts at 0, 8, and 96 hrs post 15Gy. Significant decreased levels of proliferation were observed in the untreated group ($p=0.03$; Student's t test). At 8 hrs post 15Gy IR, proliferation was significantly reduced in both groups ($p<0.05$; Student's t test). No significant difference between the *Hus1*$^{neo/\Delta 1}$ mice and littermate controls was noted. At 96 hrs, significant increased proliferation was observed at similar levels in both groups ($p<0.05$; Student's t test).

Size bar corresponds to 50 microns. Control *Hus1*$^{+}$ genotypes include *Hus1*$^{+/+}$, *Hus1*$^{+/neo}$, and *Hus1*$^{+/-1}$. n≥3 mice for each genotype and time point were used for quantitation. Quantitation was done in intact intestinal crypts and n≥5 intestinal crypts per mouse were counted. Error bars represent ±standard deviation.

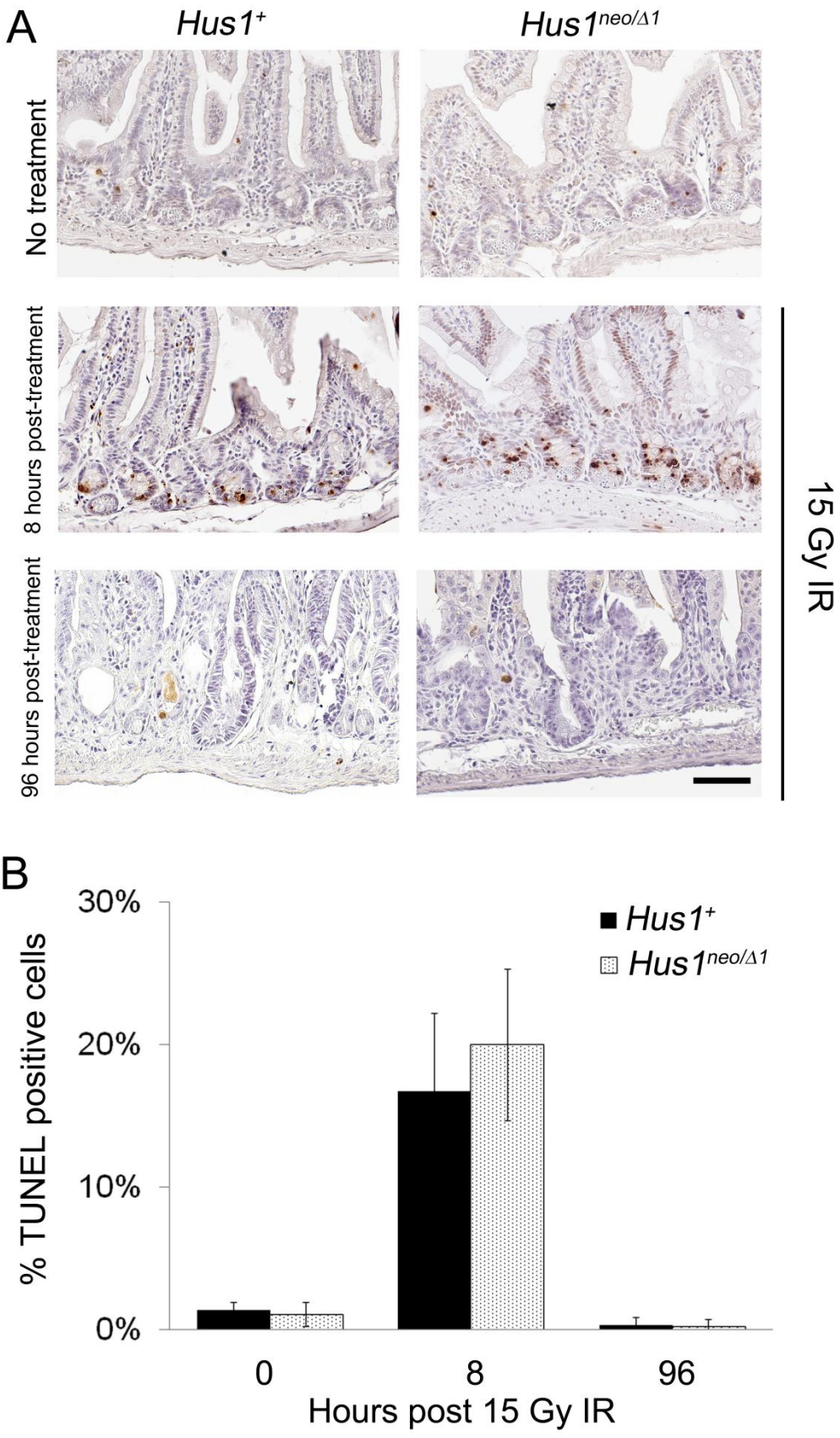
A
Hus1+
Hus1neo/Δ1
No treatment
8 hours post-treatment
96 hours post-treatment
15 Gy IR
B
% TUNEL positive cells
30%
20%
10%
0%
Hus1+
Hus1neo/Δ1
0
8
96
Hours post 15 Gy IR

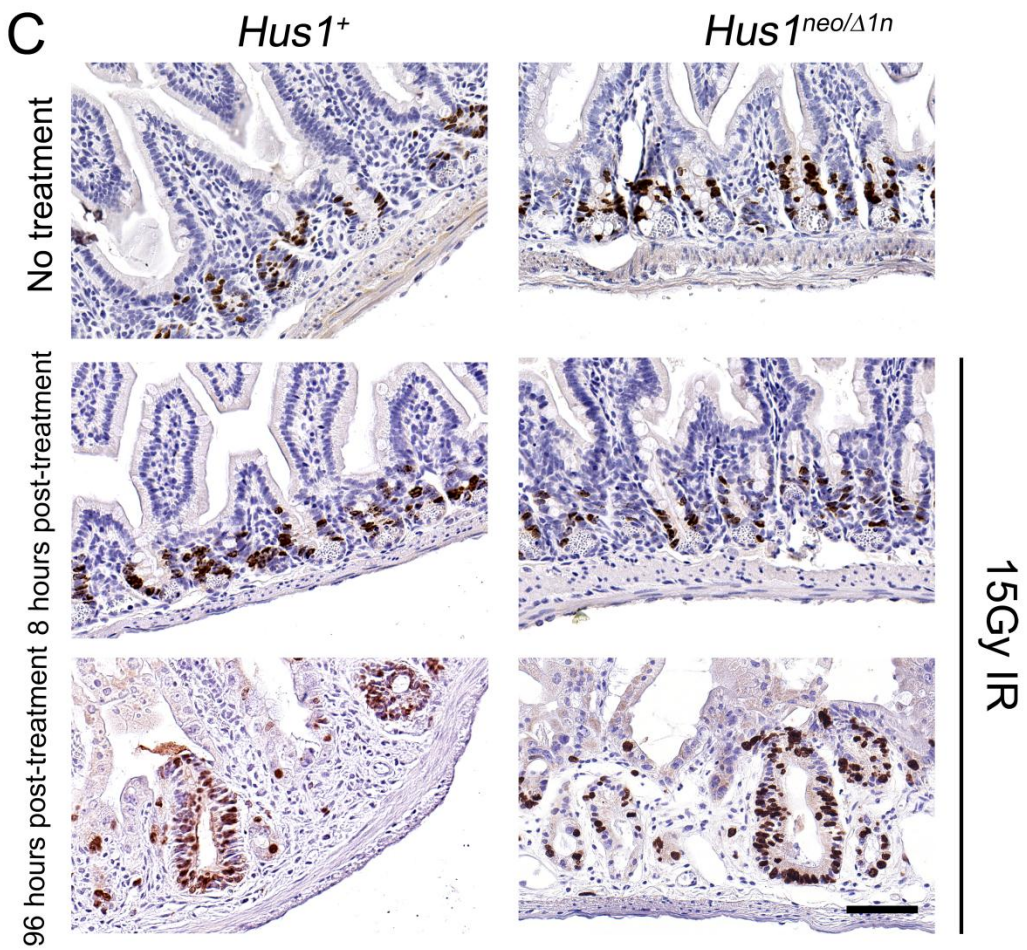
C
Hus1+
Hus1neo/Δ1n
No treatment
8 hours post-treatment
96 hours post-treatment
15Gy IR

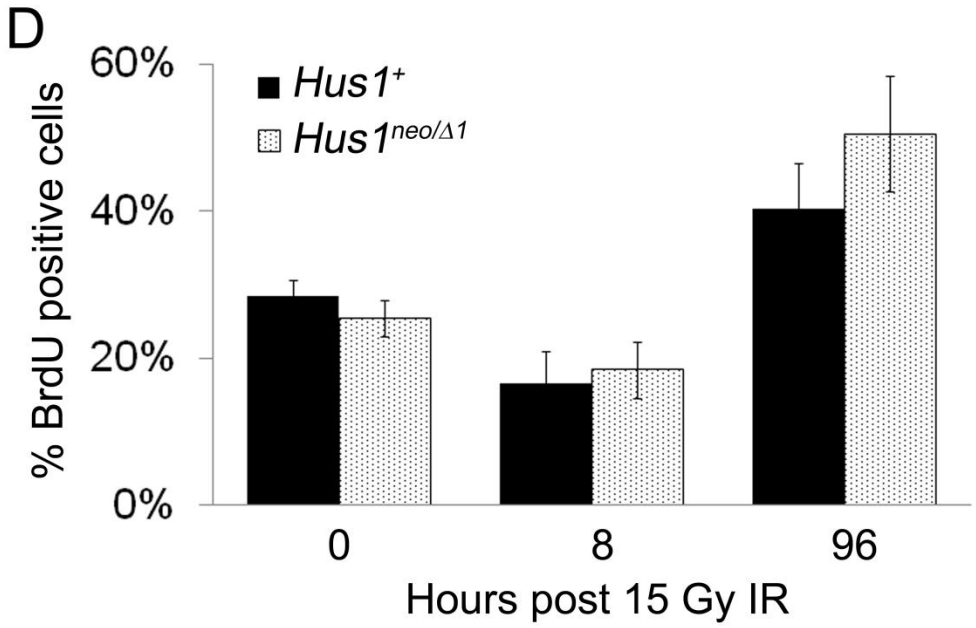
D
% BrdU positive cells
60%
40%
20%
0%
Hus1+
Hus1neo/Δ1
0
8
96
Hours post 15 Gy IR

Table 3.1 Major pathologic findings in *Hus1*$^{neo/\Delta 1}$ mice and *Hus1*$^{+}$ littermate controls after IR treatment[a].

Dose	Genotype	Major pathologic findings
9Gy	*Hus1*$^{+}$	Splenic white pulp depletion, increased red pulp macrophages, interstitial hemorrhage in testis, increased nuclear density in liver, mild neutrophilic colitis
	Hus1$^{neo/\Delta 1}$	Congested splenic red pulp, hemosiderin, EMH; colonic hyperplasia, rare neutrophils in the small intestine; moderate neutrophilic colitis
15Gy	*Hus1*$^{+}$	Severe necrotizing gastritis with hyperplasia, mild colitis with necrosis and hyperplasia, middle tubular ectasia
	Hus1$^{neo/\Delta 1}$	Severe gastric necrosis, inflammation and regeneration, SI contains mild hyperplasia and individual cell necrosis

[a]Samples were fixed in 10% formalin and processed for histology. Hematoxilin and eosin stained slides were used for assessment.

post 15 Gy IR the proliferation of the small intestinal crypt cells almost doubled when compared to the untreated groups, with *Hus1*$^{neo/\Delta 1n}$ mice showing an even higher proliferation (Figure 3.4B). These data show that differences in cell proliferation and apoptosis seen upon IR treatment in the highly replicating small intestinal crypts are not significantly affected by *Hus1* depletion. In both genotypic groups, we saw an increase in cell death at 8 hours post 15 Gy IR. These changes were accompanied by proliferative compensation at 96 hours.

To further examine the overlap between *Atm* and *Hus1* analysis of the cellular modifications in the small intestine was performed in the *Hus1*/*Atm* mice 8 hours post 4Gy IR. Preliminary data showed no significant histopathologic modifications in the *Hus1*/*Atm* mutant mice compared to the littermate representative controls (Figure 3.5). The analysis of cell proliferation and apoptosis using the BrdU and TUNEL assays showed that while increases in apoptosis and reduced proliferation were observed no differences were detected between the *Hus1*/*Atm* double mutant mice compared to control mice (Figure 3.6 A-B; C-D).

We next wanted to assess the *in vivo* levels of genomic instability in the *Hus1*/*Atm* double mutant mice using micronucleus assay. Mice of the representative genotypes were irradiated with a unique 0.7Gy whole body irradiation dose and blood was extracted before treatment (0 time point) or 24, 48 and 72 hours post treatment. Blood was fixed in methanol and process for MN assay as described in the Material and Methods. While similar kinetics of MN formation was observed in the wild type

Figure 3.5. Tissue morphology in mice with *Hus1/Atm* impairment following 4Gy ionizing radiation. Following euthanasia, isolated tissues were fixed in 10% formalin. Histological sections of paraffin-embedded tissues were stained with hematoxylin and eosin (HE) and subjected to pathological assessment. Representative images depicting tissue morphology in the small intestine from $Hus1^{neo/neo}Atm^{-/-}$ mice compared to littermate controls upon 4 Gy IR. The small intestinal crypts are grossly normal 8hrs post IR. No difference in cellularity of the crypt was observed between the genotypic groups

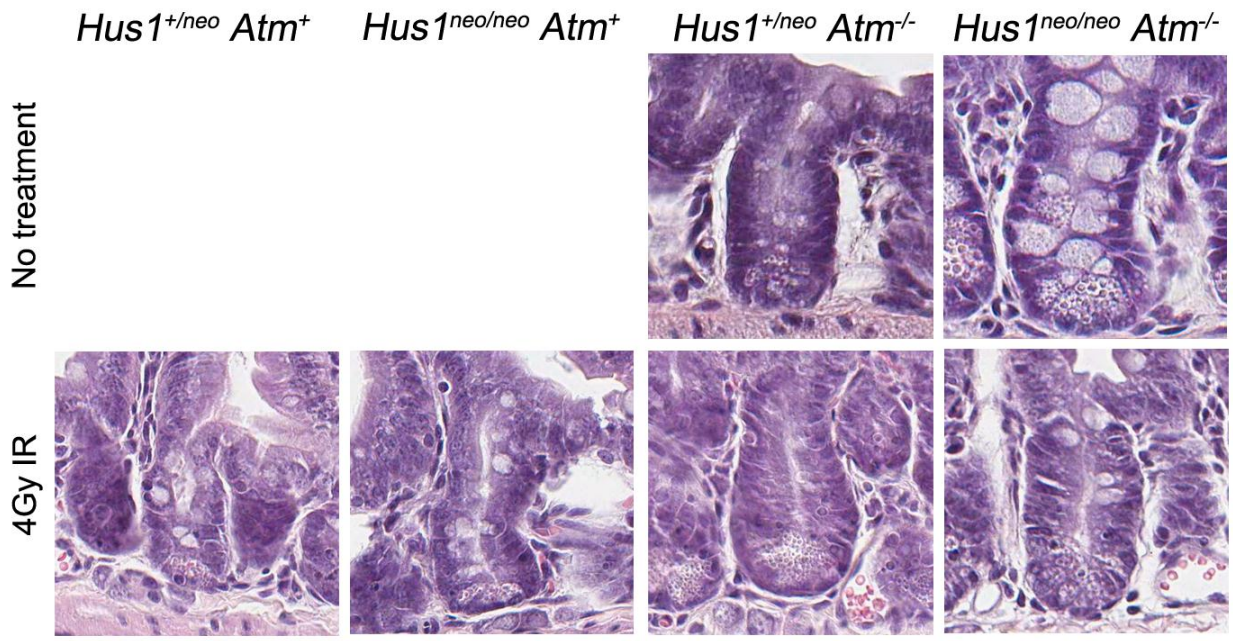
Hus1+/neo Atm+
Hus1neo/neo Atm+
Hus1+/neo Atm-/-
Hus1neo/neo Atm-/-
No treatment
4Gy IR

Figure 3.6. Analysis of cell proliferation and apoptosis in the small intestine from *Hus1/Atm double mutant mice* as compared to *Hus1* control group mice following 4Gy ionizing radiation. Immunohistochemical staining of TUNEL positive cells and BrdU positive cells in paraffin embedded small intestine sections. (A) Representative images depicting TUNEL positive cells, indicative of apoptosis, in the small intestinal crypts from $Hus1^{neo/neo}Atm^{-/-}$ mice compared to littermate controls after no treatment or the indicated time points after 4Gy IR. (B) Quantification of TUNEL positive cells in the small intestinal crypts at 0 and 8. 8 hours post 4Gy IR all genotypic groups showed significant increased levels of apoptosis when compared to the untreated group ($p<0.05$; Student's t test). No significant difference between the $Hus1^{neo/neo}Atm^{-/-}$ mice and littermate controls was noted. (C) Representative images depicting BrdU positive cells, indicative of proliferation, in the small intestinal crypts from $Hus1^{neo/neo}Atm^{-/-}$ mice as compared to littermate controls after no treatment or the indicated time points after 4Gy IR. (D) Quantification of BrdU positive cells in the small intestinal crypts at 0 and 8 hours post 4Gy. 8 hours post 4Gy IR proliferation was significantly reduced in all groups ($p<0.05$; Student's t test) except the $Hus1^{neo/neo}Atm^{-/-}$ mice. Quantitation was done in intact intestinal crypts and $n\geq5$ intestinal crypts per mouse were counted. Error bars represent ± standard deviation.

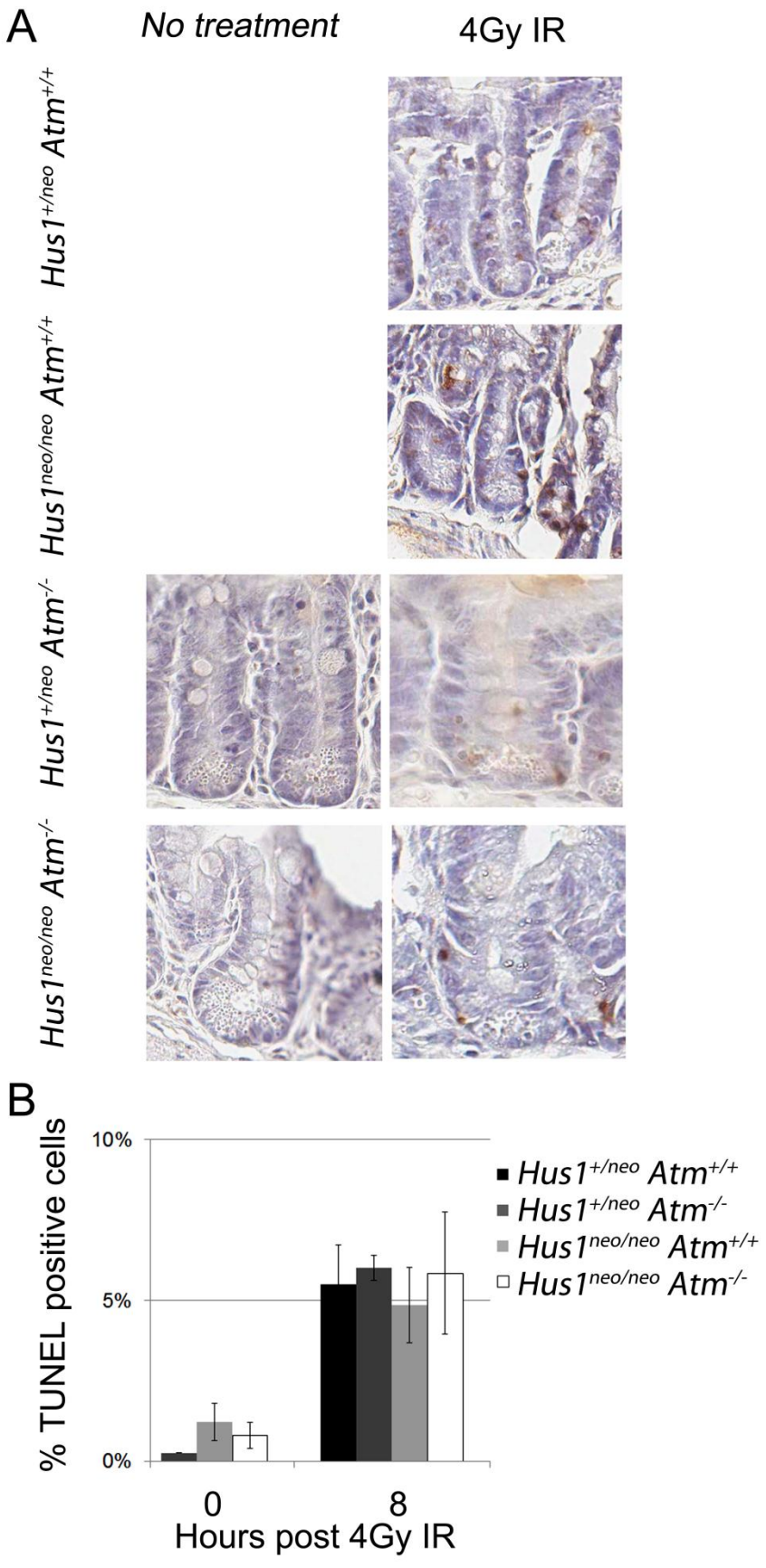
A
No treatment
4Gy IR
Hus1+/neo Atm+/+
Hus1neo/neo Atm+/+
Hus1+/neo Atm-/-
Hus1neo/neo Atm-/-
B
% TUNEL positive cells
10%
5%
0%
0
8
Hours post 4Gy IR
Hus1+/neo Atm+/+
Hus1+/neo Atm-/-
Hus1neo/neo Atm+/+
Hus1neo/neo Atm-/-

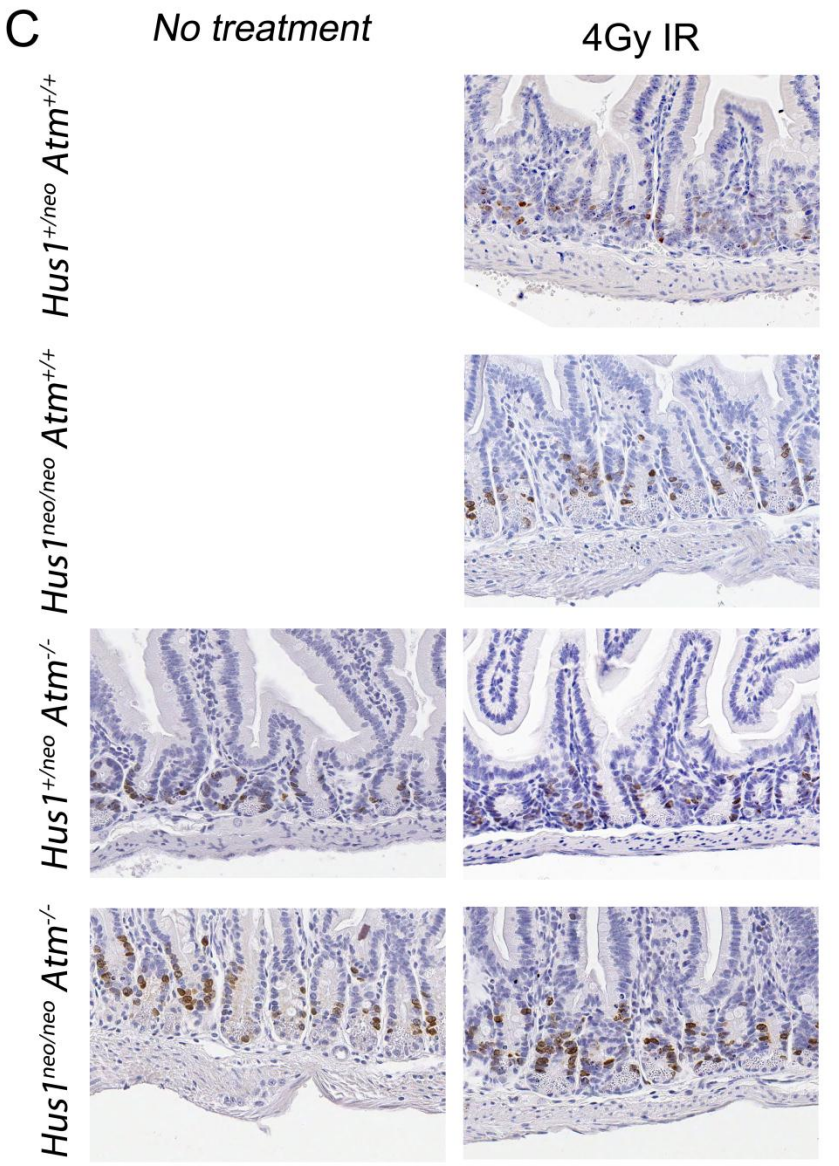
C
No treatment
4Gy IR
Hus1+/neo Atm+/+
Hus1neo/neo Atm+/+
Hus1+/neo Atm-/-
Hus1neo/neo Atm-/-

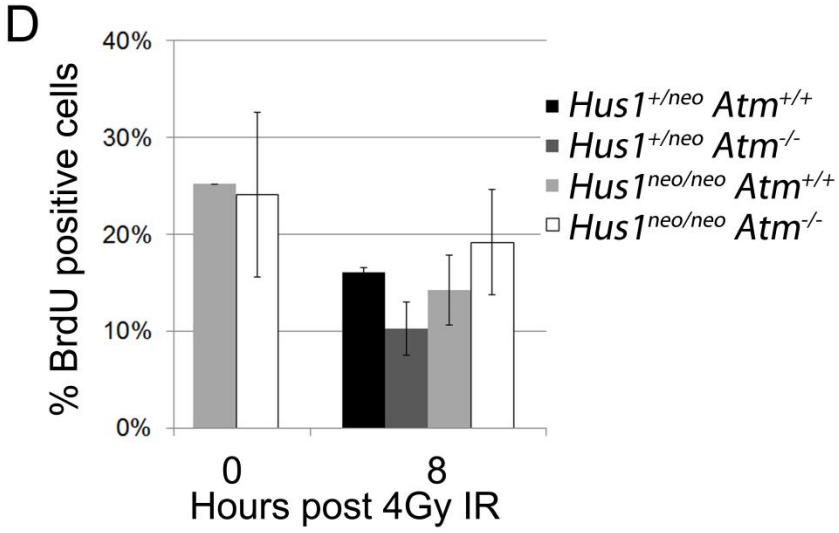
D
% BrdU positive cells
40%
30%
20%
10%
0%
0
8
Hours post 4Gy IR
Hus1+/neo Atm+/+
Hus1+/neo Atm-/-
Hus1neo/neo Atm+/+
Hus1neo/neo Atm-/-

Figure 3.7. Failure to recover from IR induced genomic instability in *Hus1*$^{neo/neo}$*Atm*$^{-/-}$ mice. A) Line chart shows the average percent of peripheral blood cells with micronuclei in mice of the indicated genotypes before treatment and 24, 48 and 72 hours post 0.7 Gy IR treatment. *Hus1*$^{neo/neo}$*Atm*$^{+/+}$ and *Hus1*$^{+/neo}$*Atm*$^{+/+}$ mice showed similar levels of GIN while *Hus1*$^{+/neo}$*Atm*$^{-/-}$ mice start with significant increase in micronucleus formation ($p<0.05$; Student's t test). All of these genotypic groups return to basal starting levels at 72 hours post IR. The combined effect of *Hus1* impairment in an *Atm* null background (*Hus1*$^{neo/neo}$*Atm*$^{-/-}$) resulted in higher basal levels of MN formation compared with all the other groups ($p<0.05$; Student's t test) and were unable to recover to starting MN levels ($p<0.05$; Student's t test).

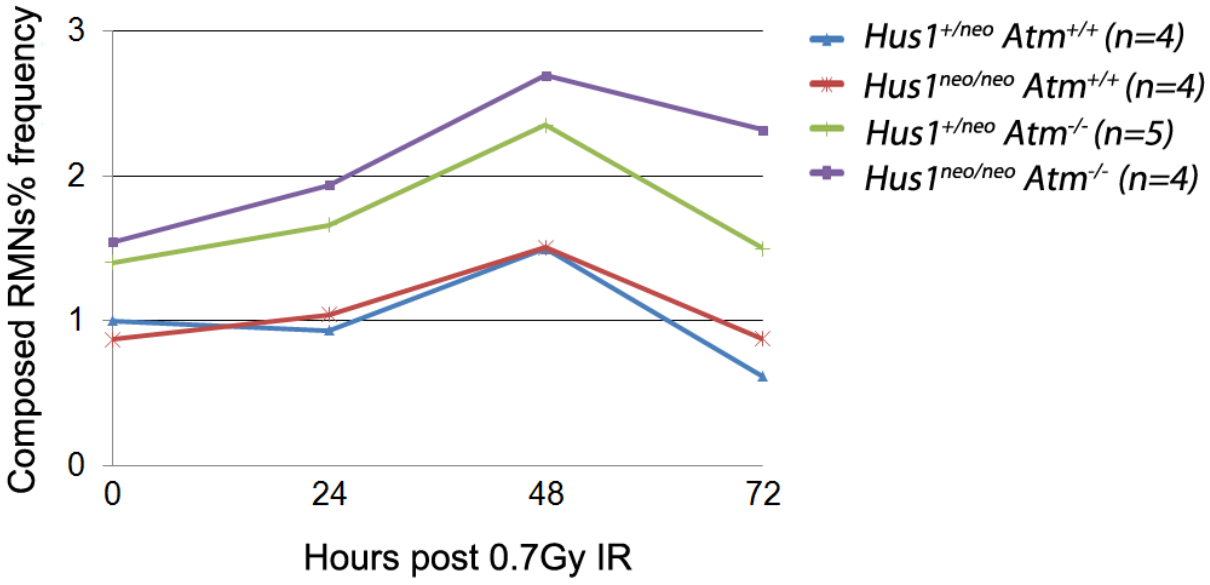
Composed RMNs% frequency
3
2
1
0
0
24
48
72
Hours post 0.7Gy IR
Hus1+/neo Atm+/+ (n=4)
Hus1neo/neo Atm+/+ (n=4)
Hus1+/neo Atm-/- (n=5)
Hus1neo/neo Atm-/- (n=4)

group and the *Hus1* and *Atm* single mutants at 24, 48 and 72 hours, the *Hus1*/*Atm* double mutant mice never recover to the initial MN levels showing that they are defective in the response to IR in the hematopoietic niche (Figure 3.7).

Our data highlight a difference in the proliferative but not apoptotic potential of untreated intestinal crypt cells between *Hus1* wild type and *Hus1* mutant mice. This is in line with the major role that the ATR pathway plays in highly replicative cells. Following IR treatment the *Hus1*/*Atm* double mutant mice fail to recover from the increased MN formed post IR, underlining a different response in this compartment.

3.4.3 ***Hus1*** **is critical for the** ***in vivo*** **response to replication stress reagents hydroxyurea and mitomycin C.**

The ATR pathway is the main responder to replication stress induced lesions and as such is critical for replication progression. Our analysis of the role of ATR deficient cells in response to replication stress inducing agents showed that these cells are highly sensitive to replication stress inducing reagents such as UV, HU or MMC (Yang, Yu et al. 2003). To explore the effect of ATR pathway deregulation *in vivo* we subjected *Hus1* deficient mice to the replication stress inducing reagents HU and MMC.

HU is a cytostatic antimetabolite that acts by inhibiting ribonucleotide reductase (RNR) (Koc, Wheeler et al. 2004). At low doses HU has been shown to be highly cytotoxic for ATR pathway deficient cells while little effect was seen in the wild

Figure 3.8. Significant increased apoptosis in *Hus1* mutant embryos following hydroxyurea treatment. Representative sections of Feulgen-Schiff staining of *Hus1*$^{neo/\Delta 1}$ embryos at E8.5. (A) Higher magnification view of neural tube showing representative apoptotic (red arrow head) and mitotic (black arrow head) figures. (B) Bar graph indicating the percent of apoptotic and mitotic cells (± standard deviation) as determined from Fuelgen-Shiff stained sections of embryos of the indicated genotypes. Student's t-test identified a significant increase in apoptosis ($p<0.05$) in *Hus1*$^{neo/\Delta 1}$ (n=3) when compared to *Hus1* controls (n=9). Control genotypes include *Hus1*$^{+/+}$, *Hus1*$^{+/neo}$, and *Hus1*$^{+/\Delta 1}$.

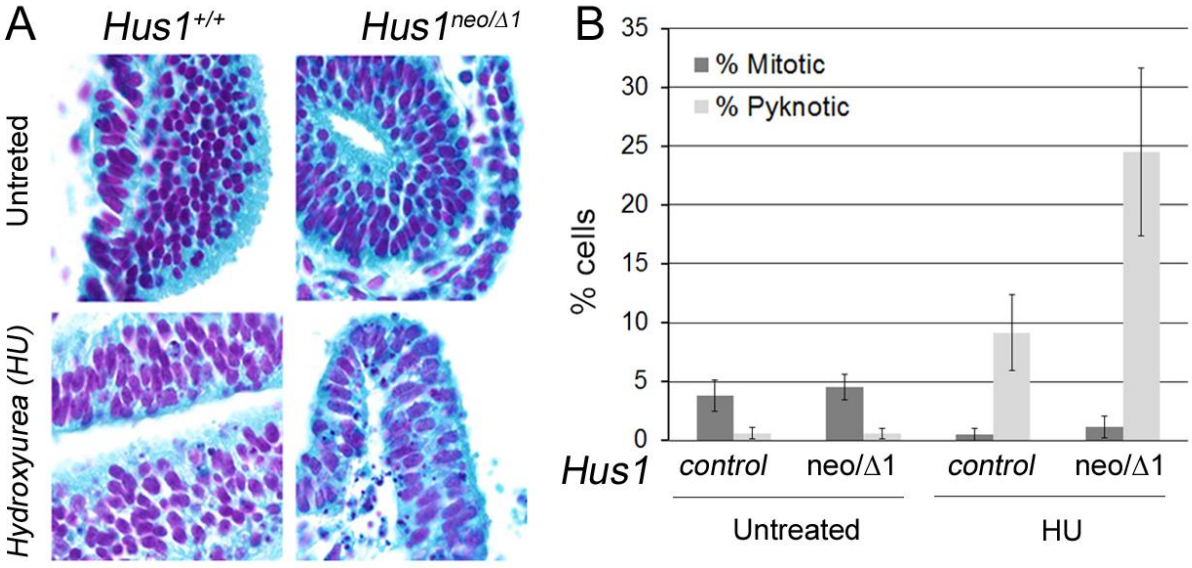
A
Hus1+/+
Hus1neo/Δ1
Untreted
Hydroxyurea (HU)
B
% Mitotic
% Pyknotic
% cells
35
30
25
20
15
10
5
0
Hus1
control
neo/Δ1
control
neo/Δ1
Untreated
HU

type control cells (Weiss, Matsuoka et al. 2002). The toxicity associated with *in vivo* administration of HU by i.p. delivery to wild type pregnant mice showed that administration of a 1g/kg body weight dose at E8.5 results in embryo lethality if pregnancy was taken to term while 400mg/kg and 800mg/kg body weight had no effect on embryo survival but determined increased cell death in the central nervous system (CNS). The increased apoptosis in the CNS was detectable as early as 3 hours post treatment. It showed the highest levels after 12 hours followed by recovery at 48 hours (Woo, Katayama et al. 2003; Woo, Katayama et al. 2004). To determine the HU toxicity associated with *Hus1* loss females from $Hus1^{+/neo}$ x $Hus1^{+/ex}$ crosses were injected IP with 400mg/kg body weigh HU at the E8 stage and the cell proliferation and apoptosis the embryos of the representative phenotypes was assessed 12 hours later using the Feulgen-Schiff staining technique as described in Material and Methods (Figure 3.8A). No difference in the percent of mitotic or pyknotic cells was seen in untreated $Hus1^{+}$ and $Hus1^{neo/\perp 1n}$ genotypes. As previously reported, HU treatment caused a significant decrease in the percentage of mitotic figures concomitant with an increase in the percentage of pyknotic nuclei, indicative of apoptosis, in the $Hus1^{+}$ group when compared to the untreated groups. More importantly, quantification of the cell proliferation and apoptosis upon treatment revealed that the $Hus1^{neo/\perp 1n}$ E8.5 embryos showed a significant increase in cell death but no change in proliferation when compared to the littermate wild-type controls (Figure 3.8 B). These data highlight the requirement for *Hus1* in the response to HU *in vivo*.

Figure 3.9. *Hus1* hypomorphic mice show hyper sensitivity to mitomycin C. Kaplan-Meyer survival analysis shows that $Hus1^{neo/\Delta 1}$ mice are hypersensitive to MMC at both 8mg/kg (A) and 4mg/kg (B) MMC doses when compared to the $Hus1^{+}$ littermate controls. (C) Kaplan-Meyer survival analysis shows that $Hus1^{neo/neo}Atm^{-/-}$ mice are hypersensitive to 4mg/kg MMC. The cohort treated included $Hus1^{+/neo}Atm^{+/+}$ (n=6); $Hus1^{neo/neo}Atm^{+/+}$ (n=11), $Hus1^{+/neo}Atm^{-/-}$ (n=4) and $Hus1^{neo/neo}Atm^{-/-}$ (n=7) mice. Mice of the indicated genotypes were treated with 8mg/kg or 4mg/kg MMC respectively via intraperotoneal delivery. Animals were monitored for survival and a chi-square statistical analysis was performed. Control $Hus1^{+}$ genotypes include $Hus1^{+/+}$, $Hus1^{+/neo}$, and $Hus1^{+/\Delta 1}$.

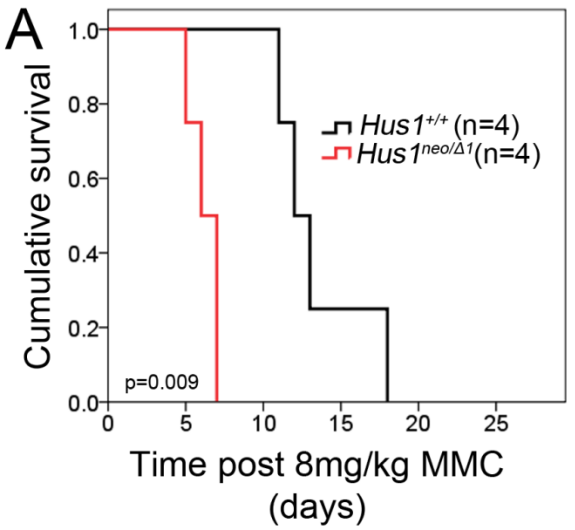
A
Cumulative survival
1.0
0.8
0.6
0.4
0.2
0.0
0
5
10
15
20
25
Hus1+/+ (n=4)
Hus1neo/Δ1(n=4)
p=0.009
Time post 8mg/kg MMC
(days)

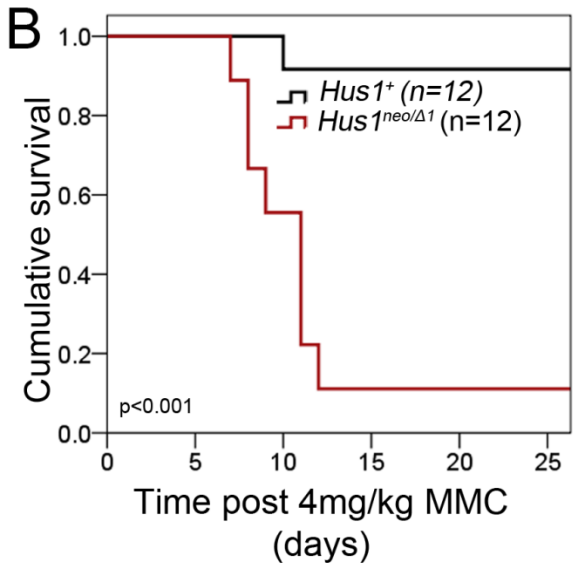
B
Cumulative survival
1.0
0.8
0.6
0.4
0.2
0.0
0
5
10
15
20
25
Hus1+ (n=12)
Hus1neo/Δ1 (n=12)
p<0.001
Time post 4mg/kg MMC
(days)

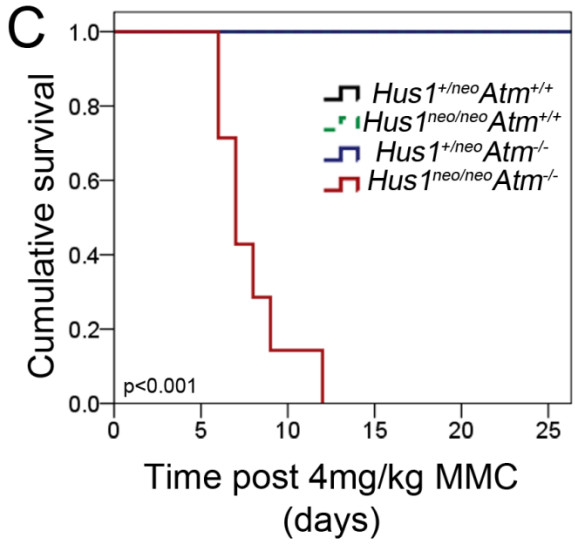
C
Cumulative survival
1.0
0.8
0.6
0.4
0.2
0.0
0
5
10
15
20
25
Hus1+/neoAtm+/+
Hus1neo/neoAtm+/+
Hus1+/neoAtm-/-
Hus1neo/neoAtm-/-
p<0.001
Time post 4mg/kg MMC
(days)

Table 3.2 Major pathologic findings in *Hus1*$^{neo/\Delta 1}$ mice and *Hus1*$^{+}$ littermate controls after MMC treatment[a].

Dose	Genotype	Major pathologic findings
4 mg/kg	*Hus1*$^{+}$	Severe necrotizing gastritis with hyperplasia, mild colitis with necrosis and hyperplasia, mild tubular ectasia in the kidney
	Hus1$^{neo/\Delta 1}$	Decreased white pulp in spleen, severe necrotizing gastritis with hyperplasia, mild colitis with necrosis and hyperplasia, mild tubular ectasia in the kidney

[a]Samples were fixed in 10% formalin and processed for histology. Hematoxilin and eosin stained slides were used for assessment.

Figure 3.10. Tissue morphology in mice with partial *Hus1* impairment following 4mg/kg mitomycin C. Tissue morphology was evaluated using Hematoxylin and Eosin staining (HE). The small intestine crypts are grossly normal 8hrs post MMC. At 96 hours post treatment both genotypic groups show enlarged crypts. Additionally, at 96 hours post treatment the small intestine from the $Hus1^{neo/\Delta 1}$ mice showed more severe pathologies: the $Hus1^{neo/\Delta 1}$ mice had completely disrupted crypts (black arrowhead) and the average crypt was larger when compared to that of the $Hus1^{+}$ group. Size bar corresponds to 50 microns. Control $Hus1^{+}$ genotypes include $Hus1^{+/+}$, $Hus1^{+/neo}$, and $Hus1^{+/\Delta 1}$.

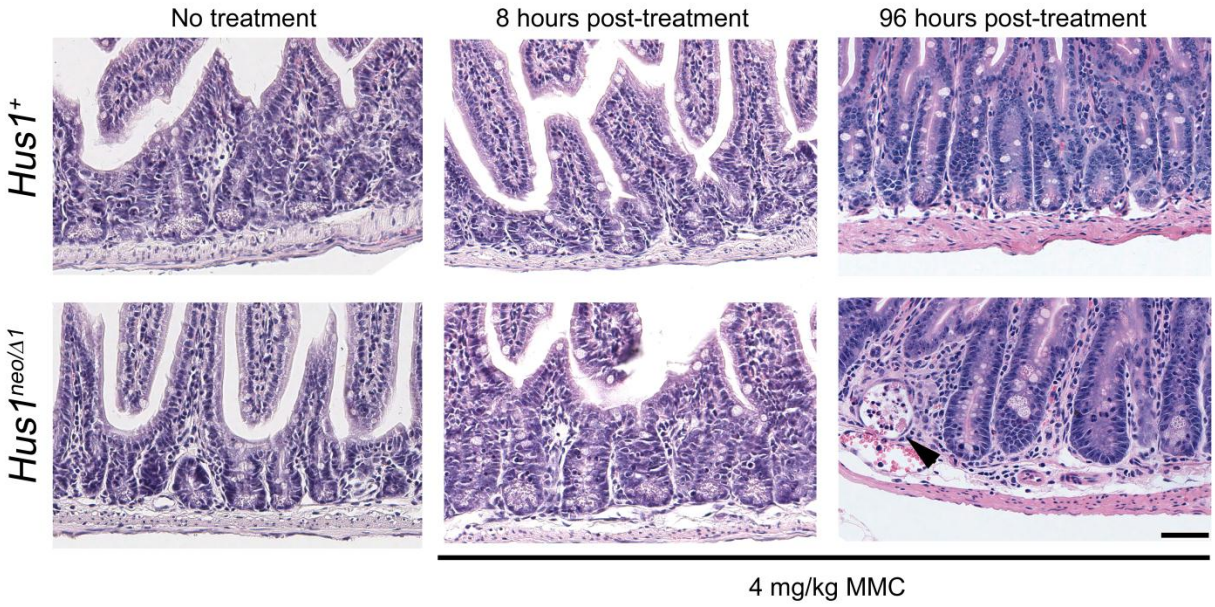
No treatment
8 hours post-treatment
96 hours post-treatment
Hus1+
Hus1neo/Δ1
4 mg/kg MMC

To extend this analysis to adult mice, MMC, a DNA cross-linking reagent was used. MMC toxicity in wild type mice has been tested previously. Mice treated with 8 mg/kg body weight MMC, representing the median lethal dose (LD50) in 14 days survival studies, suffer from hematopoietic, intestinal and renal toxicity (Crooke and Bradner 1976; Legha 1985). Mice of the *Hus1*$^{+}$ and *Hus1*$^{neo/\Delta 1n}$ representative genotypes were treated i.p. with 8mg/kg or 4mg/kg body weigh MMC and their health status was monitored for 30 days. Following treatment, independent of the dose used, *Hus1*$^{neo/\Delta 1n}$ mice showed significant hypersensitivity to MMC compared to the littermates controls (Figure 3.9A, B). This shows that *Hus1* is critical for the response to MMC *in vivo*.

Because our previous research (Chapter 2) proposed that the *Hus1*/*Atm* interaction would be critical for the response to replication stress, and to further investigate the overlap between ATM and HUS1 in the response to MMC we used *Hus1*/*Atm* double mutant mice. *Hus1*$^{+/neo}$ wild type-like controls and Hus1$^{neo/neo}$ single mutant mice showed no sensitivity to 4mg/kg body weight MMC. In contrast, and as previously reported (Kirshner, Rathavs et al. 2009), *Atm*$^{-/-}$ single mutant mice showed mild MMC sensitivity demonstrated by significant loss in body weight when compared with wild type mice (data not shown). Nevertheless, the *Atm*$^{-/-}$ single mutant mice recovered and survived treatment. In contrast, Hus1$^{neo/neo}$Atm$^{-/-}$ double mutant mice were significantly more sensitive to MMC when compared to either *Hus1* or *Atm* single mutant mice, and 100% of *Hus1*/*Atm* double mutant mice died (Figure 3.9 D).

Thus, backed up by ATM, *Hus1*$^{neo/\Delta 1n}$ mice have sufficient *Hus1* to deal with normal, physiological levels of replication stress, but when challenged with external genotoxins, such as HU or MMC, they become incapable to respond and show severe phenotypes. Moreover, we show that *Hus1* and *Atm* act in concert in response to MMC treatment, highlighting the cooperation between the ATM and ATR pathways in the response to replication stress *in vivo*.

3.4.4 **Similar mitomycin C induced responses in the small intestine of the *Hus1* mutant mice.**

Because at 96 hours post treatment histopathological examination of mice treated with 4 mg/kg body weigh MMC revealed a *Hus1* specific gastro-intestinal pathology (Table 3.2, Figure 3.10), characterized by increased crypt size in some crypts and complete depletion of others, the fate of the cells in the small intestinal crypts of *Hus1*$^{+}$ and *Hus1*$^{neo/\Delta 1n}$ mice was assessed 8 hours and 96 hours post treatment. Proliferation was quantified as percentage BrdU incorporation and apoptosis through TUNEL staining. 8 hours post MMC treatment, there was a significant increase in apoptosis in both *Hus1*$^{+}$ and *Hus1*$^{neo/\Delta 1n}$ mice, while at 96 hours post-treatment the apoptosis levels returned to untreated levels. No difference between the two genotypes was noted (Figure 3.11 A-B). Proliferation assessment showed a different proliferation pattern when the two genotypes were followed at the two time points after MMC. In the *Hus1*$^{+}$ group we could detect a decrease in the proliferation of the

Figure 3.11. Analysis of cell proliferation and apoptosis in the small intestine from *Hus1*$^{neo/\Delta 1}$ as compared to *Hus1*$^{+}$ mice following 4mg/kg mitomycin C. Immunohistochemical staining of TUNEL positive cells and BrdU positive cells in paraffin embedded small intestine sections. (A) Representative images depicting TUNEL positive cells, indicative of apoptosis, in the small intestinal crypts from *Hus1*$^{neo/\Delta 1}$ mice as compared to littermate controls after no treatment or the indicated time points after 4mg/kg MMC. (B) Quantification of TUNEL positive cells in the small intestinal crypts at 0, 8, and 96hrs post 15Gy. 8 hours post MMC treatment both genotypic groups showed significant increased levels of apoptosis when compared to the untreated group ($p<0.01$; Student's t test); no significant difference between the *Hus1*$^{neo/\Delta 1}$ mice and littermate controls was noted. At 96 hours although the crypts show severe morphology changes the apoptosis returned to untreated levels. (C) Representative images depicting BrdU positive cells, indicative of proliferation, in the small intestinal crypts from *Hus1*$^{neo/\Delta 1}$ mice as compared to littermate controls after no treatment or the indicated time points after 4mg/kg MMC. (D) Quantification of BrdU positive cells in the small intestinal crypts at 0, 8, and 96 hours post 15Gy. Significant decreased levels of proliferation were observed in the *Hus1*$^{neo/\Delta 1}$ mice as compared to littermate controls in the untreated group ($p=0.03$;

Student's t test). 8 hours post MMC treatment proliferation was significantly increased in the *Hus1*$^{neo/\perp 1}$ group ($p<0.05$; Student's t test) while in the *Hus1*$^{+}$ group proliferation was decreased ($p=0.1$; Student's t test). At 96 hours proliferation returned at similar untreated levels. Size bar corresponds to 50 microns. Control *Hus1*$^{+}$ genotypes include *Hus1*$^{+/+}$, *Hus1*$^{+/neo}$, and *Hus1*$^{+/\perp 1}$. $n\geq 3$ mice for each genotype and time point were used for quantitation. Quantitation was done in intact intestinal crypts and $n\geq 5$ intestinal crypts per mouse were counted. Error bars represent standard deviation.

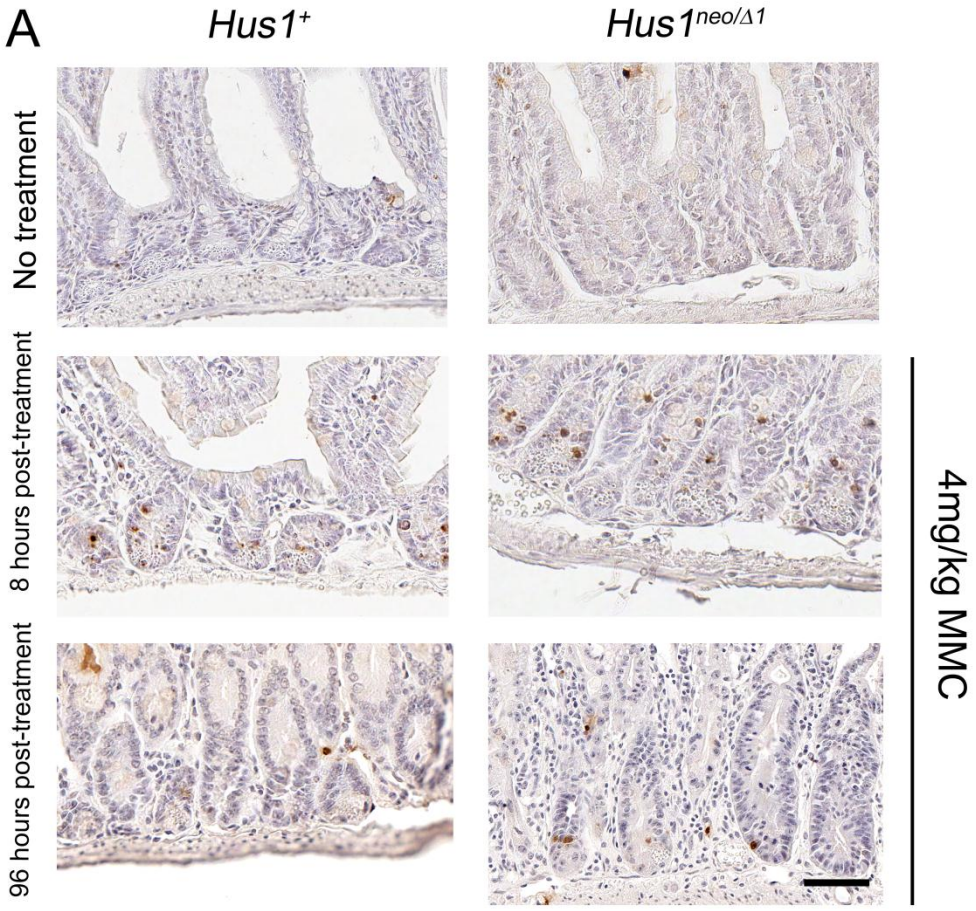
A
Hus1+
Hus1neo/Δ1
No treatment
8 hours post-treatment
96 hours post-treatment
4mg/kg MMC

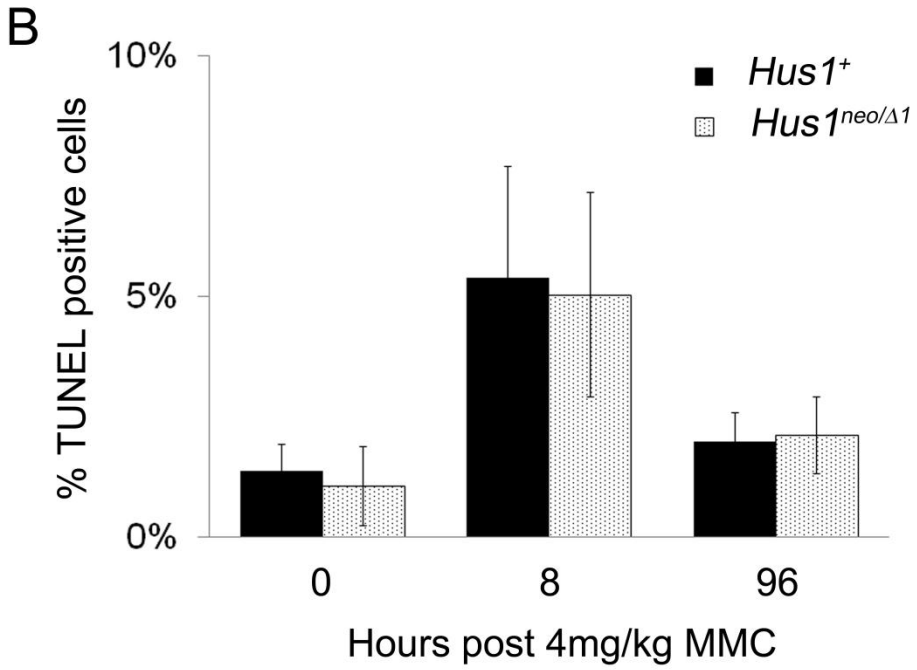
B
10%
5%
0%
% TUNEL positive cells
Hus1+
Hus1neo/Δ1
0
8
96
Hours post 4mg/kg MMC

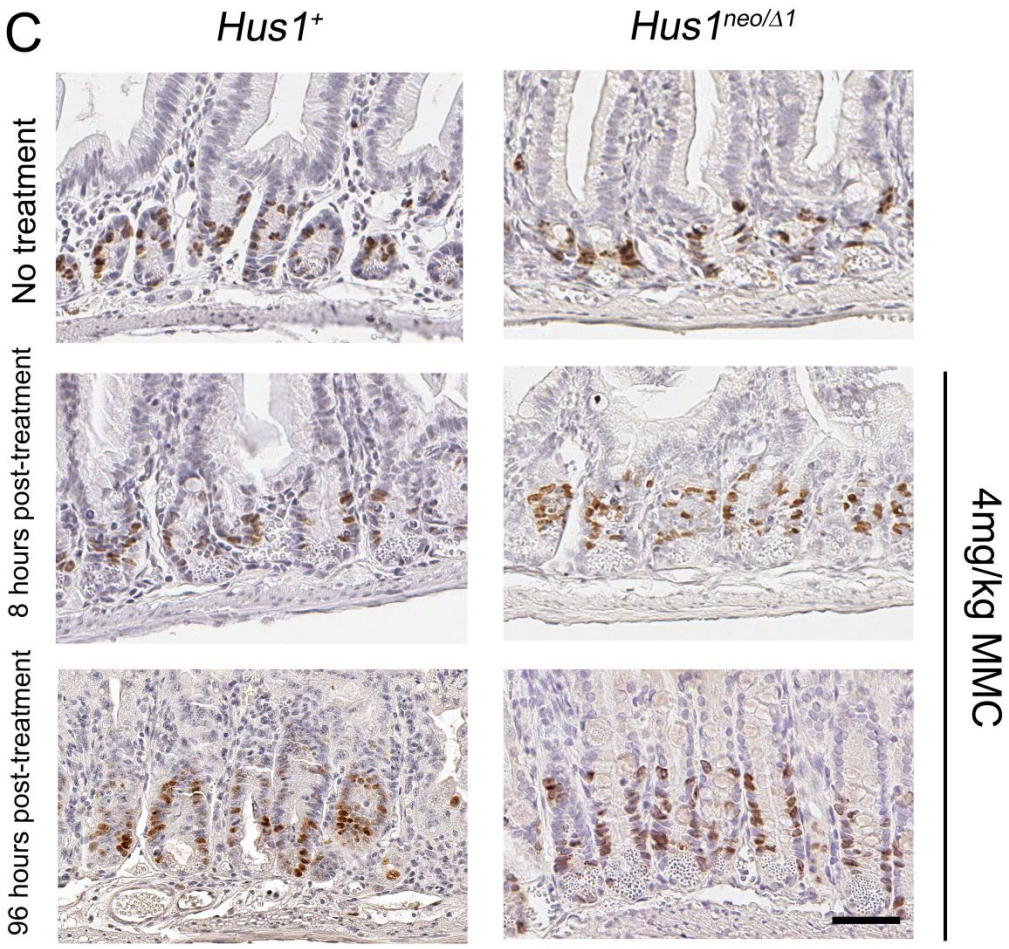
C
Hus1+
Hus1neo/Δ1
No treatment
8 hours post-treatment
96 hours post-treatment
4mg/kg MMC

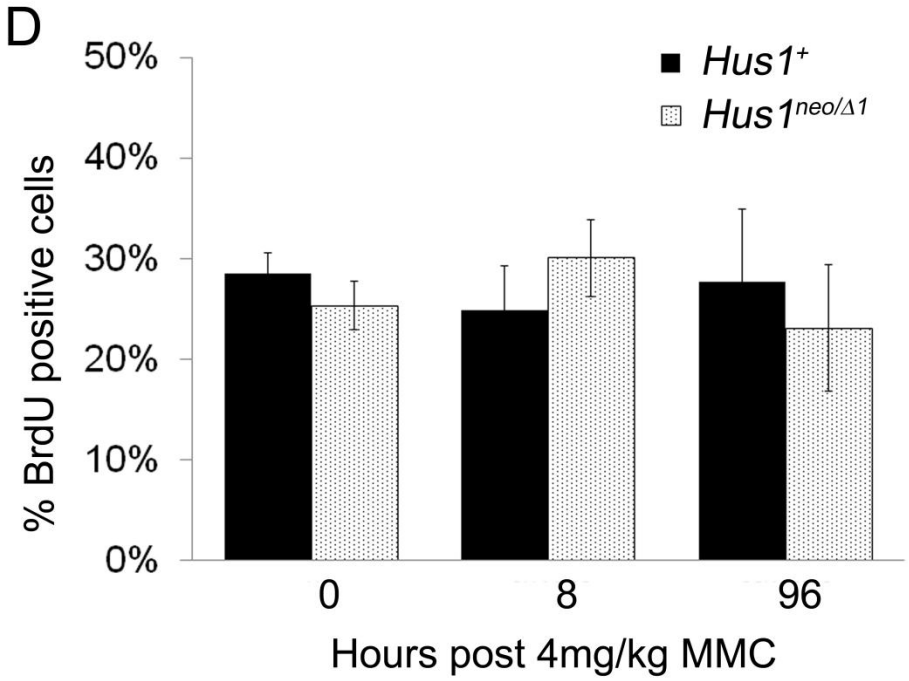
D
Hus1+
Hus1neo/Δ1
% BrdU positive cells
50%
40%
30%
20%
10%
0%
0
8
96
Hours post 4mg/kg MMC

cells of the small intestinal crypt 8 hours post MMC and a recovery to untreated levels at 96 hours. In contrast, quantification of the BrdU positive cells in the *Hus1*$^{neo/\Delta 1n}$ crypts revealed that at 8 hours post treatment there was an increase in proliferation followed by recovery at 96 hours (Figure 3.11 B-C). The MMC analysis of the cell proliferation and apoptosis in the small intestine at 8 and 96 hours post-treatment show that while *Hus1* deficient mice present a mild proliferation phenotype cannot explain the associated lethality.

Together these results show that *Hus1* is critical for the response to the replication stress inducing reagent MMC, and that when the ATR pathway is impaired the ATM pathway compensates for its loss.

3.5 Discussion

The ATR pathway is critical for the response to replication stress inducing agents by initiating a signal transduction pathway that activates the DDR. ATR pathway defective cells and organisms cannot cope with the replication induced stress and show lethal phenotypes. Here we used the *Hus1* mouse model as a unique genetic tool for the understanding of the importance of the ATR pathway in response to genotoxin treatment *in vivo*. We show for the first time that the mice showing reduced *Hus1* levels can respond as well as wild type mice to the DSB inducing reagent IR but

are hypersensitive to the replication stress reagents HU and MMC. The data presented here show that *in vivo* there is a clear parallelism between the ATR and ATM pathways.

Ionizing radiations are both a potent environmental threat for animal and human health as well as a key tool in the battle against cancer. The canonical view that the ATM and ATR pathways act in parallel with ATM being the main responder to IR induced DSBs was challenged in the past decade by biochemical and cell culture data that showed that ATR pathway deficiency results in similar sensitivities to IR, proposing that ATM and ATR act as overlapping pathways. This research proposed that although ATM is critical for DSB signaling the repair of such lesions require an intermediary step that is ATR dependent. Our data show that mice defective for the ATR pathway show similar sensitivities to different IR doses as their wild type controls, suggesting that *in vivo* the two pathways act in parallel. This idea is supported by our previous observation that *Hus1*/*Atm* double mutant mice are no more sensitive to IR stress than $Atm^{-/-}$ single mutants alone. Hence, *Hus1* response to IR is not obscured by the presence of ATM. Consistent with this observation we show that at the level of the small intestine and skin we can clearly detect an IR dependent response but no genotype specificity as both $Hus1^{neo/\Delta 1n}$ and wild type control mice show similar rates of cell death. The proliferation differences present in the $Hus1^{neo/\Delta 1n}$ mice are independent of IR treatment highlighting the critical role for the ATR

pathway in highly replicating tissues. Indeed *Hus1*$^{neo/\Delta 1n}$ mice are hypersensitive to the replication stress inducing reagents HU and MMC. One important distinction to be made is that the *Hus1* deficient mice are hypomorphic, thus the partial function present might be enough to sustain the ATR role upon IR stress. Another option is that the *Hus1* level is enough for ATR activation but not enough for *Hus1*-dependent repair. *Hus1* has been shown to be independently involved in base excision repair and translesion synthesis, both of which can be activated by replication stress (Toueille, El-Andaloussi et al. 2004). In fact a similar hypothesis was proposed based on our previous research on the genetic interaction between *Hus1* and *Atm* (Chapter 1). We have shown that while *Hus1*/*Atm* deficient mouse embryonic fibroblast can respond to genotoxin insults as well as *Atm* single mutants, *Hus1*/*Atm* double mutant mice show increased GIN levels and present with severe phenotypes. We propose that all of these phenotypes are a consequence of the inability of *Hus1*/*Atm* mice to deal with replication stress.

To test the above we treated the *Hus1* mice with the replication stress inducing reagents HU and MMC. As expected the *Hus1*$^{neo/\Delta 1}$ mice showed a marked sensitivity to these genotoxins. The hypersensitivity of the *Hus1*$^{neo/\Delta 1n}$ mice is highlighted by the low dose required to determine lethality; at half the LD50 for wild type mice 90% of the *Hus1*$^{neo/\Delta 1n}$ mice die within 10 days of exposure. Although the pathological findings showed differential pathologies when the two *Hus1* genotypic groups were

compared (*Hus1*$^{+}$ vs. *Hus1*$^{neo/\perp 1}$) in the gastrointestinal track, hematopoietic system and kidney, surprisingly no difference between the two genotypes was observed when cell proliferation and apoptosis was quantified at 8 hours and 96 hours in the small intestine. This might be due to the time points after treatment used for sampling. While IR acts immediately and at the level of the entire organism, administration of MMC might require additional time to detect a cellular response.

Because the kinetics of the response to MMC is different from that to IR more sampling time points might be necessary. At 96 hours the intestinal crypts are so affected that another quantification modality might be necessary; while the proliferation and apoptosis levels at the level of the detectable crypts is not significantly different we cannot exclude that overall there are less intact crypts in the *Hus1*$^{neo/\perp 1n}$ mice. This argues again for an intermediary sampling point between 8 hours and 96 hours, where this difference might be individualized. Another plausible hypothesis is that the mice don't die because of a gastrointestinal syndrome but rather because of another organ system is failing. Other than gastrointestinal deficiency, in wild type mice MMC has been shown to determine hematopoietic syndrome and kidney failure. The analysis of these systems at 8 hours and 96 hours showed that while we see a mild hematopoietic phenotype in the spleen and bone marrow the kidney is not affected. To further understand the effect of MMC on the

hematopoietic system analysis complete blood counts will be performed before treatment and at different time points after treatment.

The survival data indicate that the *Hus1* dependent molecular mechanisms are involved in the response to the replication stress genotoxin MMC. Like *Hus1*$^{neo/\Delta 1n}$ mice, the *Hus1*/*Atm* double mutants are also hypersensitive to MMC, but not IR. This shows that after MMC treatment *Hus1*$^{neo/\Delta 1n}$ and *Hus1*^{neo1eon} deficient mice cannot repair the induced lesions that collapse into DSBs and require the ATM pathway for survival, thus explaining the differential sensitivity to MMC between *Hus1* and *Atm* single mutants and *Hus1*/*Atm* double mutants. Thus, in response to replication stress there is a clear cooperation between the two pathways to allow for survival. We cannot exclude though a direct role of *Hus1* in signaling to the Fanconi anemia complementation group genes that are critical for the response to cross-linking reagents like MMC (Knipscheer, Raschle et al. 2009). Recent evidence showing that combined *Atm*/Fanconi anemia deficiency results in synthetic lethality support this hypothesis (Perry and Tainer 2011).

The data presented here have an important impact on our understanding of the effects of the ATR pathway deficiency both in physiologic conditions as well as after genotoxin treatment. Inhibitors for the ATR pathway are currently tested in clinical trials for cancer therapy, and our data supports the use for such inhibitors concomitant with replication stress inducing reagents such as HU and MMC. We

show that the interaction between the two is very strong and such approaches are expected to give substantial results in specifically killing cancer cells if ATR pathway inhibition can be fine-tuned. We also show that such approaches might be even more efficient for tumors that are deficient for the ATM pathway, which may represent as many as 30% of all cancers.

3.6 Acknowledgements

The data presented in this Chapter are the result of the collaboration between different members of the Weiss Lab. Specifically, Kelly Hume helped in the initiation of this project and the analysis of the MMC survival; Amy Cassano did the analysis of the embryonic analysis to HU; Josette Pierre has done much of the immunohistochemistry analysis of IR treated mice; Aaron Oswald has done much of the immunohistochemistry analysis of MMC treated mice; Rachel Peters and Teresa Southard did the pathology assessment of the IR and MMC treated mice.

CHAPTER 4

SUMMARY, MODELS, AND FUTURE DIRECTIONS

HUS1 plays a critical role in ATR pathway activation as part the 911 complex, and germline deletion of *Hus1* results in early embryonic lethality (Weiss, Enoch et al. 2000). This lethality phenotype was overcome by engineering *Hus1* hypomorphic alleles where *Hus1* was disabled to different degrees. The *Hus1* impaired mice show no overt phenotypes, are born at expected mendelian frequencies, have no increased predisposition to forming tumors but have increased genomic instability (Levitt, Zhu et al. 2007). These observations suggest that *Hus1* deficient mice rely on other pathways to promote organism survival and that although the low levels of *Hus1* present are enough for the response to normal replication stress they might not be enough when this pathway is challenged.

Although much was known about the relationship between the ATM and ATR pathways in cell culture, less was known about the *in vivo* relationship between these pathways due to the limited mammalian models available for *Atr* deficiency. Moreover, since ATR pathway inhibition shows such promising results for cancer treatment efficacy (Brooks, Oakes et al. 2012; Tang, Dai et al. 2012), it was imperative to learn more about the effect of ATR deficiency in normal tissues. Here we took advantage of the unique *Hus1* mouse model to answer these questions.

4.1 Disease severity in a mouse model of Ataxia Telangiectasia is modulated by the DNA damage checkpoint gene HUS1

We show that simultaneous *Atm* and *Hus1* defects caused phenotypes that were not merely additive but strongly synergistic. The lowest level of *Hus1* in the allelic series, which on its own is fully compatible with normal development, resulted in high levels of apoptosis and mid-gestational lethality in the absence of *Atm*. Increased H2AX phosphorylation and p53 accumulation also were observed, revealing that the checkpoint apparatus is remarkably robust, permitting DNA damage signaling even when the two primary checkpoint pathways are dysfunctional (Figure 4.1). A less severe *Hus1* defect resulted in partial embryonic lethality in the context of *Atm* deficiency. Surviving *Atm*/*Hus1* double mutant mice showed severe dwarfism, craniofacial abnormalities, and digit abnormalities, phenotypes that could not have been predicted based on knowledge of the individual single mutants.

Unlike what has been observed in other DNA repair mutants, the striking dwarfism in *Atm*/*Hus1* double mutant mice was independent of the GHR/IGF1 axis. The craniofacial defects, which resemble those seen in human patients with genomic instability syndromes, stemmed from defects in a specific subset of cells in the skull and illustrate how checkpoint failure differentially impacts particular lineages

Figure 4.1. Hypothetical model showing synthetic lethal interactions following *Atm* inactivation and partial *Hus1* impairment. Previous studies have indicated that *Hus1* impairment leads to the accumulation of DSB due to defects in checkpoint signaling and/or repair (Weiss, Enoch et al. 2000; Levitt, Zhu et al. 2007; Zhu and Weiss 2007). We hypothesize that DNA damage that arises when *Hus1* expression is sub-optimal creates a greater requirement for ATM-mediated genome protection and leads to synthetic lethality in *Atm*/*Hus1* double mutant mice. The fact that activation of canonical checkpoint signaling factors such as CHK2, CHK1, and p53 appeared similar in *Atm* single and *Atm*/*Hus1* double mutants suggests that ATR may remain active in the context of modest HUS1 impairment or that other DNA damage-responsive kinases, such as DNA-PK, can mediate the signaling as illustrated. See text for additional details.

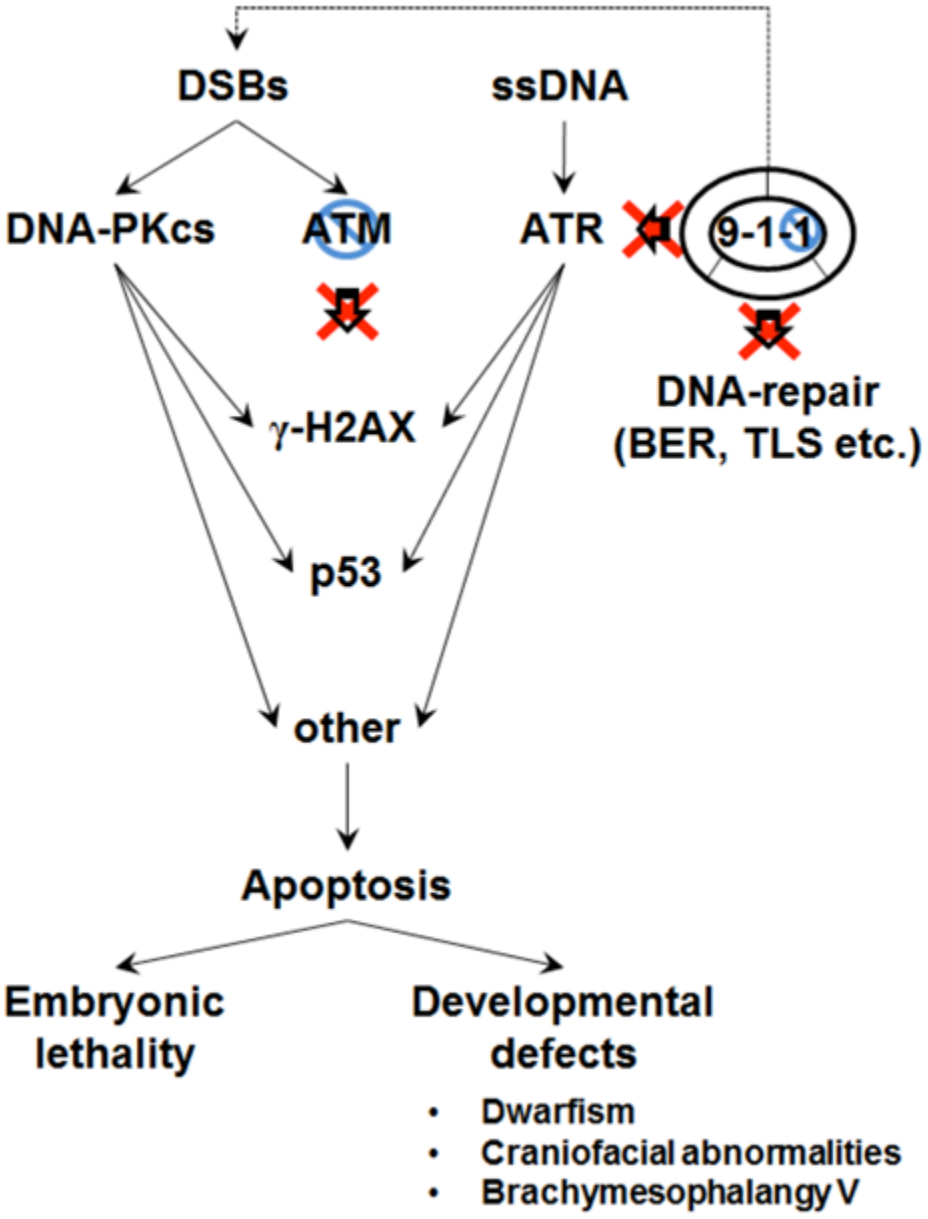
DSBs
ssDNA
DNA-PKcs
ATM
ATR
9-1-1
γ-H2AX
DNA-repair
(BER, TLS etc.)
p53
other
Apoptosis
Embryonic lethality
Developmental defects
• Dwarfism
• Craniofacial abnormalities
• Brachymesophalangy V

The highly specific consequences of defective genome maintenance were further apparent from our analysis of the double mutant limbs, where one particular bone (the mesophalanx of digit V) was affected. The same abnormality is observed in certain human genomic instability syndromes as well as following fetal teratogen exposure, suggesting that it may be a broader indicator of developmental genomic instability. Overall, the constellation of phenotypes in the *Atm/Hus1* double mutant mice is similar to that observed in a severe variant form of A-T, A-T_{Fresno}, raising the possibility that HUS1 or other ATR pathway components could be modifiers of A-T disease severity in humans.

Moreover, the developmental phenotypes in *Atm/Hus1* double mutant mice were associated with synergistic increases in genomic instability, but tumor-free survival was unaffected. That tumor development was not altered despite significantly increased genomic instability further illustrates the complex tissue-specific consequences of checkpoint failure, findings with important implications for cancer therapy strategies based on checkpoint inhibition. Of particular note with respect to the underlying molecular mechanisms is our observation that despite the combined defects in two checkpoint genes, checkpoint signaling was not further impaired beyond what is observed in the respective single mutants. In fact, the basal level of checkpoint signaling was actually increased in double mutant cells, leading us to

propose a model in which DNA repair defects associated with *Hus1* impairment drive the synthetic phenotypes.

4.2 ATM pathway mediates the primary response to IR, while HUS1 and the ATR pathway are the *in vivo* responders to replication stress

The lack of a mouse model for ATR pathway deficiency impeded the analysis of the subsequent effects on the response of normal tissues to replication stress as well as their response following chemotherapeutic treatment.

While the role for the ATM pathway in response to genotoxin treatment was extensively described *in vivo* little was known about the ATR role in response to different clastogens. For the first time we show that *in vivo Hus1* is not obligatory for the response to IR since upon different treatment doses no significant differences are seen between the $Hus1^{neo/\Delta 1n}$ group and the control $Hus1^{+}$ group. Moreover, analysis of different tissues at specific time points post-IR showed minimal *Hus1* dependency. Together with data from the *Hus1*/*Atm* double mutant mice showing that *Hus1* does not impact the IR sensitivity of $Atm^{-/-}$ mice, we conclude that the ATM pathway is the main responder to DSBs inducing genotoxins *in vivo* (Figure 4.2).

On the other hand analysis of the *in vivo* sensitivity to the replication stress reagents MMC and HU showed that at very low doses, $Hus1^{neo/\Delta 1n}$ impaired mice readily die underlining a severe requirement for HUS1 and the ATR pathway. The

Figure 4.2. Hypothetical model showing the interaction between the ATM and ATR pathways in response to genotoxic stress caused by IR or MMC. While *Atm* null mice are hypersensitive to IR independent of the *Hus1* status, suboptimal *Hus1* expression creates a greater requirement for ATM-mediated genome protection to DSBs and leads to synthetic lethality in *Atm*/*Hus1* double mutant mice upon increased replication stress as caused by MMC. We propose that because of synthetic lethal interaction impairment of the ATR pathway through specific inhibitors can be used to sensitize tumor cells to specific chemotherapies.

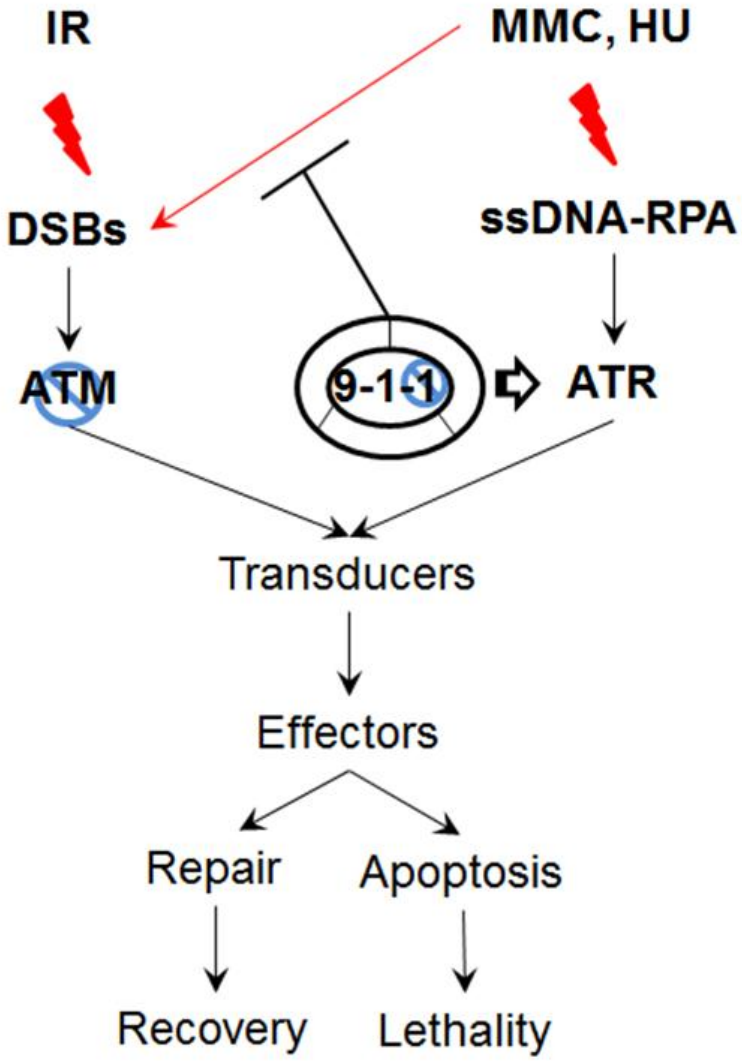
IR
MMC, HU
DSBs
ssDNA-RPA
ATM
9-1-1
ATR
Transducers
Effectors
Repair
Apoptosis
Recovery
Lethality

survival data presented, gives clear hints on the molecular mechanism underlying these sensitivities. HUS1 is necessary for the response to MMC induced lesions and when HUS1 levels are low in the *Hus1* impaired mice these lesions, most likely stalled forks, collapse and are transformed into DSBs that are repaired by the ATM pathway. This is highlighted by the fact that while $Hus1^{neo/neo}$ or $Atm^{-/-}$ single mutant mice show no sensitivity to MMC, $Hus1^{neo/neo}Atm^{-/-}$ mice are hypersensitive to the same dose although they show no specific hypersensitivity to IR when compared to $Atm^{-/-}$ single mutants alone (Figure 4.2). We need to further understand though what are the specific molecular steps that require HUS1 for the repair of MMC induced lesions. We hypothesize that HUS1 might be important for the ATR mediated signaling to FA complementation group or could play an important repair role, independent of ATR.

Corroborated with current data from our laboratory and from others that show that components of the ATR pathway, including RAD9, RAD1, HUS1, and CHK1, are important for tumor progression (Bartek, Mistrik et al. 2012; Brooks, Oakes et al. 2012; Ma, Cai et al. 2012; Origanti, Cai et al. 2012; Tang, Dai et al. 2012; Stephanie A. Yazinsky in preparation) we think that ATR pathway inhibitors could be successfully associated with chemotherapy to specifically kill cancer cells. Moreover, based on the data presented in this thesis, critical for the success of such therapies will be an

Figure 4.3. Distinct roles of the DDR pathways during multistep tumorigenesis. In normal circumstances the transformation of normal cells (depicted in black) to transformed cells is kept in check by the ATM pathway. If the ATM pathway gets mutated (depicted in red are cells defective for ATM pathway that would eventually initiate a tumor), protection is lost and tumor progression takes place. ATM deficiency comes with a great toll for these cancers that become defective for the response to DSBs formation and thus sensitive to chemotherapeutics. With time, the cancer cells become resistant to these treatments because they adapt to the increased GIN by upregulation of the activity of the ATR pathway. The ATR pathway is proposed to play an important role in this adaptation and future tumor survival by allowing them to deal with replication and genotoxin induced stress. Based on our data, in these instances, a cocktail of MMC/ATRi would specifically kill the cancer cells with very little effect on normal surrounding cells since these cells are intact for the ATM pathway.

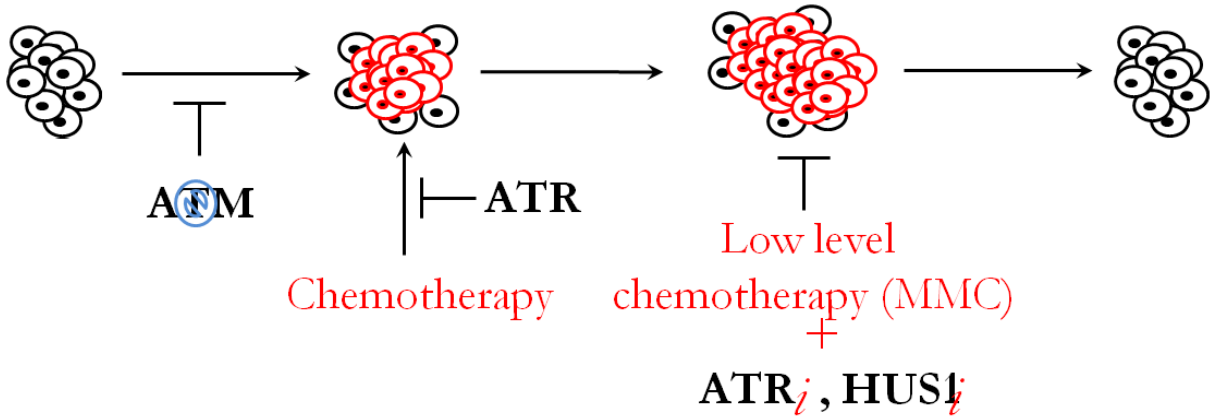
ATM
ATR
Chemotherapy
Low level
chemotherapy (MMC)
+
ATRi , HUSLi

initial understanding of the ATM pathway status of these tumors as well as their replication potential. We predict that ATM pathway deficient tumors would be highly sensitive to low doses of MMC combined with ATR pathway inhibitors while normal surrounding tissues that are ATM proficient will suffer very mild toxicity (Figure 4.3).

4.3 Future Directions

While the data presented here ilustrate the strong relationship between the main DDR pathways lead by ATM and ATR for both for development and cancer protection many surprising observations remain unexplained.

HUS1 and ATM cooperate for normal development but the requirement for this interaction is limited to specific cell populations, since this combined deficiency results in very specific phenotypes. Since we see increased GIN during development and in the hematopoietic system in the adult but not in the liver that is a replication quiet organ we think that the replication status of a specific tissue is critical for this interaction. More experiments are needed to be done to clearly demonstrate this hypothesis. Moreover, we think that different cell types deal differently with lack of these factors. This was previously observed in the *Hus1* conditional knock-out, where *Hus1* deletion was better supported in the lung and mammary gland, highlighting

Table 4.1. Association between genomic instability syndromes and developmental defects.

Syndrome	OMIM	Gene	GIN	GR	CD	BMF-V
Ataxia Telangiectasia (A-T)	208900	ATM	+	+	-	-
Seckel Syndrome (SCKL)	210600	ATR	+	+	+	+
Nijmegen Breakage Syndrome (NBS)	251260	NBS1	+	+	+	+
Ataxia Telangiectasia like (ATLD)		MRE11	+	+	-	-
Williams-Beuren Syndrome	194050	del7q11.23 (*RFC2)*	+			+
Rothmund Thomson Syndrome	268400	REQ4	+			+
Bloom Syndrome	604610	BLM	+		+	+
Warsaw Breakage Syndrome	613398	DDX11	+	+	+	+
Fanconi anemia	605724	>11 genes	+	+	+	+
Trichothiodystrophy	278730	XPD	+	-	-	+
Lig4 Syndrome	606593	Lig4	+	+	+	+
Nijmegen breakage syndrome-like disorder	604040	Rad50	+	+	+	+
Lig1 Syndrome	126391	Lig1	+	+	-	
Werner syndrome	277700	WRN	+	+	-	+
Omenn Syndrome	603554	Artemis	+	+	-	-
Severe Combined Immune Deficiency Syndrome	600899	DNA-PK	+	+	-	-
NHEJ1 Syndrome	611290	NHEJ1	+	+	+	+

Genomic instability (GIN); growth retardation (GR); craniofacial defects (CD) and brachymesophalangy V (BMP-V); the data was parsed using OMIM database.

varying requirements in different tissues (Levitt, Liu et al. 2005). We think the same happens in the *Hus1/Atm* double mutant mice where the craniofacial phenotype as well as the lack of a difference in tumor predisposition could be attributed to different tissue sensitivities. This could be done both at the level of the embryo as well as in adults, with and without genotoxin treatment. Transcript analysis by Q-PCR for members of the two pathways (p21, PUMA, Bax etc.) as well as immunohistochemistry staining for γ-H2AX and p53 could be executed in spleen, kidney, small intestine, thymus, brain, liver and testes(ovaries) of the Hus1/Atm double mutant mice and compared to the representative littermate controls.

The dwarfism present in our mice remains a very interesting phenotype to be dissected. One question that remains to be answered is if the hormonal growth pathways are intact in our mice. While Igf1 and GhR are not deregulated we cannot reject the implication of the Igf1 binding proteins (IGF1BP) or other Igf family members (*Igf2; Igf1R*) in the promotion of this phenotype. For all these factors transcript analysis by Q-PCR from E13.5 and neonatal livers could be performed. Additionally, to completely rule out the implication of the IGF1BP's ELISA assays could be performed from the serum of our mice to establish if the circulating levels of these proteins is changed. Preliminary *Igf1R* transcript analysis revealed no change in the level of this transcript in E10.5 embryos (Figure 4.4.A). Moreover I think that we will see no difference in the levels of the IGF1-BP because of the direct correlation

between IGF1 levels and IGF1-BP3 (that is 80% of the IGF-BP`s that binds IGF1 the rest is shared by the other 6 IGF1-BP) (Robinson 2010). Although initially we have postulated that this phenotype could arise due to increase cell death at the level of the bones growth plates, as reported in other dwarf models (Li, Chen et al. 1999), preliminary analysis showed that the growth plates of the *Hus1/Atm* double mutant mice have similar morphologies in all the mice, excluding this hypothesis (Figure 4.4B). We thus favor the idea that the dwarfism is due to a cell autonomous defect: the increased GIN during development results in marked cell death causing the depletion of both somatic and stem cells thus creating a cellular shortage translated into a small body size.

The skeletal defects featured by the *Atm/Hus1* mice are also very striking. We think that the craniofacial defects could be due to an increase cell death in particular cell niches, like the neural crest progenitor cells. Like in a mouse model for Treacher-Collins syndrome (Jones, Lynn et al. 2008), I would expect this to be due to increased cell death in this compartment via a p53 dependent mechanism. Furthermore the embryo analysis performed in the Hus1/Atm double mutant showed increased p53 levels that correlated with increased apoptosis. To test this, mice of the representative genotypes could be treated during embryonic development (starting E6.5 daily) with a potent p53 inhibitor, pifithrin-alpha (Alexis Biochemicals) at 2.2 mg per kg (body weight) in PBS by intraperitoneal injection. Inhibition of p53 could lead to apoptosis

inhibition triggering the abolition of the craniofacial phenotype (McKeown and Bronner-Fraser 2008). Moreover p53 inhibition might save the dwarfism phenotype like in the case of the Treacher-Collins mouse model (favoring the cell autonomous hypothesis). The caveat of such an experiment would be related to the toxicity associated with pifithrin-alpha daily injection or because *Hus1* has been implicated in p53-independent apoptosis (Yazinski, Westcott et al. 2009).

The brachymesophalangy V phenotype is a unique and very specific phenotype. Recently, it has been shown that deletion of *mir-17-92* cluster in mice causes an array of developmental defects including brachymesophalangy V (Ventura, Young et al. 2008; de Pontual, Yao et al. 2011). Additionally the *mir-17-92* cluster has been shown to be repressed by p53, fitting well with our model where p53 is activated (Yan, Xue et al. 2009). The *mir-17-92* family of miRNA is composed of 3 related polycistronic miRNA genes that collectively encode for a total of 15 miRNAs (Concepcion, Bonetti et al. 2012). To test if the brachymesophalangy V arose due to *mir17-92* depletion we have performed Taq-Man Q-PCR analysis and analyzed the levels of two of the mature *mir17-92* members (*mir17* and *mir19b*) –(Figure 4.5 A) as well as the levels of expression of the two pri-miRNA's (Figure 4.5B). Our preliminary analysis didn't reveal any difference in the transcript levels of the *mir17-92* family members. Although at this point we cannot completely exclude the deregulation of this cluster we think that in the Feingold syndrome model the *mir17-92* depletion is a secondary

Figure 4.4. Analysis of the dwarfism phenotype in *Hus1/Atm* double mutant and control mice. (A) Bar graph shows the fold expression level of *Igf1R* in E10.5 from embryos (n=3) of the indicated genotypes relative to $Hus1^{+/neo}Atm^{+/+}$. Total RNA was extracted using RNA STAT-60 reagent (Tel-Test, Friendswood, TX) and SYBR Green Q-PCR using the forward (TGCTGTCTATGTCAAGGCTG) and reverse (AGAGGAAGAGTTTGATGCTGAG) Igf1R primers. No significant differences were detected. (B) Tibias dissected from 6-week old littermate male mice of the indicated genotypes were isolated, decalcified and processed for histopathological staining. Sarfanin O staining differentially detects the cartilage, mucin, and mast cell granules on formalin-fixed, paraffin-embedded tibia tissue sections. Representative 40X images of the growth plates of the representative genotypic groups show no difference in the morphology of the growth plates.

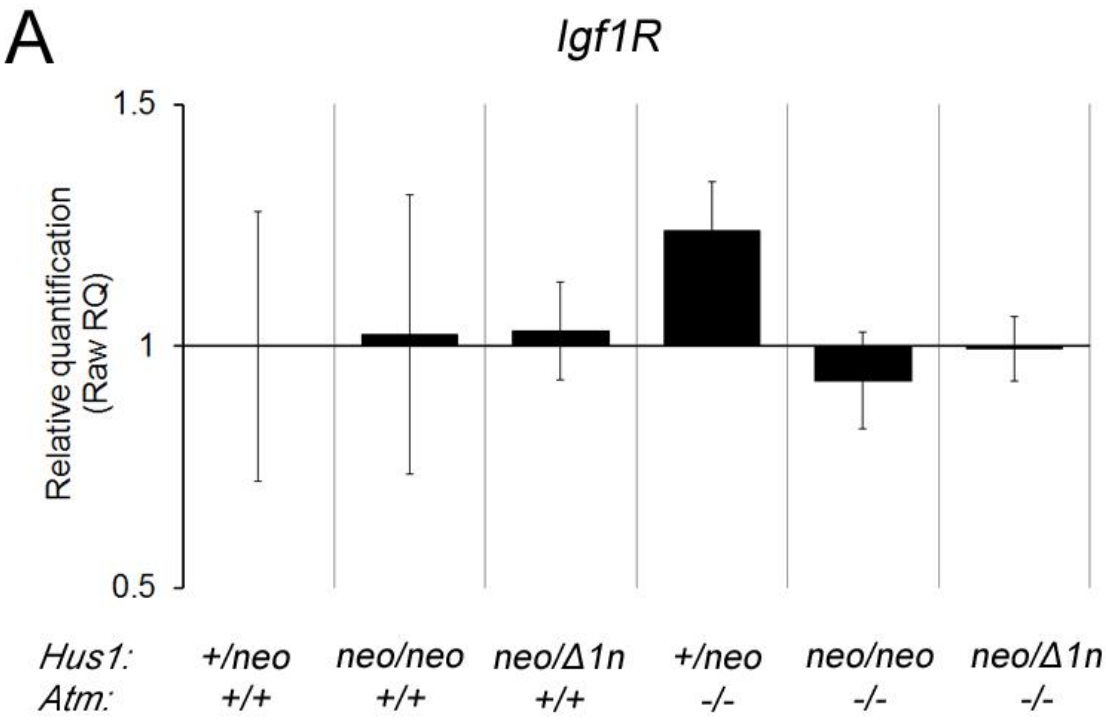
A
Igf1R
1.5
1
0.5
Relative quantification
(Raw RQ)
Hus1: +/neo neo/neo neo/Δ1n +/neo neo/neo neo/Δ1n
Atm: +/+ +/+ +/+ -/- -/- -/-

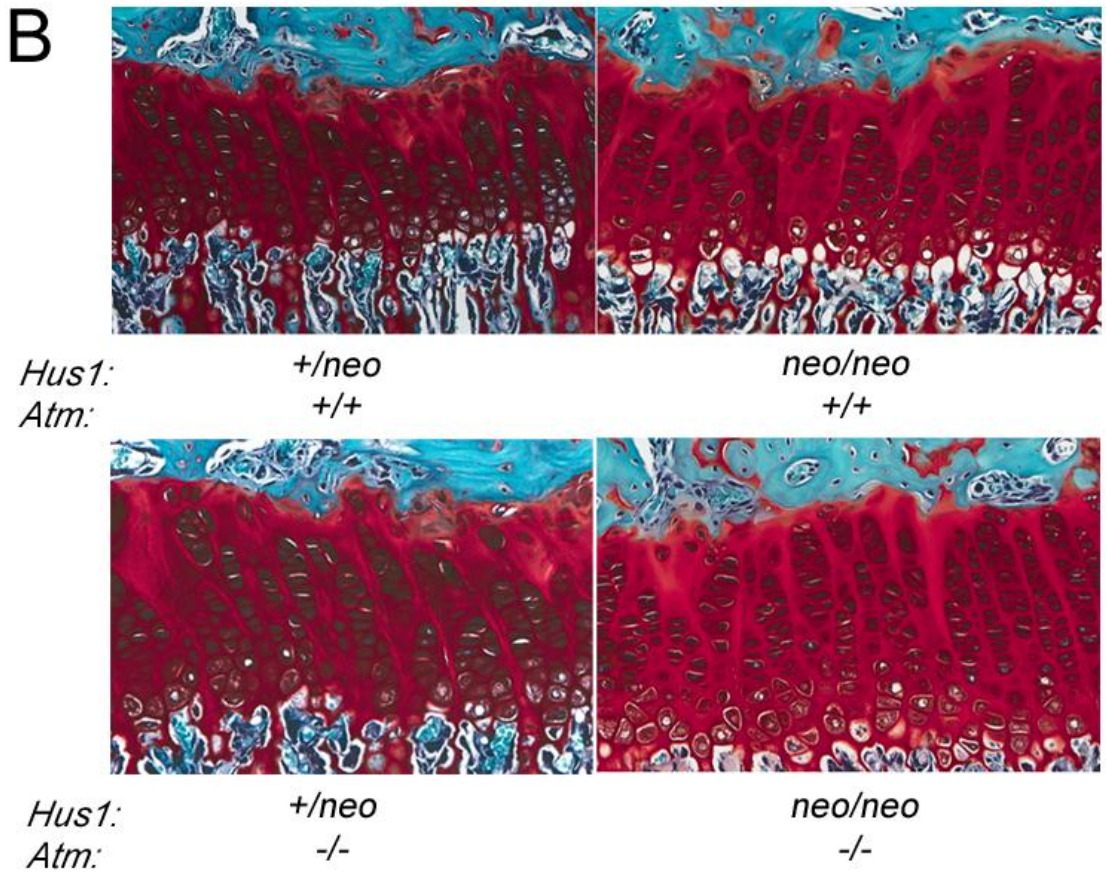
B
Hus1: +/neo neo/neo
Atm: +/+ +/+
Hus1: +/neo neo/neo
Atm: -/- -/-

effect to activated p53 due to possible increased GIN. Many human genomic instability syndromes present with brachymesophalangy V and teratogen exposure during pregnancy leads to similar phenotypes (Mancinelli, Binetti et al. 2007). To test this hypothesis wild-type mice could be treated with HU during embryonic development and the digit phenotypes of the offspring could be assessed. In parallel Q-PCR analysis for the other mature members of the *mir17-92* pathway could be performed. If the GIN hypothesis stands true, then we would expect that the *mir17-92* mice to have increased GIN, while other DDR mutant mice should present brachymesophalangy V, and indeed preliminary data shows that the $ATR^{S/S}$ mice show similar defects. These observations would have an important impact on our understanding of the effects of GIN during development and would also point to a specific skeletal defect that could be used for diagnosis of genomic instability syndromes during early pregnancy.

The analysis of the DDR response in the *Hus1*/*Atm* primary MEFs, revealed no signaling defect. We think that this might be due to the redundancy with another PIKK, DNA-PK. To test this we could use DNA-PK specific inhibitors and test if this inhibition could abolish signaling in the double mutant MEFs. Because preliminary analysis shows that the DNA-PK involvement is minimal we favor the hypothesis that the level of *Hus1* present in our mice is sufficient for promoting ATR signaling, and the increased GIN that we see is due to a *Hus1* repair defect. To test

Figure 4.5. Figure 4.4. Analysis of the *mir17-92* expression level in the *Hus1/Atm* double mutant and control mice. (A) Bar graph shows the fold expression level of primary microRNAs (pri-miRNAs) of the *mir17-92's* using total RNA E10.5 embryo samples (n=3) from embryos of the indicated genotypes relative to $Hus1^{+/neo}Atm^{+/+}$. Pri-miRNA are long noncoding RNA transcripts with at least one precursor microRNAs (pre-miRNAs) containing mature microRNA 17-92 cluster (miRNA) sequences. No significant differences were detected. (B) Bar graph shows the fold expression level of *mir17* and *mir-19b* in total RNA E10.5 embryo samples (n=3) from embryos of the indicated genotypes relative to $Hus1^{+/neo}Atm^{+/+}$. No significant differences were detected.

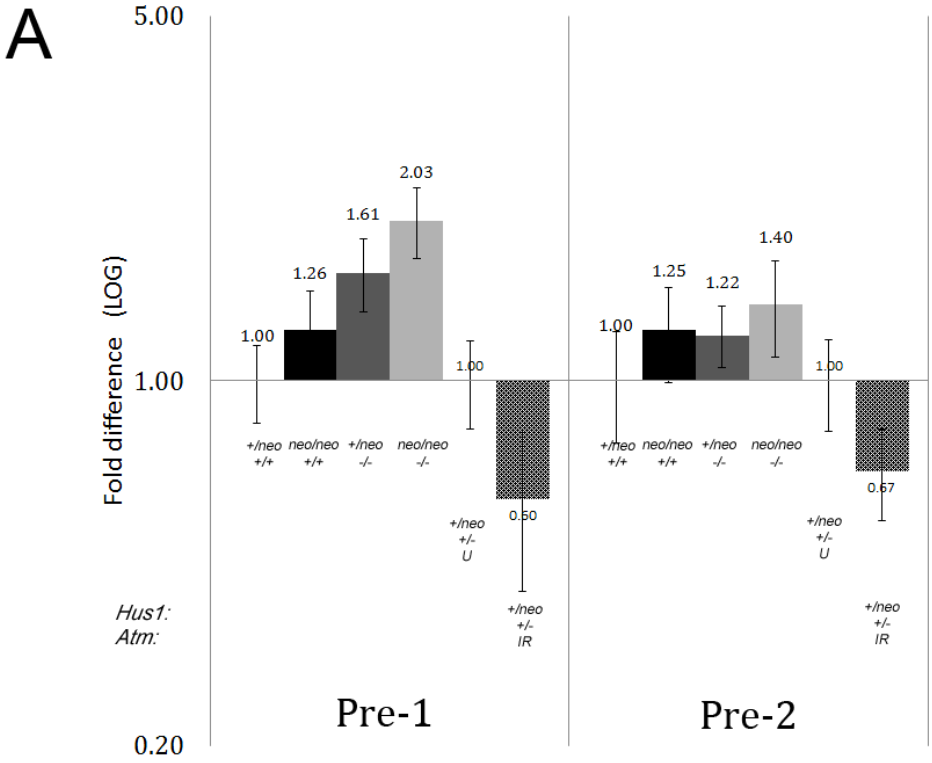
A
5.00
1.00
0.20
Fold difference (LOG)
1.00
1.26
1.61
2.03
1.00
0.50
1.00
1.25
1.22
1.40
1.00
0.67
+/neo +/+
neo/neo +/+
+/neo -/-
neo/neo -/-
+/neo +/- U
+/neo +/- IR
Hus1:
Atm:
Pre-1
Pre-2

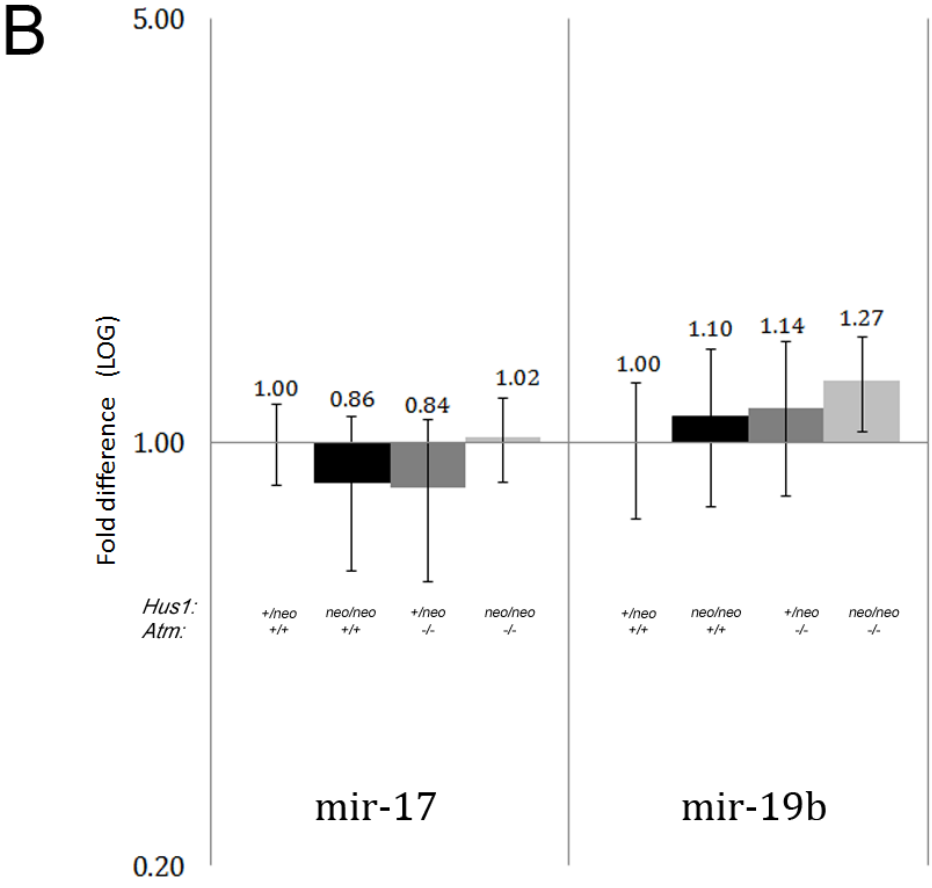
B
5.00
1.00
0.20
Fold difference (LOG)
1.00
0.86
0.84
1.02
1.00
1.10
1.14
1.27
+/neo +/+
neo/neo +/+
+/neo -/-
neo/neo -/-
Hus1:
Atm:
mir-17
mir-19b

this hypothesis we could use ATR inhibitors in MEFs and I propose that upon treatment signaling to the downstream kinase CHK1 could be diminished.

The analysis of the *Hus1* requirement for genotoxin response *in vivo* showed a very clear survival difference: Hus1 is not required for IR response but is critical for MMC response. The analysis of cell proliferation and apoptosis in the MMC small intestine samples showed though no significant difference in apoptosis at the different time points when the correspondent genotypes were compared. This might be due to that fact that the MMC lethality is due to increased cell death in another compartment, like the hematopoietic system, or because we are not looking at the right time interval. Histopathology assessment of MMC treated samples revealed a splenic pathology consistent with increased anemia. To test this hypothesis *Hus1* impaired mice and littermates controls could be treated with a 4mg/kg MMC and complete blood counts (CBC's) could be performed at 0, 24, 48 and 76 hours. This will allow us to see if anemia is a specific pathology in the *Hus1* impaired mice. We could complete the analysis with the exploration of the cell proliferation and apoptosis following MMC at additional time points (2hrs and 24 hours).

To resolve the mechanistic role for *Hus1* in cross-link repair we could use both tissues and MEFs from *Hus1* impaired mice from MMC treated and untreated groups and test for the effect of *Hus1* deregulation on signaling to the FA complementation group. We could test the activation level of FancD2, a protein positioned

downstream of ATR and target of its phosphorylation. Additionally, if signaling is intact we could test the involvement of HUS1 directly in repair by looking at the accumulation of cross-link repair factors like MUS81.

Finally, based on our model *Atm*/*Hus1* deficient tumor cells should be hypersensitive to low levels of MMC when compared to the single mutants alone. To test this hypothesis we could isolate thymic tumor T cells from either $Atm^{-/-}$ or *Hus1*/*Am* double mutant mice and subject them to MMC treatment. We expect that the *Hus1*/*Atm* T cells could readily die when compared to the $Atm^{-/-}$ single mutant ones, confirming our model (Figure 4.3). If this holds true we could cross *Hus1* on different tumor bearing backgrounds and re-test our hypothesis. These observation will bring vital information on the use of ATR inhibitors for cancer therapy and propose HUS1 specifically for the development of small molecule inhibitors.

Together the data presented here outline the importance of the *Hus1* gene for both development and the response to genotoxins and proposes a model where HUS1 or ATR impairment could be used in our fight against cancer.

REFERENCES

Abraham, A. T., X. Zhou, et al. (2001). "Metallobleomycin-mediated cleavage of DNA not involving a threading-intercalation mechanism." J Am Chem Soc **123**(22): 5167-5175.

Abraham, R. T. (2001). "Cell cycle checkpoint signaling through the ATM and ATR kinases." Genes Dev **15**(17): 2177-2196.

Abraham, R. T. and T. D. Halazonetis (2012). DNA Damage Checkpoint Signaling Pathways in Human Cancer

Signaling Pathways in Cancer Pathogenesis and Therapy. D. A. Frank, Springer New York**:** 23-37.

Achari, Y. and S. P. Lees-Miller (2000). "Detection of DNA-dependent protein kinase in extracts from human and rodent cells." Methods Mol Biol **99**: 85-97.

Al-Dosari, M. S., R. Shaheen, et al. (2010). "Novel CENPJ mutation causes Seckel syndrome." J Med Genet **47**(6): 411-414.

Alderton, G. K., H. Joenje, et al. (2004). "Seckel syndrome exhibits cellular features demonstrating defects in the ATR-signalling pathway." Hum Mol Genet **13**(24): 3127-3138.

Angele, S., P. Romestaing, et al. (2003). "ATM haplotypes and cellular response to DNA damage: association with breast cancer risk and clinical radiosensitivity." Cancer Research **63**(24): 8717-8725.

Antoni, L., N. Sodha, et al. (2007). "CHK2 kinase: cancer susceptibility and cancer therapy - two sides of the same coin?" Nat Rev Cancer **7**(12): 925-936.

Araki, R., R. Fukumura, et al. (1999). "Enhanced phosphorylation of p53 serine 18 following DNA damage in DNA-dependent protein kinase catalytic subunit-deficient cells." Cancer Res **59**(15): 3543-3546.

Arlander, S. J., B. T. Greene, et al. (2008). "DNA protein kinase-dependent G2 checkpoint revealed following knockdown of ataxia-telangiectasia mutated in human mammary epithelial cells." Cancer Res **68**(1): 89-97.

Ashwell, S. and S. Zabludoff (2008). "DNA damage detection and repair pathways--recent advances with inhibitors of checkpoint kinases in cancer therapy." Clinical Cancer Research **14**(13): 4032-4037.

Bai, H., A. Madabushi, et al. (2010). "Interaction between human mismatch repair recognition proteins and checkpoint sensor Rad9-Rad1-Hus1." DNA Repair (Amst) **9**(5): 478-487.

Bakkenist, C. J. and M. B. Kastan (2003). "DNA damage activates ATM through intermolecular autophosphorylation and dimer dissociation." Nature **421**(6922): 499-506.

Balmus, G., M. Zhu, et al. (2012). "Disease severity in a mouse model of ataxia telangiectasia is modulated by the DNA damage checkpoint gene Hus1." Human Molecular Genetics.

Barlow, C., S. Hirotsune, et al. (1996). "Atm-deficient mice: a paradigm of ataxia telangiectasia." Cell **86**(1): 159-171.

Bartek, J., J. Bartkova, et al. (2007). "DNA damage signalling guards against activated oncogenes and tumour progression." Oncogene **26**(56): 7773-7779.

Bartek, J., C. Lukas, et al. (2004). "Checking on DNA damage in S phase." Nat. Rev. Mol. Cell Biol. **5**(10): 792-804.

Bartek, J., M. Mistrik, et al. (2012). "Thresholds of replication stress signaling in cancer development and treatment." Nature Structural & Molecular Biology **19**(1): 5-7.

Bartek, J., M. Mistrik, et al. (2012). "Thresholds of replication stress signaling in cancer development and treatment." Nat Struct Mol Biol **19**(1): 5-7.

Bartkova, J., Z. Horejsi, et al. (2005). "DNA damage response as a candidate anti-cancer barrier in early human tumorigenesis." Nature **434**(7035): 864-870.

Bianchi, V., E. Pontis, et al. (1986). "Changes of deoxyribonucleoside triphosphate pools induced by hydroxyurea and their relation to DNA synthesis." Journal of Biological Chemistry **261**(34): 16037-16042.

Bonner, W. M., C. E. Redon, et al. (2008). "GammaH2AX and cancer." Nat Rev Cancer **8**(12): 957-967.

Borchiellini, D., M. C. Etienne-Grimaldi, et al. (2012). "The impact of pharmacogenetics on radiation therapy outcome in cancer patients. A focus on DNA damage response genes." Cancer Treatment Reviews **38**(6): 737-759.

Branzei, D. and M. Foiani (2008). "Regulation of DNA repair throughout the cell cycle." Nat Rev Mol Cell Biol **9**(4): 297-308.

Branzei, D. and M. Foiani (2010). "Maintaining genome stability at the replication fork." Nat Rev Mol Cell Biol **11**(3): 208-219.

Brooks, K., V. Oakes, et al. (2012). "A potent Chk1 inhibitor is selectively cytotoxic in melanomas with high levels of replicative stress." Oncogene.

Brown, E. J. and D. Baltimore (2000). "ATR disruption leads to chromosomal fragmentation and early embryonic lethality." Genes Dev **14**(4): 397-402.

Budzowska, M., I. Jaspers, et al. (2004). "Mutation of the mouse Rad17 gene leads to embryonic lethality and reveals a role in DNA damage-dependent recombination." EMBO J **23**(17): 3548-3558.

Bunz, F., P. M. Hwang, et al. (1999). "Disruption of p53 in human cancer cells alters the responses to therapeutic agents." The Journal of clinical investigation **104**(3): 263-269.

Callen, E., M. Jankovic, et al. (2009). "Essential role for DNA-PKcs in DNA double-strand break repair and apoptosis in ATM-deficient lymphocytes." Mol Cell **34**(3): 285-297.

Chabner, B. A. and T. G. Roberts, Jr. (2005). "Timeline: Chemotherapy and the war on cancer." Nature reviews. Cancer **5**(1): 65-72.

Chanoux, R. A., B. Yin, et al. (2009). "ATR and H2AX cooperate in maintaining genome stability under replication stress." J Biol Chem **284**(9): 5994-6003.

Cheng, C. K., L. W. Chow, et al. (2005). "The cell cycle checkpoint gene Rad9 is a novel oncogene activated by 11q13 amplification and DNA methylation in breast cancer." Cancer Research **65**(19): 8646-8654.

Cimprich, K. A. and D. Cortez (2008). "ATR: an essential regulator of genome integrity." Nat. Rev. Mol. Cell Biol. **9**(8): 616-627.

Collis, S. J., T. L. DeWeese, et al. (2005). "The life and death of DNA-PK." Oncogene **24**(6): 949-961.

Concepcion, C. P., C. Bonetti, et al. (2012). "The MicroRNA-17-92 Family of MicroRNA Clusters in Development and Disease." Cancer Journal **18**(3): 262-267.

Cook, A. J., L. Oganesian, et al. (2003). "Reduced switching in SCID B cells is associated with altered somatic mutation of recombined S regions." J Immunol **171**(12): 6556-6564.

Cook, M. J. (1965). The anatomy of the laboratory mouse. London, New York,, Academic Press.

Cotta-Ramusino, C., E. R. McDonald, 3rd, et al. (2011). "A DNA damage response screen identifies RHINO, a 9-1-1 and TopBP1 interacting protein required for ATR signaling." Science **332**(6035): 1313-1317.

Cotter, T. G. (2009). "Apoptosis and cancer: the genesis of a research field." Nat Rev Cancer **9**(7): 501-507.

Crooke, S. T. and W. T. Bradner (1976). "Mitomycin C: a review." Cancer Treatment Reviews **3**(3): 121-139.

Crosnier, C., D. Stamataki, et al. (2006). "Organizing cell renewal in the intestine: stem cells, signals and combinatorial control." Nat Rev Genet **7**(5): 349-359.

Davies, A. A., A. Neiss, et al. (2010). "Ubiquitylation of the 9-1-1 checkpoint clamp is independent of rad6-rad18 and DNA damage." Cell **141**(6): 1080-1087.

De Kerviler, E., A. Guermazi, et al. (2000). "The clinical and radiological features of Fanconi's anaemia." Clin Radiol **55**(5): 340-345.

de Klein, A., M. Muijtjens, et al. (2000). "Targeted disruption of the cell-cycle checkpoint gene ATR leads to early embryonic lethality in mice." Curr Biol **10**(8): 479-482.

de la Torre, J., A. Gil-Moreno, et al. (2008). "Expression of DNA damage checkpoint protein Hus1 in epithelial ovarian tumors correlates with prognostic markers." International Journal of Gynecological Pathology **27**(1): 24-32.

de Lange, T. (2002). "Protection of mammalian telomeres." Oncogene **21**(4): 532-540.

de Pontual, L., E. Yao, et al. (2011). "Germline deletion of the miR-17 approximately 92 cluster causes skeletal and growth defects in humans." Nature Genetics **43**(10): 1026-1030.

Dean Fraga, Tea Meulia, et al. (2008). "Real-Time PCR." Current Protocols Essential Laboratory Techniques **UNIT 10.3**.

Delacroix, S., J. M. Wagner, et al. (2007). "The Rad9-Hus1-Rad1 (9-1-1) clamp activates checkpoint signaling via TopBP1." Genes Dev **21**(12): 1472-1477.

Deng, C., P. Zhang, et al. (1995). "Mice lacking p21CIP1/WAF1 undergo normal development, but are defective in G1 checkpoint control." Cell **82**(4): 675-684.

Digweed, M. and K. Sperling (2004). "Nijmegen breakage syndrome: clinical manifestation of defective response to DNA double-strand breaks." DNA Repair (Amst) **3**(8-9): 1207-1217.

Donehower, L. A., M. Harvey, et al. (1992). "Mice deficient for p53 are developmentally normal but susceptible to spontaneous tumours." Nature **356**(6366): 215-221.

Dore, A. S., M. L. Kilkenny, et al. (2009). "Crystal structure of the rad9-rad1-hus1 DNA damage checkpoint complex--implications for clamp loading and regulation." Mol Cell **34**(6): 735-745.

Ellisen, L. W. (2011). "PARP inhibitors in cancer therapy: promise, progress, and puzzles." Cancer Cell **19**(2): 165-167.

Elson, A., Y. Wang, et al. (1996). "Pleiotropic defects in ataxia-telangiectasia protein-deficient mice." Proc Natl Acad Sci U S A **93**(23): 13084-13089.

Enoch, T., A. M. Carr, et al. (1992). "Fission yeast genes involved in coupling mitosis to completion of DNA replication." Genes & Development **6**(11): 2035-2046.

Fang, Y., C. C. Tsao, et al. (2004). "ATR functions as a gene dosage-dependent tumor suppressor on a mismatch repair-deficient background." EMBO Journal **23**(15): 3164-3174.

Fernandez-Capetillo, O. (2010). "Intrauterine programming of ageing." EMBO Rep **11**(1): 32-36.

Fortini, P. and E. Dogliotti (2007). "Base damage and single-strand break repair: mechanisms and functional significance of short- and long-patch repair subpathways." DNA Repair (Amst) **6**(4): 398-409.

Francia, S., R. S. Weiss, et al. (2007). "Need telomere maintenance? Call 911." Cell Div **2**: 3.

Francia, S., R. S. Weiss, et al. (2006). "Telomere and telomerase modulation by the mammalian Rad9/Rad1/Hus1 DNA-damage-checkpoint complex." Curr Biol **16**(15): 1551-1558.

Friedrich-Heineken, E., M. Toueille, et al. (2005). "The two DNA clamps Rad9/Rad1/Hus1 complex and proliferating cell nuclear antigen differentially regulate flap endonuclease 1 activity." J Mol Biol **353**(5): 980-989.

Fu, Y., Y. Zhu, et al. (2008). "Rad6-Rad18 mediates a eukaryotic SOS response by ubiquitinating the 9-1-1 checkpoint clamp." Cell **133**(4): 601-611.

Gangolli, S. and Royal Society of Chemistry (Great Britain) (1999). The dictionary of substances and their effects. Cambridge, UK, Royal Society of Chemistry.

Gatei, M., K. Sloper, et al. (2003). "Ataxia-telangiectasia-mutated (ATM) and NBS1-dependent phosphorylation of Chk1 on Ser-317 in response to ionizing radiation." J Biol Chem **278**(17): 14806-14811.

Gilad, S., L. Chessa, et al. (1998). "Genotype-phenotype relationships in ataxia-telangiectasia and variants." Am. J. Hum. Genet. **62**(3): 551-561.

Goodarzi, A. A., A. T. Noon, et al. (2008). "ATM signaling facilitates repair of DNA double-strand breaks associated with heterochromatin." Mol Cell **31**(2): 167-177.

Goodship, J., H. Gill, et al. (2000). "Autozygosity mapping of a seckel syndrome locus to chromosome 3q22. 1-q24." Am. J. Hum. Genet. **67**(2): 498-503.

Greenow, K. R., A. R. Clarke, et al. (2009). "Chk1 deficiency in the mouse small intestine results in p53-independent crypt death and subsequent intestinal compensation." Oncogene **28**(11): 1443-1453.

Griffith, E., S. Walker, et al. (2008). "Mutations in pericentrin cause Seckel syndrome with defective ATR-dependent DNA damage signaling." Nat Genet **40**(2): 232-236.

Griffith, J. D., L. A. Lindsey-Boltz, et al. (2002). "Structures of the human Rad17-replication factor C and checkpoint Rad 9-1-1 complexes visualized by glycerol spray/low voltage microscopy." Journal of Biological Chemistry **277**(18): 15233-15236.

Gudkov, A. V. and E. A. Komarova (2003). "The role of p53 in determining sensitivity to radiotherapy." Nat Rev Cancer **3**(2): 117-129.

Guidos, C. J., C. J. Williams, et al. (1996). "V(D)J recombination activates a p53-dependent DNA damage checkpoint in scid lymphocyte precursors." Genes Dev **10**(16): 2038-2054.

Gurley, K. E. and C. J. Kemp (2007). "Ataxia-telangiectasia mutated is not required for p53 induction and apoptosis in irradiated epithelial tissues." Mol Cancer Res **5**(12): 1312-1318.

Hamner, R. W., R. Verani, et al. (1983). "Mitomycin-associated renal failure. Case report and review." Archives of Internal Medicine **143**(4): 803-807.

Han, L., Z. Hu, et al. (2010). "Mouse Rad1 deletion enhances susceptibility for skin tumor development." Mol Cancer **9**(1): 67.

Harlow, E. and D. Lane (2006). "Lysing Tissue-Culture Cells for Immunoprecipitation." Cold Spring Harb Protoc; doi:10.1101/pdb.prot4531.

Helt, C. E., W. Wang, et al. (2005). "Evidence that DNA damage detection machinery participates in DNA repair." Cell Cycle **4**(4): 529-532.

Herzog, K. H., M. J. Chong, et al. (1998). "Requirement for Atm in ionizing radiation-induced cell death in the developing central nervous system." Science **280**(5366): 1089-1091.

Hoeijmakers, J. H. (2001). "Genome maintenance mechanisms for preventing cancer." Nature **411**(6835): 366-374.

Hoff, J. (2000). "Methods of blood collection in the mouse." Lab. Animal **29**(10): 47-53.

Holmes, L. B., B. C. Kleiner, et al. (1987). "Predictive value of minor anomalies: II. Use in cohort studies to identify teratogens." Teratology **36**(3): 291-297.

Hopkins, K. M., W. Auerbach, et al. (2004). "Deletion of mouse rad9 causes abnormal cellular responses to DNA damage, genomic instability, and embryonic lethality." Mol Cell Biol **24**(16): 7235-7248.

Hsiang, Y. H., M. G. Lihou, et al. (1989). "Arrest of replication forks by drug-stabilized topoisomerase I-DNA cleavable complexes as a mechanism of cell killing by camptothecin." Cancer Research **49**(18): 5077-5082.

Hu, Z., Y. Liu, et al. (2008). "Targeted deletion of Rad9 in mouse skin keratinocytes enhances genotoxin-induced tumor development." Cancer Research **68**(14): 5552-5561.

Ikegami, S., T. Taguchi, et al. (1978). "Aphidicolin prevents mitotic cell division by interfering with the activity of DNA polymerase-alpha." Nature **275**(5679): 458-460.

Inagaki, A., E. Sleddens-Linkels, et al. (2011). "Human RAD18 interacts with ubiquitylated chromatin components and facilitates RAD9 recruitment to DNA double strand breaks." PloS one **6**(8): e23155.

International Standing Committee on Human Cytogenetic Nomenclature., L. G. Shaffer, et al. (2009). ISCN 2009 : an international system for human cytogenetic nomenclature (2009). Basel ; Unionville, CT, Karger.

Jackson, S. P. and J. Bartek (2009). "The DNA-damage response in human biology and disease." Nature **461**(7267): 1071-1078.

Jansen, J. G., M. I. Fousteri, et al. (2007). "Send in the clamps: control of DNA translesion synthesis in eukaryotes." Mol Cell **28**(4): 522-529.

Jazayeri, A., J. Falck, et al. (2006). "ATM- and cell cycle-dependent regulation of ATR in response to DNA double-strand breaks." Nat. Cell Biol. **8**(1): 37-45.

Jimenez, G. S., F. Bryntesson, et al. (1999). "DNA-dependent protein kinase is not required for the p53-dependent response to DNA damage." Nature **400**(6739): 81-83.

Jones, N. C., M. L. Lynn, et al. (2008). "Prevention of the neurocristopathy Treacher Collins syndrome through inhibition of p53 function." Nat Med **14**(2): 125-133.

Kai, M. and T. S. Wang (2003). "Checkpoint activation regulates mutagenic translesion synthesis." Genes and Development **17**(1): 64-76.

Kalay, E., G. Yigit, et al. (2011). "CEP152 is a genome maintenance protein disrupted in Seckel syndrome." Nat Genet **43**(1): 23-26.

Kaufman, M. H. (1992). The atlas of mouse development. London ; San Diego, Academic Press.

Kemp, M. and A. Sancar (2009). "DNA distress: just ring 9-1-1." Curr Biol **19**(17): R733-734.

Kirshner, M., M. Rathavs, et al. (2009). "Analysis of the relationships between ATM and the Rad54 paralogs involved in homologous recombination repair." DNA Repair (Amst) **8**(2): 253-261.

Kjaer, I., N. Hansen, et al. (2001). "Craniofacial morphology, dentition, and skeletal maturity in four siblings with Seckel syndrome." Cleft Palate Craniofac J **38**(6): 645-651.

Klingseisen, A. and A. P. Jackson (2011). "Mechanisms and pathways of growth failure in primordial dwarfism." Genes Dev **25**(19): 2011-2024.

Knipscheer, P., M. Raschle, et al. (2009). "The Fanconi anemia pathway promotes replication-dependent DNA interstrand cross-link repair." Science **326**(5960): 1698-1701.

Koc, A., L. J. Wheeler, et al. (2004). "Hydroxyurea arrests DNA replication by a mechanism that preserves basal dNTP pools." The Journal of biological chemistry **279**(1): 223-230.

Komotar, R. J., M. L. Otten, et al. (2008). "Radiotherapy plus concomitant and adjuvant temozolomide for glioblastoma-a critical review." Clin Med Oncol **2**: 421-422.

Lam, M. H., Q. Liu, et al. (2004). "Chk1 is haploinsufficient for multiple functions critical to tumor suppression." Cancer Cell **6**(1): 45-59.

Lavin, M. F. (2008). "Ataxia-telangiectasia: from a rare disorder to a paradigm for cell signalling and cancer." Nat Rev Mol Cell Biol **9**(10): 759-769.

Lavin, M. F. and Y. Shiloh (1997). "The genetic defect in ataxia-telangiectasia." Annu Rev Immunol **15**: 177-202.

Lee, J. H., Y. Jin, et al. (2012). "Hypoxia activates the tumor suppressor p53 by inducing ATR-Chk1 kinase cascade-mediated phosphorylation and consequent 14-3-3gamma inactivation of MDMX." Journal of Biological Chemistry.

Legha, S. S. (1985). "A review of mitomycin regimens in advanced breast cancer therapy." Clinical Therapeutics **7**(3): 286-307.

Lehnert, S. (1998). "From DNA damage to cell death: the role of nuclear structure in the response to cancer therapy. Overview of the proceedings: from loose loops to sticky ends." Radiation Research **149**(4): 317-318.

Levitt, P. S., H. Liu, et al. (2005). "Conditional inactivation of the mouse Hus1 cell cycle checkpoint gene." Genomics **86**(2): 212-224.

Levitt, P. S., M. Zhu, et al. (2007). "Genome maintenance defects in cultured cells and mice following partial inactivation of the essential cell cycle checkpoint gene Hus1." Mol Cell Biol **27**(6): 2189-2201.

Lewis, K. A., J. Bakkum-Gamez, et al. (2007). "Mutations in the ataxia telangiectasia and rad3-related-checkpoint kinase 1 DNA damage response axis in colon cancers." Genes, Chromosomes and Cancer **46**(12): 1061-1068.

Lewis, K. A., S. Mullany, et al. (2005). "Heterozygous ATR mutations in mismatch repair-deficient cancer cells have functional significance." Cancer Research **65**(16): 7091-7095.

Li, C., L. Chen, et al. (1999). "A Lys644Glu substitution in fibroblast growth factor receptor 3 (FGFR3) causes dwarfism in mice by activation of STATs and ink4 cell cycle inhibitors." Human Molecular Genetics **8**(1): 35-44.

Li, G. M. (2008). "Mechanisms and functions of DNA mismatch repair." Cell Res **18**(1): 85-98.

Linette, D. C., K. H. McGee, et al. (1992). "Mitomycin-induced pulmonary toxicity: case report and review of the literature." Annals of Pharmacotherapy **26**(4): 481-484.

Liu, Q., S. Guntuku, et al. (2000). "Chk1 is an essential kinase that is regulated by Atr and required for the G(2)/M DNA damage checkpoint." Genes Dev **14**(12): 1448-1459.

Liu, Q., S. Guntuku, et al. (2000). "Chk1 is an essential kinase that is regulated by Atr and required for the G(2)/M DNA damage checkpoint." Genes and Development **14**(12): 1448-1459.

Liu, X. J., A. Matsuda, et al. (2008). "Ataxia-telangiectasia and Rad3-related and DNA-dependent protein kinase cooperate in G(2) checkpoint activation by the DNA strand-breaking nucleoside analogue 2 '-C-cyano-2 '-deoxy-1-beta-D-arabino-pentofuranosylcytosine." Molecular Cancer Therapeutics **7**(1): 133-142.

Loeb, L. A. and R. J. Monnat, Jr. (2008). "DNA polymerases and human disease." Nat Rev Genet **9**(8): 594-604.

Lord, C. J. and A. Ashworth (2012). "The DNA damage response and cancer therapy." Nature **481**(7381): 287-294.

Lui, J. C. and J. Baron (2011). "Mechanisms limiting body growth in mammals." Endocr Rev **32**(3): 422-440.

Luo, J., N. L. Solimini, et al. (2009). "Principles of cancer therapy: oncogene and non-oncogene addiction." Cell **136**(5): 823-837.

Luo, Y., S. K. Rockow-Magnone, et al. (2001). "Blocking Chk1 expression induces apoptosis and abrogates the G2 checkpoint mechanism." Neoplasia **3**(5): 411-419.

Lupu, F., J. D. Terwilliger, et al. (2001). "Roles of growth hormone and insulin-like growth factor 1 in mouse postnatal growth." Dev Biol **229**(1): 141-162.

Ma, C. X., S. Cai, et al. (2012). "Targeting Chk1 in p53-deficient triple-negative breast cancer is therapeutically beneficial in human-in-mouse tumor models." Journal of Clinical Investigation **122**(4): 1541-1552.

Majka, J. and P. M. Burgers (2004). "The PCNA-RFC families of DNA clamps and clamp loaders." Progress in Nucleic Acid Research and Molecular Biology **78**: 227-260.

Mancinelli, R., R. Binetti, et al. (2007). "Woman, alcohol and environment: Emerging risks for health." Neuroscience and Biobehavioral Reviews **31**(2): 246-253.

Manning, M. A. and H. Eugene Hoyme (2007). "Fetal alcohol spectrum disorders: a practical clinical approach to diagnosis." Neurosci Biobehav Rev **31**(2): 230-238.

Matsuoka, S., B. A. Ballif, et al. (2007). "ATM and ATR substrate analysis reveals extensive protein networks responsive to DNA damage." Science **316**(5828): 1160-1166.

McKeown, S. J. and M. Bronner-Fraser (2008). "Saving face: rescuing a craniofacial birth defect." Nat Med **14**(2): 115-116.

McKinnon, P. J. (2012). "ATM and the Molecular Pathogenesis of Ataxia Telangiectasia." Annu. Rev. Pathol. **7**: 303-321.

McKinnon, P. J. and K. W. Caldecott (2007). "DNA strand break repair and human genetic disease." Annu Rev Genomics Hum Genet **8**: 37-55.

Meek, D. W. (2009). "Tumour suppression by p53: a role for the DNA damage response?" Nat Rev Cancer **9**(10): 714-723.

Meek, K., V. Dang, et al. (2008). "DNA-PK: the means to justify the ends?" Adv Immunol **99**: 33-58.

Mellor, H. R. and R. Callaghan (2008). "Resistance to chemotherapy in cancer: a complex and integrated cellular response." Pharmacology **81**(4): 275-300.

Menoyo, A., H. Alazzouzi, et al. (2001). "Somatic mutations in the DNA damage-response genes ATR and CHK1 in sporadic stomach tumors with microsatellite instability." Cancer Research **61**(21): 7727-7730.

Michel, C. (1989). "Radiation embryology." Experientia **45**(1): 69-77.

Minniti, G., V. De Sanctis, et al. (2008). "Radiotherapy plus concomitant and adjuvant temozolomide for glioblastoma in elderly patients." Journal of Neuro-Oncology **88**(1): 97-103.

Moldovan, G. L. and A. D. D'Andrea (2009). "How the fanconi anemia pathway guards the genome." Annual Review of Genetics **43**: 223-249.

Mostoslavsky, R., K. F. Chua, et al. (2006). "Genomic instability and aging-like phenotype in the absence of mammalian SIRT6." Cell **124**(2): 315-329.

Moynahan, M. E. and M. Jasin (2010). "Mitotic homologous recombination maintains genomic stability and suppresses tumorigenesis." Nat Rev Mol Cell Biol **11**(3): 196-207.

Murga, M., S. Bunting, et al. (2009). "A mouse model of ATR-Seckel shows embryonic replicative stress and accelerated aging." Nat Genet **41**(8): 891-898.

Murga, M., S. Campaner, et al. (2011). "Exploiting oncogene-induced replicative stress for the selective killing of Myc-driven tumors." Nature Structural & Molecular Biology **18**(12): 1331-1335.

Navadgi-Patil, V. M. and P. M. Burgers (2009). "A tale of two tails: activation of DNA damage checkpoint kinase Mec1/ATR by the 9-1-1 clamp and by Dpb11/TopBP1." DNA Repair (Amst) **8**(9): 996-1003.

Niedernhofer, L. J. (2008). "Tissue-specific accelerated aging in nucleotide excision repair deficiency." Mech Ageing Dev **129**(7-8): 408-415.

Norimura, T., S. Nomoto, et al. (1996). "p53-dependent apoptosis suppresses radiation-induced teratogenesis." Nature Medicine **2**(5): 577-580.

Nussenzweig, A., C. Chen, et al. (1996). "Requirement for Ku80 in growth and immunoglobulin V(D)J recombination." Nature **382**(6591): 551-555.

O'Driscoll, M. (2008). "Haploinsufficiency of DNA Damage Response Genes and their Potential Influence in Human Genomic Disorders." Curr. Genomics **9**(3): 137-146.

O'Driscoll, M. (2009). "Life can be stressful without ATR." Nat Genet **41**(8): 866-868.

O'Driscoll, M. (2009). "Mouse models for ATR deficiency." DNA Repair (Amst) **8**(11): 1333-1337.

O'Driscoll, M., W. B. Dobyns, et al. (2007). "Cellular and clinical impact of haploinsufficiency for genes involved in ATR signaling." Am J Hum Genet **81**(1): 77-86.

O'Driscoll, M. and P. A. Jeggo (2003). "Clinical impact of ATR checkpoint signalling failure in humans." Cell Cycle **2**(3): 194-195.

O'Driscoll, M. and P. A. Jeggo (2006). "The role of double-strand break repair - insights from human genetics." Nat Rev Genet **7**(1): 45-54.

O'Driscoll, M., V. L. Ruiz-Perez, et al. (2003). "A splicing mutation affecting expression of ataxia-telangiectasia and Rad3-related protein (ATR) results in Seckel syndrome." Nat Genet **33**(4): 497-501.

Origanti, S., S. R. Cai, et al. (2012). "Synthetic lethality of Chk1 inhibition combined with p53 and/or p21 loss during a DNA damage response in normal and tumor cells." Oncogene.

Osborne, L. R. (1999). "Williams-Beuren syndrome: unraveling the mysteries of a microdeletion disorder." Mol Genet Metab **67**(1): 1-10.

Perry, J. J. and J. A. Tainer (2011). "All stressed out without ATM kinase." Science signaling **4**(167): pe18.

Ragland, R. L., M. F. Arlt, et al. (2009). "Mice hypomorphic for Atr have increased DNA damage and abnormal checkpoint response." Mamm Genome **20**(6): 375-385.

Raschle, M., P. Knipscheer, et al. (2008). "Mechanism of replication-coupled DNA interstrand crosslink repair." Cell **134**(6): 969-980.

Rauch, A., C. T. Thiel, et al. (2008). "Mutations in the pericentrin (PCNT) gene cause primordial dwarfism." Science **319**(5864): 816-819.

Reaper, P. M., M. R. Griffiths, et al. (2011). "Selective killing of ATM- or p53-deficient cancer cells through inhibition of ATR." Nat. Chem. Biol. **7**(7): 428-430.

Rens, W., B. Fu, et al. (2006). "Cross-species chromosome painting." Nat. Protoc. **1**(2): 783-790.

Renwick, A., D. Thompson, et al. (2006). "ATM mutations that cause ataxia-telangiectasia are breast cancer susceptibility alleles." Nat Genet **38**(8): 873-875.

Robinson, I. C. A. F. (2010). GH & IGF1: Aspects of Global and Local Release and Actions

IGFs:Local Repair and Survival Factors Throughout Life Span. D. Clemmons, I. C. A. F. Robinson and Y. Christen, Springer Berlin Heidelberg**:** 1-10.

Rosset, A., L. Spadola, et al. (2004). "OsiriX: an open-source software for navigating in multidimensional DICOM images." J Digit Imaging **17**(3): 205-216.

Ruzankina, Y., C. Pinzon-Guzman, et al. (2007). "Deletion of the developmentally essential gene ATR in adult mice leads to age-related phenotypes and stem cell loss." Cell Stem Cell **1**(1): 113-126.

Ruzankina, Y., D. W. Schoppy, et al. (2009). "Tissue regenerative delays and synthetic lethality in adult mice after combined deletion of Atr and Trp53." Nature Genetics **41**(10): 1144-1149.

Rypens, F., J. Dubois, et al. (2006). "Obstetric US: watch the fetal hands." Radiographics **26**(3): 811-829; discussion 830-811.

Sabbioneda, S., B. K. Minesinger, et al. (2005). "The 9-1-1 checkpoint clamp physically interacts with polzeta and is partially required for spontaneous polzeta-dependent mutagenesis in Saccharomyces cerevisiae." J Biol Chem **280**(46): 38657-38665.

Schoppy, D. W., R. L. Ragland, et al. (2012). "Oncogenic stress sensitizes murine cancers to hypomorphic suppression of ATR." The Journal of clinical investigation **122**(1): 241-252.

Schoppy, D. W., R. L. Ragland, et al. (2012). "Oncogenic stress sensitizes murine cancers to hypomorphic suppression of ATR." Journal of Clinical Investigation **122**(1): 241-252.

Schubert, R., N. Schmitz, et al. (2009). "Growth hormone supplementation increased latency to tumourigenesis in Atm-deficient mice." Growth Factors **27**(5): 265-273.

Sekiguchi, J., D. O. Ferguson, et al. (2001). "Genetic interactions between ATM and the nonhomologous end-joining factors in genomic stability and development." Proc Natl Acad Sci U S A **98**(6): 3243-3248.

Shi, G., D. Y. Chang, et al. (2006). "Physical and functional interactions between MutY glycosylase homologue (MYH) and checkpoint proteins Rad9-Rad1-Hus1." Biochemical Journal **400**(1): 53-62.

Shiloh, Y. (2003). "ATM and related protein kinases: safeguarding genome integrity." Nat. Rev. Cancer **3**(3): 155-168.

Shima, N., S. A. Hartford, et al. (2003). "Phenotype-based identification of mouse chromosome instability mutants." Genetics **163**(3): 1031-1040.

Shiotani, B. and L. Zou (2009). "ATR signaling at a glance." J Cell Sci **122**(Pt 3): 301-304.

Shirakawa, K., S. Morita, et al. (1993). "[Mitomycin C associated hemolytic uremic syndrome--a case report and review of the Japanese cases]." Gan to Kagaku Ryoho **20**(13): 2057-2061.

Sinclair, W. K. (1973). "N-ethylmaleimide and the cyclic response to x-rays of synchronous Chinese hamster cells." Radiation Research **55**(1): 41-57.

Skinner, M. (2010). "Oxidative stress: ATM bonds under stress." Nature reviews. Molecular cell biology **11**(12): 818-819.

Smith, G. C. and S. P. Jackson (1999). "The DNA-dependent protein kinase." Genes Dev **13**(8): 916-934.

Smith, J., L. M. Tho, et al. (2010). "The ATM-Chk2 and ATR-Chk1 pathways in DNA damage signaling and cancer." Advances in Cancer Research **108**: 73-112.

Sohn, S. Y. and Y. Cho (2009). "Crystal structure of the human rad9-hus1-rad1 clamp." J Mol Biol **390**(3): 490-502.

Stephanie A. Yazinsky, G. B., Pei Xin Lim, Lee G. Gewwitz, Tiffany Shard, Teresa Southard, and Robert S. Weiss (in preparation). "A partial defect in the checkpoint protein HUS1 impairs cellular transformation and tumor development."

Stevens, M. F., J. A. Hickman, et al. (1987). "Antitumor activity and pharmacokinetics in mice of 8-carbamoyl-3-methyl-imidazo[5,1-d]-1,2,3,5-tetrazin-4(3H)-one (CCRG 81045; M & B 39831), a novel drug with potential as an alternative to dacarbazine." Cancer Research **47**(22): 5846-5852.

Stiff, T., S. A. Walker, et al. (2006). "ATR-dependent phosphorylation and activation of ATM in response to UV treatment or replication fork stalling." EMBO J **25**(24): 5775-5782.

Stracker, T. H., S. S. Couto, et al. (2008). "Chk2 suppresses the oncogenic potential of DNA replication-associated DNA damage." Mol Cell **31**(1): 21-32.

Stracker, T. H., M. Morales, et al. (2007). "The carboxy terminus of NBS1 is required for induction of apoptosis by the MRE11 complex." Nature **447**(7141): 218-221.

Stracker, T. H. and J. H. Petrini (2011). "The MRE11 complex: starting from the ends." Nature reviews. Molecular cell biology **12**(2): 90-103.

Takai, H., K. Naka, et al. (2002). "Chk2-deficient mice exhibit radioresistance and defective p53-mediated transcription." EMBO Journal **21**(19): 5195-5205.

Takai, H., K. Naka, et al. (2002). "Chk2-deficient mice exhibit radioresistance and defective p53-mediated transcription." EMBO J **21**(19): 5195-5205.

Takai, H., K. Naka, et al. (2002). "Chk2-deficient mice exhibit radioresistance and defective p53-mediated transcription." The EMBO journal **21**(19): 5195-5205.

Takai, H., K. Tominaga, et al. (2000). "Aberrant cell cycle checkpoint function and early embryonic death in Chk1(-/-) mice." Genes Dev **14**(12): 1439-1447.

Tang, Y., Y. Dai, et al. (2012). "Enhancing CHK1 inhibitor lethality in glioblastoma." Cancer biology & therapy **13**(6).

Thorstenson, Y. R., A. Roxas, et al. (2003). "Contributions of ATM mutations to familial breast and ovarian cancer." Cancer Research **63**(12): 3325-3333.

Todaro, G. J. and H. Green (1963). "Quantitative studies of the growth of mouse embryo cells in culture and their development into established lines." J Cell Biol **17**: 299-313.

Toledo, L. I., M. Murga, et al. (2011). "A cell-based screen identifies ATR inhibitors with synthetic lethal properties for cancer-associated mutations." Nature Structural & Molecular Biology **18**(6): 721-727.

Toueille, M., N. El-Andaloussi, et al. (2004). "The human Rad9/Rad1/Hus1 damage sensor clamp interacts with DNA polymerase beta and increases its DNA substrate utilisation efficiency: implications for DNA repair." Nucleic Acids Res **32**(11): 3316-3324.

Tsutakawa, S. E., A. W. Van Wynsberghe, et al. (2011). "Solution X-ray scattering combined with computational modeling reveals multiple conformations of covalently bound ubiquitin on PCNA." Proceedings of the National Academy of Sciences of the United States of America **108**(43): 17672-17677.

van de Ven, M., J. O. Andressoo, et al. (2006). "Adaptive stress response in segmental progeria resembles long-lived dwarfism and calorie restriction in mice." PLoS Genet. **2**(12): e192.

Vassileva, V., A. Millar, et al. (2002). "Genes involved in DNA repair are mutational targets in endometrial cancers with microsatellite instability." Cancer Research **62**(14): 4095-4099.

Venclovas, C. and M. P. Thelen (2000). "Structure-based predictions of Rad1, Rad9, Hus1 and Rad17 participation in sliding clamp and clamp-loading complexes." Nucleic Acids Res **28**(13): 2481-2493.

Ventura, A., A. G. Young, et al. (2008). "Targeted deletion reveals essential and overlapping functions of the miR-17 through 92 family of miRNA clusters." Cell **132**(5): 875-886.

Verdun, R. E. and J. Karlseder (2006). "The DNA damage machinery and homologous recombination pathway act consecutively to protect human telomeres." Cell **127**(4): 709-720.

Volkmer, E. and L. M. Karnitz (1999). "Human homologs of Schizosaccharomyces pombe rad1, hus1, and rad9 form a DNA damage-responsive protein complex." Journal of Biological Chemistry **274**(2): 567-570.

Wang, L., C. L. Hsu, et al. (2004). "Human checkpoint protein hRad9 functions as a negative coregulator to repress androgen receptor transactivation in prostate cancer cells." Molecular and Cellular Biology **24**(5): 2202-2213.

Wang, S., M. Guo, et al. (2000). "The catalytic subunit of DNA-dependent protein kinase selectively regulates p53-dependent apoptosis but not cell-cycle arrest." Proc Natl Acad Sci U S A **97**(4): 1584-1588.

Wang, W., L. A. Lindsey-Boltz, et al. (2006). "Mechanism of stimulation of human DNA ligase I by the Rad9-rad1-Hus1 checkpoint complex." J Biol Chem **281**(30): 20865-20872.

Weiss, R. S., T. Enoch, et al. (2000). "Inactivation of mouse Hus1 results in genomic instability and impaired responses to genotoxic stress." Genes Dev **14**(15): 1886-1898.

Weiss, R. S., T. Enoch, et al. (2000). "Inactivation of mouse Hus1 results in genomic instability and impaired responses to genotoxic stress." Genes and Development **14**(15): 1886-1898.

Weiss, R. S., C. F. Kostrub, et al. (1999). "Mouse Hus1, a homolog of the Schizosaccharomyces pombe hus1+ cell cycle checkpoint gene." Genomics **59**(1): 32-39.

Weiss, R. S., P. Leder, et al. (2003). "Critical role for mouse Hus1 in an S-phase DNA damage cell cycle checkpoint." Mol Cell Biol **23**(3): 791-803.

Weiss, R. S., S. Matsuoka, et al. (2002). "Hus1 acts upstream of chk1 in a mammalian DNA damage response pathway." Current Biology **12**(1): 73-77.

Weiss, R. S., S. Matsuoka, et al. (2002). "Hus1 acts upstream of chk1 in a mammalian DNA damage response pathway." Curr Biol **12**(1): 73-77.

Weterings, E. and D. J. Chen (2008). "The endless tale of non-homologous end-joining." Cell Res **18**(1): 114-124.

Wirth-Dzieciolowska, E., J. Karaszewska, et al. (2009). "Selected peripheral blood cell parameters in twelve inbred strains of laboratory mice." Animal Science Papers and Reports **27**(1): 69-77.

Woo, G. H., K. Katayama, et al. (2004). "Effects of prenatal hydroxyurea-treatment on mouse offspring." Experimental and Toxicologic Pathology **56**(1-2): 1-7.

Woo, G. H., K. Katayama, et al. (2003). "Hydroxyurea (HU)-induced apoptosis in the mouse fetal tissues." Histology and Histopathology **18**(2): 387-392.

Woo, R. A., K. G. McLure, et al. (1998). "DNA-dependent protein kinase acts upstream of p53 in response to DNA damage." Nature **394**(6694): 700-704.

Xu, M., L. Bai, et al. (2009). "Structure and functional implications of the human rad9-hus1-rad1 cell cycle checkpoint complex." J Biol Chem **284**(31): 20457-20461.

Xu, Y., T. Ashley, et al. (1996). "Targeted disruption of ATM leads to growth retardation, chromosomal fragmentation during meiosis, immune defects, and thymic lymphoma." Genes Dev **10**(19): 2411-2422.

Xu, Y. and D. Baltimore (1996). "Dual roles of ATM in the cellular response to radiation and in cell growth control." Genes Dev **10**(19): 2401-2410.

Yan, H. L., G. Xue, et al. (2009). "Repression of the miR-17-92 cluster by p53 has an important function in hypoxia-induced apoptosis." The EMBO journal **28**(18): 2719-2732.

Yang, J., Y. Yu, et al. (2003). "ATM, ATR and DNA-PK: initiators of the cellular genotoxic stress responses." Carcinogenesis **24**(10): 1571-1580.

Yazinski, S. A., P. M. Westcott, et al. (2009). "Dual inactivation of Hus1 and p53 in the mouse mammary gland results in accumulation of damaged cells and impaired tissue regeneration." Proc Natl Acad Sci U S A **106**(50): 21282-21287.

Yazinski, S. A., P. M. Westcott, et al. (2009). "Dual inactivation of Hus1 and p53 in the mouse mammary gland results in accumulation of damaged cells and impaired tissue regeneration." Proceedings of the National Academy of Sciences of the United States of America **106**(50): 21282-21287.

Yoo, H. Y., A. Kumagai, et al. (2007). "Ataxia-telangiectasia mutated (ATM)-dependent activation of ATR occurs through phosphorylation of TopBP1 by ATM." J Biol Chem **282**(24): 17501-17506.

Zhu, A., C. X. Zhang, et al. (2008). "Rad9 has a functional role in human prostate carcinogenesis." Cancer Research **68**(5): 1267-1274.

Zhu, M. and R. S. Weiss (2007). "Increased common fragile site expression, cell proliferation defects, and apoptosis following conditional inactivation of mouse Hus1 in primary cultured cells." Mol Biol Cell **18**(3): 1044-1055.

Zhu, M. and R. S. Weiss (2007). "Increased common fragile site expression, cell proliferation defects, and apoptosis following conditional inactivation of mouse Hus1 in primary cultured cells." Molecular Biology of the Cell **18**(3): 1044-1055.

Zighelboim, I., A. P. Schmidt, et al. (2009). "ATR mutation in endometrioid endometrial cancer is associated with poor clinical outcomes." Journal of Clinical Oncology **27**(19): 3091-3096.

Zou, L. and S. J. Elledge (2003). "Sensing DNA damage through ATRIP recognition of RPA-ssDNA complexes." Science **300**(5625): 1542-1548.